1992

Distance analysis of Patterson calculations and molecular mechanics as aids in structure solution

Catherine Lucia Day
Iowa State University

Order Number 9301999

Distance analysis of Patterson calculations and molecular mechanics as aids in structure solution

Day, Catherine Lucia, Ph.D.

Iowa State University, 1992

U·M·I
300 N. Zeeb Rd.
Ann Arbor, MI 48106

Distance analysis of Patterson calculations and molecular mechanics as aids in structure solution

by

Catherine Lucia Day

A Dissertation Submitted to the
Graduate Faculty in Partial Fulfillment of the
Requirements for the Degree of
DOCTOR OF PHILOSOPHY

Department: Chemistry
Major: Physical Chemistry

Approved:

Signature was redacted for privacy.

In Charge of Major Work

Signature was redacted for privacy.

For the Major Department

Signature was redacted for privacy.

For the Graduate College

Iowa State University
Ames, Iowa

1992

TABLE OF CONTENTS

CHAPTER 1. INTRODUCTION

Less than 50 years ago, solving one crystal structure was the basis for a PhD in crystallography. Today, X-ray structure determination has become a tool to the synthetic chemist in the characterization of new compounds. With the advent of direct methods which often furnishes at least a partial solution and "user-friendly" structure solution packages which lead the novice crystallographer by the hand, routine crystal structures can be solved with only rudimentary knowledge of crystallographic theory. However, with the increasing sophistication of synthetic techniques leading to the increasing complexity of the molecules prepared, the likelihood of the crystal structures resisting solution has also increased. (Degree of difficulty increases approximately as the square of the number of atoms.) It is these cases which spur the crystallographer into pursuing new and novel structure elucidation techniques.

In the solution of a crystal structure, the primary goal is to obtain information regarding space group symmetry and atomic positions which lead to bond lengths and bond angles. To this end, two main methods for initial model development are currently in use. Direct methods are by far the choice of solution for crystals containing no heavy atoms. Even though

the mathematics used in direct methods is quite complicated, today's fast computers and advanced software packages make direct methods an easy to use, black-box technique. Additionally, advances in the direct methods techniques allow direct methods to often give at least a partial solution even when the molecule contains heavy atoms; therefore, direct methods has become the method of first choice for initial model development for the novice crystallographer attempting a crystal solution. When direct methods fail, however, the crystallographer often returns to an older method of solution, the Patterson method.

Since the direct methods technique is based on statistics, it doesn't give the physical insight of the Patterson function. By the nature of the method, the Patterson function contains an image of the structure. However, this image, for a structure containing N atoms, is superimposed with N-1 other images making interpretation of even a simple structure nontrivial. The difficulty in obtaining a solution from a Patterson map often inhibits the novice crystallographer from using the technique.

The images revealed in the Patterson function can be partially unscrambled by means of Patterson superposition techniques. This method superimposes a Patterson map with another Patterson map whose origin has been shifted by a carefully chosen interatomic vector. Depending on the shift

chosen, the resultant map can provide a clearer picture of the structure.

Though the Patterson superposition map provides a partial deconvolution of the Patterson map, some interpretation is usually still necessary to reveal the structure. The program SUPSYMM was written to aid in these interpretations. Before going into the details of the program, it is necessary to understand the theory of Patterson and the Patterson superposition methods. Chapter 2 will discuss the continuing evolution of these techniques. Chapter 3 will delve into the program, SUPSYMM, which, using the distances between and vector projections associated with the superposition peaks, interprets the superposition map by finding related peaks and their symmetry elements. The program has been tested on several real structures. These structures are discussed in Chapter 4.

Another technique, one combining the strengths of molecular mechanics and those of X-ray crystallography, has been developed for particular application to those crystal structures involving largely organic organometallic complexes. Crystallographic methods such as the previously discussed Patterson superposition calculations can usually provide at least the heavier atom positions. In large organometallic complexes, these heavy atoms alone may not be enough to phase the reflections well enough to readily reveal the rest of the

structure. Using the known heavy atom positions as anchor points for molecular mechanics routines, the rest of the molecule can be modeled. Chapter 5 discusses a technique devised to take the results from molecular mechanics refinement as input to crystallographic least-squares refinement in order to obtain a complete trial model. Chapter 6 shows the results of the technique on both a known and an unknown structure.

A summary of the two techniques and plans for their future extensions are included in Chapter 7.

Two programs designed to teach the basics of both powder and single crystal X-ray diffraction methods to undergraduate physical chemistry students or first year graduate students were developed and are discussed in Appendix A. Additional, crystal structures solved through normal crystallographic routes are presented in Appendix B.

CHAPTER 2. PATTERSON AND PATTERSON SUPERPOSITION TECHNIQUES

Patterson and Patterson superposition techniques are neither new nor novel but the information provided by these techniques has lead to countless crystal solutions. In fact, until the early 1950s, almost all crystal structures were solved via analysis of the Patterson function. Even though Patterson methods have been largely overshadowed since the development of "direct methods", Patterson techniques continue to be a viable option when direct methods fail to reveal a solution.

The Patterson Method

In 1934, A. L. Patterson[1] introduced and discussed the physical significance of a Fourier series which can be directly calculated from experimental intensity data. This function

$$P(\mathbf{u}) = \int_V \rho(\mathbf{r}+\mathbf{u})\,\rho(\mathbf{r})\,d\tau \qquad (2.1)$$

is an average distribution of the product of the electron density at any fractional coordinate $\mathbf{r} = (x,y,z)$ and $\mathbf{r}+\mathbf{u} = (x+u,y+v,z+w)$ where the electron density is given by

$$\rho(\boldsymbol{x}) = \frac{1}{V}\sum_{\boldsymbol{h}} F_{\boldsymbol{h}}\, e^{i2\pi(\boldsymbol{h}\cdot\boldsymbol{x})}$$
$$\rho(\boldsymbol{x}+\boldsymbol{u}) = \frac{1}{V}\sum_{\boldsymbol{h}} F_{\boldsymbol{h}}\, e^{i2\pi(\boldsymbol{h}\cdot(\boldsymbol{x}+\boldsymbol{u}))} \qquad (2.2)$$

and the summation extends from $-\infty$ to ∞. (Letters in bold indicate vector quantities.) P(u) may be evaluated by substituting (2.2) into (2.1) to give

$$P(\boldsymbol{u}) = \frac{1}{V^2}\int_V \left(\sum_{\boldsymbol{h}'} F^*_{\boldsymbol{h}'} e^{-2\pi i\boldsymbol{h}'\cdot(\boldsymbol{x}+\boldsymbol{u})} \sum_{\boldsymbol{h}} F_{\boldsymbol{h}} e^{2\pi i\boldsymbol{h}\cdot\boldsymbol{x}}\right) d\tau \qquad (2.3)$$

where **h′** and **h** indices lie within the same range but are independent of each other. Remembering that the integral of a sum is the sum of the integrals of the separate terms leads to

$$P(\boldsymbol{u}) = \frac{1}{V^2}\sum_{\boldsymbol{h}}\sum_{\boldsymbol{h}'} F^*_{\boldsymbol{h}'} F_{\boldsymbol{h}} e^{-2\pi i(\boldsymbol{h}'\cdot\boldsymbol{u})} \int_V e^{2\pi i(\boldsymbol{h}-\boldsymbol{h}')\cdot\boldsymbol{x}} d\tau \qquad (2.4)$$

The exponential function in the integral part of this expression is periodic and consequently is, in general, zero. However, if **h′**= **h** then $\int_V d\tau = V$ leaving

$$P(\boldsymbol{u}) = \frac{1}{V}\sum_{\boldsymbol{h}(\text{or }\boldsymbol{h}')} |F_{\boldsymbol{h}}|^2 e^{-2\pi i(\boldsymbol{h}\cdot\boldsymbol{u})} \qquad (2.5)$$

where the index h (or h′) ranges from $-\infty$ to ∞. Since $-\infty \rightarrow 0$ gives the same values with only a different sign as $0 \rightarrow \infty$ and using de Moivre's theorem

$$e^{\pm i\phi} = \cos\phi \pm i\sin\phi \tag{2.6}$$

the Patterson function becomes

$$P(\boldsymbol{u}) = \frac{2}{V}\sum_{\boldsymbol{h}}|F_{\boldsymbol{h}}|^2\cos 2\pi\boldsymbol{h}\cdot\boldsymbol{u} \tag{2.7}$$

An important feature to recognize is that the Patterson function is related to the square of the structure factor which, defined as the intensity, can be directly measured by X-ray diffraction.

Further examination of this function allows the square of the magnitude of the structure factors, which here include the temperature factors, to be written as

$$\begin{aligned} |F_{\boldsymbol{h}}|^2 &= F_{\boldsymbol{h}}\,F_{-\boldsymbol{h}} \\ &= \left|\left(\sum_j f_j e^{-2\pi i\boldsymbol{h}\cdot\boldsymbol{r}_j}\right)\right|^2 \\ &= \sum_i\sum_j f_j f_i\, e^{2\pi i\boldsymbol{h}\cdot(\boldsymbol{r}_i-\boldsymbol{r}_j)} \\ &= \sum_{\substack{j \\ i=j}} f_j^2 + \sum_i\sum_{\substack{j \\ i\neq j}} f_j f_i e^{2\pi i\boldsymbol{h}\cdot(\boldsymbol{r}_i-\boldsymbol{r}_j)} \end{aligned} \tag{2.8}$$

Thus substituting (2.8) into (2.5) gives

$$P(\mathbf{u}) = \frac{1}{V}\sum_{h}\sum_{j} f_j^2 e^{-2\pi i(\mathbf{h}\cdot\mathbf{u})} + \frac{1}{V}\sum_{h}\sum_{i}\sum_{\substack{j \\ i\neq j}} f_i f_j e^{2\pi i\mathbf{h}\cdot(\mathbf{r}_i-\mathbf{r}_j)}\, e^{-2\pi i\mathbf{h}\cdot\mathbf{u}} \qquad (2.9)$$

(a) (b)

The interpretation of (2.9) can be accomplished in parts. The average of (a) will be zero unless $\mathbf{u} = 0$ which yields a peak at the origin whose magnitude is proportional to ΣZ_j^2 since f_j is related to the atomic number of the jth atom. The magnitude of (b) will be small unless $\mathbf{r}_i-\mathbf{r}_j = \mathbf{u}$. The quantity $\mathbf{u}$ is a vector terminating at the point $(x_i-x_j, y_i-y_j, z_i-z_j)$ and proportional to Z_iZ_j. This is equivalent to putting atom j at the origin and mapping a peak at the location of atom i. This illustrates another important physical aspect of the Patterson function. The Patterson function gives a composite picture of the molecule, one that would be obtained by placing each atom in the unit cell in turn at the origin and putting peaks at the positions where all other atoms would reside.

By the above argument a Patterson peak occurs when two atoms are separated by the vector $\mathbf{u}$. Therefore, for a molecule containing N atoms in a unit cell, the Patterson will show N^2 peaks which corresponds to the N possible vectors which can be drawn from each of the N atoms (Figure 2.1)[2]. The set of interatomic vectors between atom 1 through atom N

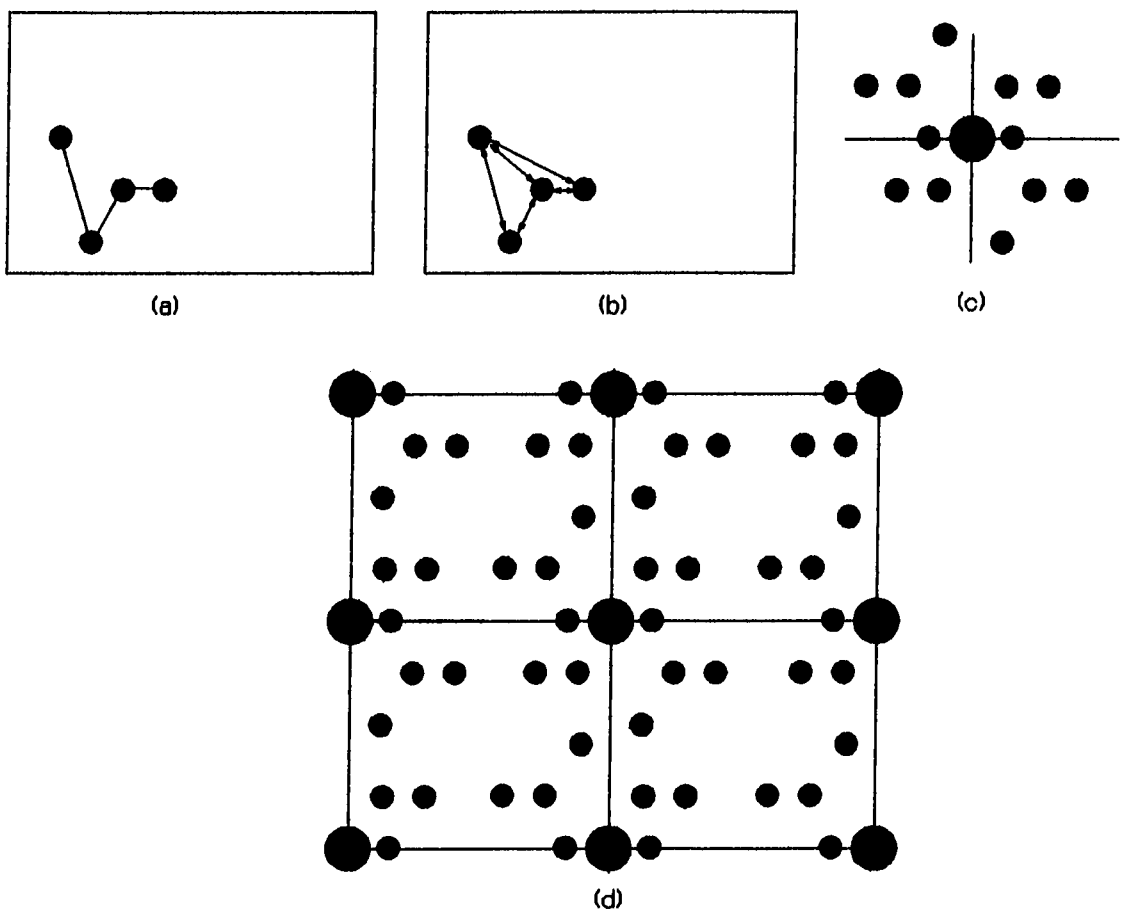

Figure 2.1. (a) A set of points (b) Interatomic vectors (c) Patterson peaks about the origin; ●, origin peak (d) Patterson peaks in four unit cells

of a structure can be represented in vector set notation where $\{A_i - A_1\}$, i=1 to N. Therefore, the Patterson function gives

$$\begin{aligned}[P(u)] &\equiv \{A_i - A_1\} \cup \{A_i - A_2\} \cup \ldots \cup \{A_i - A_N\} \\ &\equiv \{A_i - A_j\}, \quad i,j=1 \text{ to } N\end{aligned} \tag{2.10}$$

Of these N^2 peaks, N will coincide at the origin and $\frac{1}{2}N(N-1)$ peaks are related to the remaining $\frac{1}{2}N(N-1)$ peaks by a center of symmetry. The center of symmetry arises due to the fact that the vector from r_i-r_j is equal in magnitude but opposite in sign to the vector r_j-r_i. As a consequence of this center of symmetry inherent in the Patterson function, the 230 space groups available do not necessarily correspond to the Patterson symmetry but do correspond to the Laue group.

Evaluating the Patterson function using vectors related to symmetry was first introduced by D. Harker[3] in 1936. In the evaluation of a crystal with a 2-fold axis parallel with the b axis, if there is an atom at (x,y,z), the coordinates of the symmetry related pair will be (-x,y,-z). A maximum in the Patterson function occurs at the interatomic vector between the two or at (2x,0,2z). Consequently, given a Patterson peak of the type (u,0,w), the x and z coordinates can be established by solving the relations: x = u/2 and z = w/2. Nothing can be said about the y coordinate for this

relationship. The vector (u,0,w) is called a Harker vector. Table 2.1 lists the Harker vectors and planes corresponding to some of the more common symmetry elements.

Table 2.1. Some Harker vectors and planes

Symmetry element	Harker vector or plane
2-fold axis ‖ a, b, c	(0,v,w); (u,0,w); (u,v,0)
2-fold screw ‖ a, b, c	(½,u,w); (u,½,w); (u,v,½)
m plane perpendicular to a, b, c	(u,0,0); (0,v,0); (0,0,w)
a glide perpendicular to b, c	(½,v,0); (½,0,w)
b glide perpendicular to a, c	(u,½,0); (0,½,w)
c glide perpendicular to a, b	(u,0 ½); (0,v,½)

A practical example of the usefulness of Harker vectors is illustrated by my solution of the structure $[BrC_{15}N_1O_4H_{24}]Cl \cdot CCl_2H_2$. The bromine atom was located from Harker vector analysis of the Patterson map. $[BrC_{15}N_1O_4H_{24}]Cl \cdot CCl_2H_2$ forms in the orthorhombic space group $P2_12_12_1$. Harker vectors for this space group are (½ ± 2x, ± 2y, ½), (½, ½ ± 2y, ± 2z), and (± 2x, ½, ½ ± 2z). Larger Patterson peaks attributable to Br-Br interactions were found at (0.5741,0.0645,0.5000), (0.500,0.4342,0.6697) and (0.0781,0.5000,0.8306); assuming them to be the Harker vectors, a bromine atom is established

to reside at (0.0370,-0.03225,0.3348). Correct placement of the bromine atom provided phases of sufficient correctness to determine the rest of the structure. Complete experimental details for this structure are given in Appendix B.

Although Patterson maps can be quite complicated even for simple structures, the Patterson method is the most general method; it does not require any special knowledge regarding space groups while it contains all the necessary information about the structure. Attempts have been made to solve structures semi-automatically from Patterson syntheses[4,5,6]. These methods have not been adopted for general use because existing programs are not as automatic as direct methods program packages such as TEXSAN[7] and SHELXS[8]. Even though the Patterson search methods have considerable effectiveness and flexibility, the extensive user input required usually does not make them the method of first choice.

What is needed is a way to at least partially unscramble the picture presented in the Patterson function to make interpretation less complicated. A technique devised by Buerger[9] showed that a Patterson map with N superimposed images can, in a systematic way, be pared down to a map with one or, as usually occurs, some number between 1 and N images by correctly displacing two copies of the Patterson map and noting the positions of peak overlap.

The Patterson Superposition Method

The Patterson superposition method is based upon correctly displacing the images in the Patterson function by some interatomic vector and superimposing this shifted map with another copy of the Patterson map. Comparing the positions of peak overlap, using a suitable comparison function - usually a minimum function - lead to at least a partial unshuffling of the Patterson. In the following approach, no chemical knowledge need be directly used.

Vector notation can be used to illustrate this concept. Taking a unique interatomic vector S, such that $\mathbf{S} = (\mathbf{A}_2 - \mathbf{A}_1)$, as the shift vector, the superposition can be written as the intersection between the set of Patterson vectors and the set of Patterson vectors shifted by S or

$$[\{\mathbf{A}_j - \mathbf{A}_1\} + (\mathbf{A}_2 - \mathbf{A}_1)] \cap [\{\mathbf{A}_j - \mathbf{A}_1\}] \qquad (2.11)$$

which corresponds to two images where

$$\begin{aligned} &j = 1 \text{ gives the set } \{\mathbf{A}_2 - \mathbf{A}_1\} \qquad i = 1 \text{ to } N \\ &i = 2 \text{ gives the set } \{\mathbf{A}_j - \mathbf{A}_1\} \qquad j = 1 \text{ to } N \end{aligned} \qquad (2.12)$$

In theory, these two images can be reduced into one by choosing an additional superposition vector, S2, where S2 = $(\mathbf{A}_3 - \mathbf{A}_1)$ which can be written as

$$[\{\mathbf{A}_j - \mathbf{A}_i\} + (\mathbf{A}_2 - \mathbf{A}_1)] \cap [\{\mathbf{A}_j - \mathbf{A}_i\} + (\mathbf{A}_3 - \mathbf{A}_1)] \qquad (2.13)$$

whose image is given by

$$[\{\mathbf{A}_i - \mathbf{A}_1\}] \qquad i=1 \text{ to } N \qquad (2.14)$$

The above shift vectors are assumed to be single. In practice, however, multiple vectors (ie. another vector, e.g. $(\mathbf{A}_5 - \mathbf{A}_4)$, equal to the original shift vector $(\mathbf{A}_2 - \mathbf{A}_1)$) are easier to find and more likely to be used in the superposition.

Another case that needs to be considered is one where overlap between non-related peaks occur. Such accidental overlaps arise from the fact that peaks in the Patterson map have a certain breadth. These spurious peaks further complicate an already difficult analysis. To minimize these extraneous overlaps, sharpening using a procedure outlined by Jacobson, Wunderlich, and Lipscomb[10] is employed. Sharpening techniques try to minimize the peak width as well as to minimize rippling due to termination-of-series effects.

Peaks in a superposition map can still be related to Harker vectors. Usually there is a shift in the origin as well. Locating the position of the symmetry elements helps to establish the origin and, thus, the atom positions.

In general, an m-fold vector gives 2m remaining images. Superposition maps which still contain multiple images are the input to SUPSYMM. (For further details on the superposition method consult references 11, 12, and 13).

CHAPTER 3. DETAILS OF SUPSYMM

The Patterson superposition approach is a powerful tool in crystal structure determination. Interpretation of a superposition map, however, remains one of the main roadblockS for the novice crystallographer when using this method. Using distance analysis and vector projections, SUPSYMM is a program designed to aid the less experienced crystallographer in the meaningful interpretation of the superposition map.

Elements of Symmetry

More than 99% of all structure investigated have some elements of symmetry present in the unit cell. Testing for the presence and position of symmetry elements and noting peaks related by these symmetry elements is the path taken by SUPSYMM in the interpretation of the Patterson superposition map.

Crystals form in one of seven crystal systems as shown in Table 3.1. SUPSYMM calculations, at this point, extend through the orthorhombic system. For the organometallic compounds or compounds containing heavy atoms on which Patterson methods have the greatest success, approximately 90% will fall into orthorhombic, monoclinic or triclinic symmetry.

Table 3.1. The seven crystal systems

Crystal system	Parameters	Laue symmetry
Triclinic	$a \neq b \neq c$; $\alpha \neq \beta \neq \gamma$	-1
Monoclinic	$a \neq b \neq c$; $\alpha = \gamma = 90^\circ$; $\beta \neq 90^\circ$	2/m
Orthorhombic	$a \neq b \neq c$; $\alpha = \beta = \gamma = 90^\circ$	mmm
Tetragonal	$a = b \neq c$; $\alpha = \beta = \gamma = 90^\circ$	4/mmm
Rhombohedral	$a = b = c$; $\alpha = \beta = \gamma \neq 90^\circ$	-3/m
Hexagonal	$a = b \neq c$; $\alpha = \beta = 90^\circ$; $\gamma = 120^\circ$	6/mmm
Cubic	$a = b = c$; $\alpha = \beta = \gamma = 90^\circ$	m3m

Because of their underlying importance in the analysis performed by SUPSYMM, the symmetry elements available to the triclinic, monoclinic and orthorhombic systems need to be discussed. The description of symmetry elements can be broken down into two simple types of symmetry: reflection and rotation.

If every point in the structure is reflected through a plane, that plane is designated as a mirror plane. The reflected points are said to be related by mirror symmetry. Figure 3.1(a) depicts two points related by a mirror plane. Two atoms related by a mirror plane perpendicular to the b axis will have coordinates (x,y,z) and (x,-y,z).

Rotation occurs about an axis. For the seven crystal systems, 1-, 2-, 3-, 4- 6-fold axes can occur. For systems

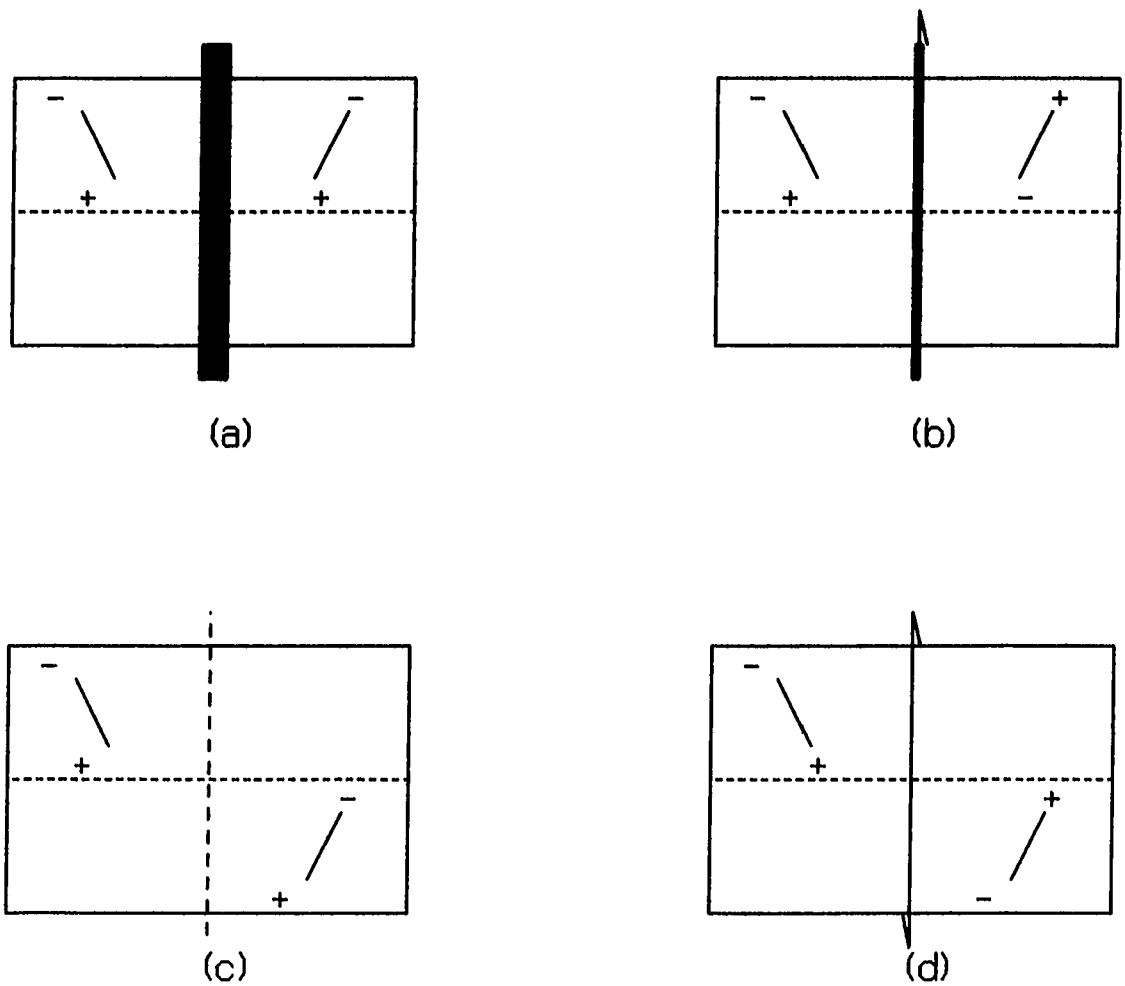

Figure 3.1. Symmetry elements: (a) mirror, (b) 2-fold rotation, (c) glide and (d) screw; (+)-indicates line is in front of the plane of the paper, (-)-indicates line is behind the plane of the paper

through orthorhombic symmetry, only the 2-fold rotation is present. The 2-fold rotation is a 180° rotation about one of the crystallographic axes. Figure 3.1(b) illustrates a 2-fold rotation. Two atoms with coordinates (x,y,z) and (-x,y,-z) are said to be related by a 2-fold rotation about the b axis.

These two symmetry elements may be combined to produce other symmetry. Combining a mirror with a 2-fold rotation yields an inversion center - a center of symmetry. If a molecule contains an inversion center or is centrosymmetric, a point (x,y,z) will be transformed to (-x,-y,-z).

Combining a mirror plane with a half unit cell translation parallel to the reflecting plane produces a glide plane (Figure 3.1(c)). The translation can occur along the axis or along a diagonal. A glide plane is designated by a, b, or c if the translation is a/2, b/2, or c/2 and by n if (a+b)/2, (a+c)/2, or (b+c)/2. Symbolically, the point (x,y,z) is said to be related to the point (x,-y,z+½) by a c-glide.

A half unit cell translation can also be merged with a 2-fold rotation to produce a 2_1 screw axis. The direction of such an axis is usually along a unit cell edge and the translation is along the rotation axis. Two points related by a 2_1 screw axis along the b direction would have coordinates (x,y,z) and (-x,y+½,-z), respectively (Figure 3.1(d)).

Distance Relationships for Symmetry Element Identification

SUPSYMM requires no chemical information except the lattice parameters of the crystal and a list of superposition peak positions. Using calculated interatomic distances, atom pairs are grouped into sets of "equivalent distances". Because of approximations in Fourier series analysis, equivalent here means equal within a tolerance. The tolerance is determined by an examination of the quality of the data and the resolution of the peaks. Any tolerance level can be chosen; however, a smaller tolerance is more apt to eliminate coincident correspondences while a larger tolerance is likely to find relationships that are not there. Using pairs from these equivalent distance groups, a search is carried out for possible symmetry relationships.

The first step in this search for possible symmetry relationships is to calculate the shortest interatomic distance between all pairs of peaks of the Patterson superposition map using

$$\begin{aligned} d = (&\Delta x^2 \cdot a^2 + \Delta y^2 \cdot b^2 + \Delta z^2 \cdot c^2 \\ &+ 2 \cdot \Delta x \cdot \Delta y \cdot a \cdot b \cdot \cos\gamma \\ &+ 2 \cdot \Delta x \cdot \Delta z \cdot a \cdot c \cdot \cos\beta \\ &+ 2 \cdot \Delta y \cdot \Delta z \cdot b \cdot c \cdot \cos\alpha)^{1/2} \end{aligned} \qquad (3.1)$$

where $\Delta x \equiv (x_B - x_A)$, $\Delta y \equiv (y_B - y_A)$, and $\Delta z \equiv (z_B - z_A)$. Unit cell translations are taken into account in order to obtain the shortest distance to atom B and are noted and used in all subsequent calculations involving atom B of the pair. Distances are sorted in ascending order to identify potential distance relationships.

If two pairs of atoms pass the initial distance equivalence within tolerance, they are subjected to further tests to check for a symmetry relationship. If the two atom pairs, A-B and A′-B′, are related by the following symmetry elements - inversion, 2-fold rotation about any axis, 2_1 screw about any axis, mirror perpendicular to any axis, or glide symmetry perpendicular or diagonal to any axis, the distances between A-A′, B-B′, A-B′, and A′-B must meet specific criteria.

If the pairs are related by an inversion (Figure 3.2) then $(x_A, y_A, z_A) \rightarrow (-x_A, -y_A, -z_A)$ and $(x_B, y_B, z_B) \rightarrow (-x_B, -y_B, -z_B)$ give the following relationships as shown in Table 3.2:

Table 3.2. Difference criteria ($\Delta x, \Delta y, \Delta z$) for inversion

	$A' \equiv (-x_A, -y_A, -z_A)$	$B' \equiv (-x_B, -y_B, -z_B)$
$A \equiv (x_A, y_A, z_A)$	$2x_A, 2y_A, 2z_A$ =d6	$(x_A+x_B)(y_A+y_B)(z_A+z_B)$ =d4
$B \equiv (x_B, y_B, z_B)$	$(x_B+x_A)(y_B+y_A)(z_B+z_A)$ =d3	$2x_B, 2y_B, 2z_B$ =d5

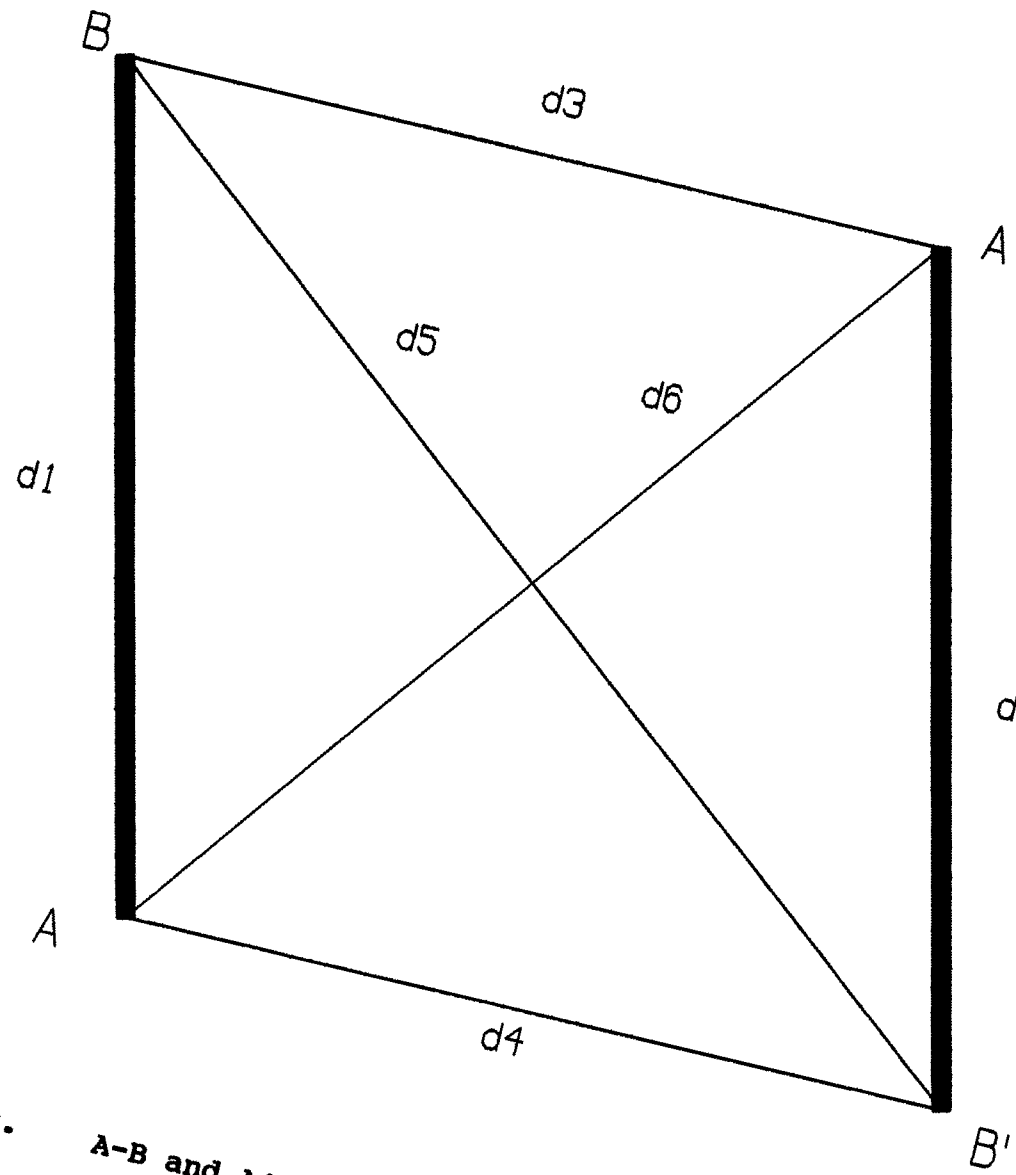

Figure 3.2. **A-B and A′-B′ related by inversion**

As shown in Tables 3.3 to 3.6, if the pairs are related by 2-fold rotation, screw, mirror, or glide symmetry (Figure 3.3), the following relationships arise:

Table 3.3. Difference criteria ($\Delta x, \Delta y, \Delta z$) for mirror perpendicular to b

	$A' \equiv (x_A, -y_A, z_A)$	$B' \equiv (x_B, -y_B, z_B)$
$A \equiv (x_A, y_A, z_A)$	$0, 2y_A, 0$ =d4	$(x_A - x_B)(y_A + y_B)(z_A - z_B)$ =d6
$B \equiv (x_B, y_B, z_B)$	$(x_B - x_A)(y_B + y_A)(z_B - z_A)$ =d5	$0, 2y_B, 0$ =d3

Table 3.4. Difference criteria ($\Delta x, \Delta y, \Delta z$) for 2-fold rotation about b

	$A' \equiv (-x_A, y_A, -z_A)$	$B' \equiv (-x_B, y_B, -z_B)$
$A \equiv (x_A, y_A, z_A)$	$2x_A, 0, 2z_A$ =d4	$(x_A + x_B)(y_A - y_B)(z_A + z_B)$ =d6
$B \equiv (x_B, y_B, z_B)$	$(x_B + x_A)(y_B - y_A)(z_B + z_A)$ =d5	$2x_B, 0, 2z_B$ =d3

Table 3.5. Difference criteria ($\Delta x, \Delta y, \Delta z$) for c-glide perpendicular to b

	$A' \equiv (x_A, -y_A, z_A+\frac{1}{2})$	$B' \equiv (x_B, -y_B, z_B+\frac{1}{2})$
$A \equiv (x_A, y_A, z_A)$	$0, 2y_A, \frac{1}{2}$ =d4	$(x_A-x_B)(y_A+y_B)(z_A-z_B-\frac{1}{2})$ =d6
$B \equiv (x_B, y_B, z_B)$	$(x_B-x_A)(y_B+y_A)(z_B-z_A-\frac{1}{2})$ =d5	$0, 2y_B, \frac{1}{2}$ =d3

Table 3.6. Difference criteria ($\Delta x, \Delta y, \Delta z$) for 2_1 about b

	$A' \equiv (-x_A, y_A+\frac{1}{2}, -z_A)$	$B' \equiv (-x_B, y_B+\frac{1}{2}, -z_B)$
$A \equiv (x_A, y_A, z_A)$	$2x_A, \frac{1}{2}, 2z_A$ =d4	$(x_A+x_B)(y_A-y_B\frac{1}{2})(z_A+z_B)$ =d6
$B \equiv (x_B, y_B, z_B)$	$(x_B+x_A)(y_B-y_A-\frac{1}{2})(z_B+z_A)$ =d5	$2x_B, \frac{1}{2}, 2z_B$ =d3

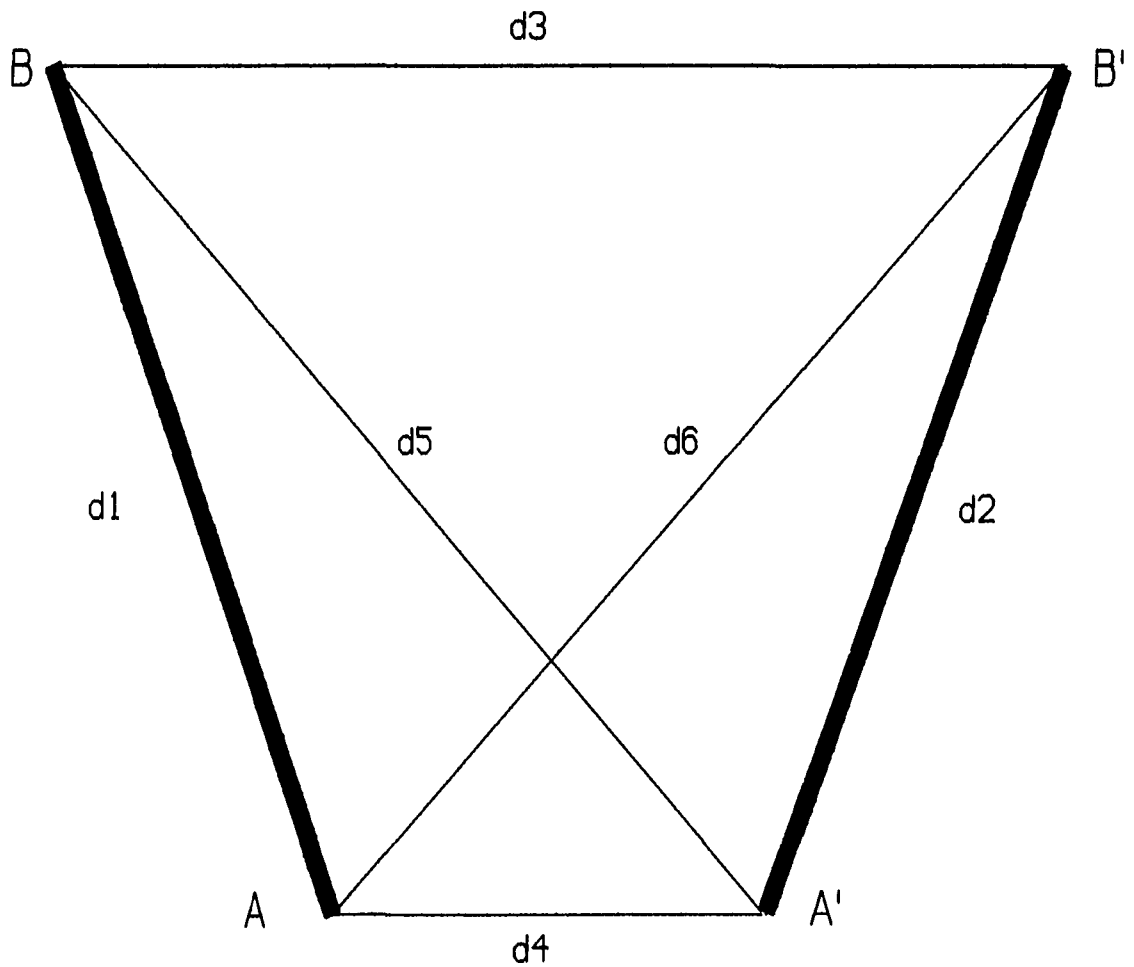

Figure 3.3. **A-B and A'B' related by mirror, rotation, glide, or screw symmetry**

The difference criteria of Tables 3.3 - 3.6 hold for relationships about any axis not just the b axis as illustrated.

Using the (Δx,Δy,Δz) difference criteria from Tables 3.2 - 3.6 the distances between atom pairs can be calculated using equation 3.1. These distance calculations indicate that if the two pairs of atoms, A-B and A′-B′, are related by any one of the above listed symmetry elements, in addition to this distance pair, at least one of the other of the two sets of distances [(1) A-A′ and B-B′, and (2) A-B′ and A′-B] must be equivalent. If this distance equivalency is not met, the pairs can not be related by any of these symmetry elements.

From Table 3.2, atom pairs related by an inversion can be distinguished from the other symmetry elements by noting that the crossed pair in Figure 3.2, denoted A-A′ and B-B′, distances are equal while A-B′ and A′-B are not equal for the inversion. This leaves the midpoint of A-A′ and the midpoint of B-B′ equal to one another and equal to the inversion center. On the other hand, for the rest of the symmetry elements as denoted in Figure 3.3 and Tables 3.3 - 3.6, A-B′ and A′-B distances are equal while A-A′ and B-B′ are not equal. The midpoints of the crossed pairs in Figure 3.3, designated as A-B′ and A′-B, are not equivalent. Since the original distance calculation does not differentiate between a vector written as A′-B′ or B′-A′, all of the distance pairs

must be calculated and their midpoints checked for agreement. After the possibility of an inversion center has been eliminated (Figure 3.4) by the initial distance equivalent checks, further tests are required to determine if one of the other types of symmetry elements is present.

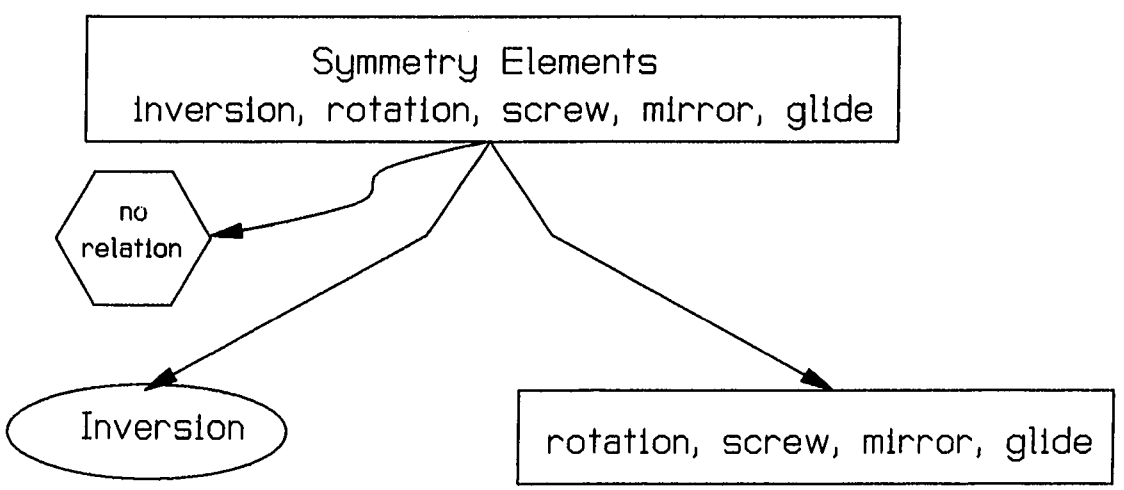

Figure 3.4. Distance equivalent test performed by SUPSYMM to determine the existence of an inversion center, other symmetry or no relationship

Projection Relationships for Symmetry Element Identification

SUPSYMM makes no assumptions regarding the symmetry elements' relationship with the crystallographic axes. A set of orthogonal axes between the two atom pairs are set up in order to eliminate any dependence of the symmetry element on a particular axis direction. The remaining tests for symmetry use this orthogonal set of axes as their basis.

V3 is set up to be perpendicular to any rotation axis or reflection plane. As shown in Figure 3.5 and Figure 3.6 and using vector addition, V3 can be calculated as follows:

$$\begin{aligned} 2 \cdot \boldsymbol{V3} &= \boldsymbol{BA} + \boldsymbol{A'B'} \\ \boldsymbol{V3} &= \frac{1}{2}(\boldsymbol{BA} + \boldsymbol{A'B'}) \end{aligned} \tag{3.2}$$

Breaking V3 into components gives

$$\begin{aligned} \boldsymbol{V3} = \frac{1}{2}[&(x_A - x_B)\boldsymbol{a} + (y_A - y_B)\boldsymbol{b} + (z_A - z_B)\boldsymbol{c}] \\ + [&(x_{B'} - x_{A'})\boldsymbol{a} + (y_{B'} - y_{A'})\boldsymbol{b} + (z_{B'} - z_{A'})\boldsymbol{c}] \end{aligned} \tag{3.3}$$

Components of B and B' are transformed according to the initial unit cell shifts required to obtain the shortest distance to A and A', respectively.

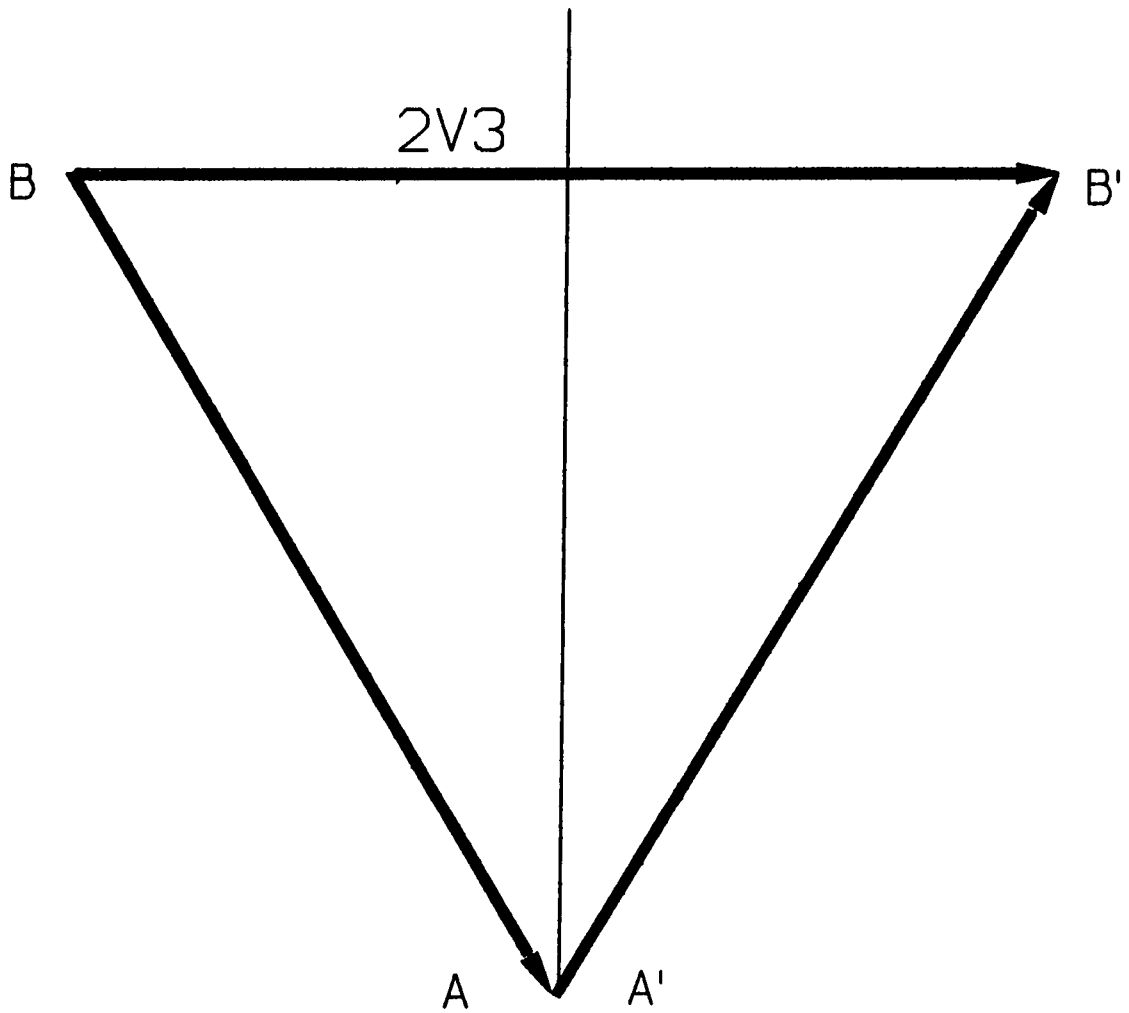

Figure 3.5. Vector basis for axis 2V3

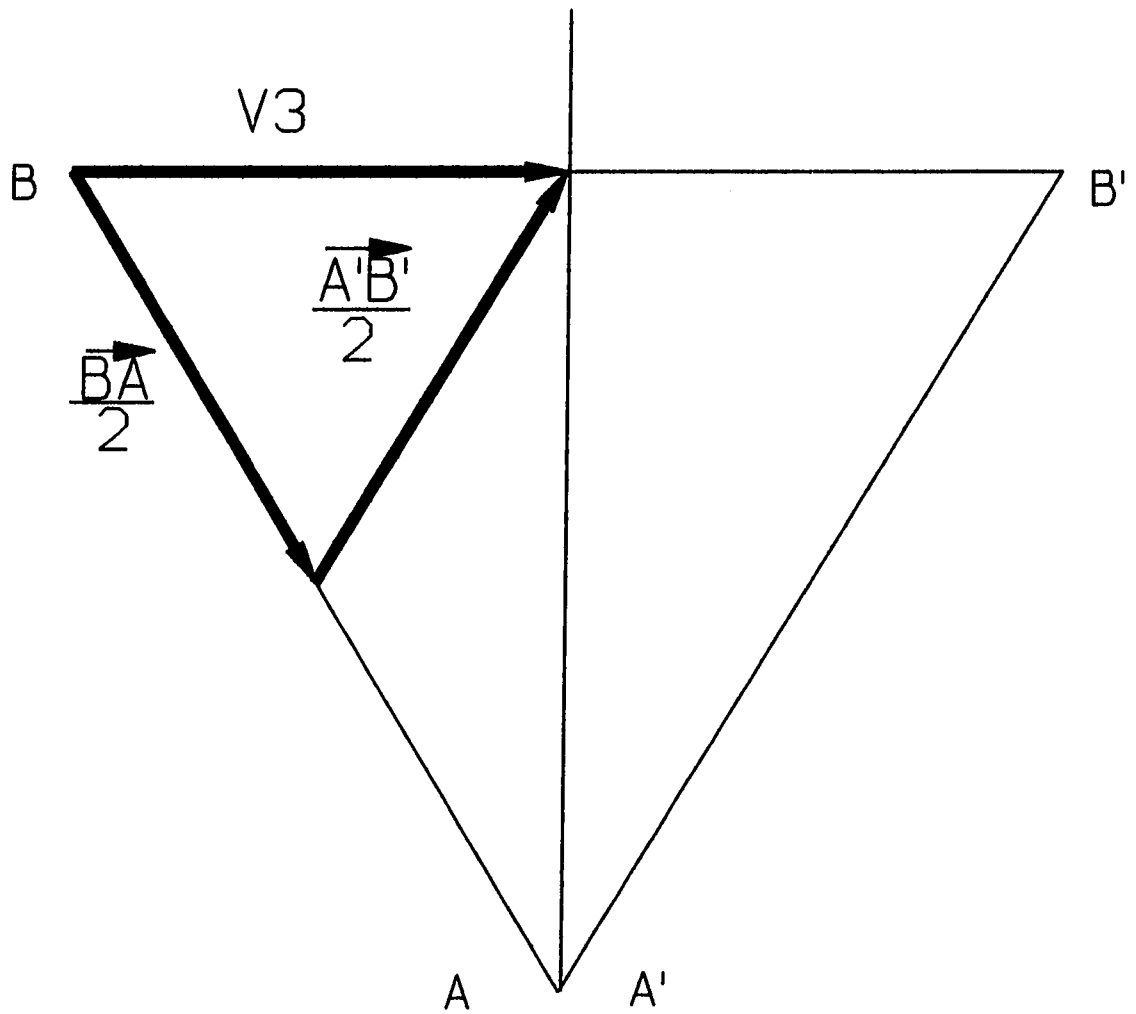

Figure 3.6. Vector basis for V3

V4 is defined such as to be perpendicular to V3 in order to obtain an orthonormal set of coordinate axes. Also by definition, V4 is set up to be contain any axis of rotation or to lie in a reflection plane. To meet these criteria, V4 is defined as

$$\begin{aligned} V4 &= AB + V3 \\ &= AB + \left[\frac{1}{2}(BA + A'B')\right] \\ &= \frac{1}{2}(AB + A'B') \end{aligned} \tag{3.4}$$

or pictured vectorily as shown in Figures 3.7 and 3.8. To complete the set of orthogonal axes, V5 must be mutually perpendicular to V3 and V4. V5 is defined by

$$\begin{aligned} V5 &= V3 \times V4 \\ &= \left[\frac{BA + A'B'}{2}\right] \times \left[\frac{AB + A'B'}{2}\right] \\ &= \frac{1}{2}(A'B' \times AB) \end{aligned} \tag{3.5}$$

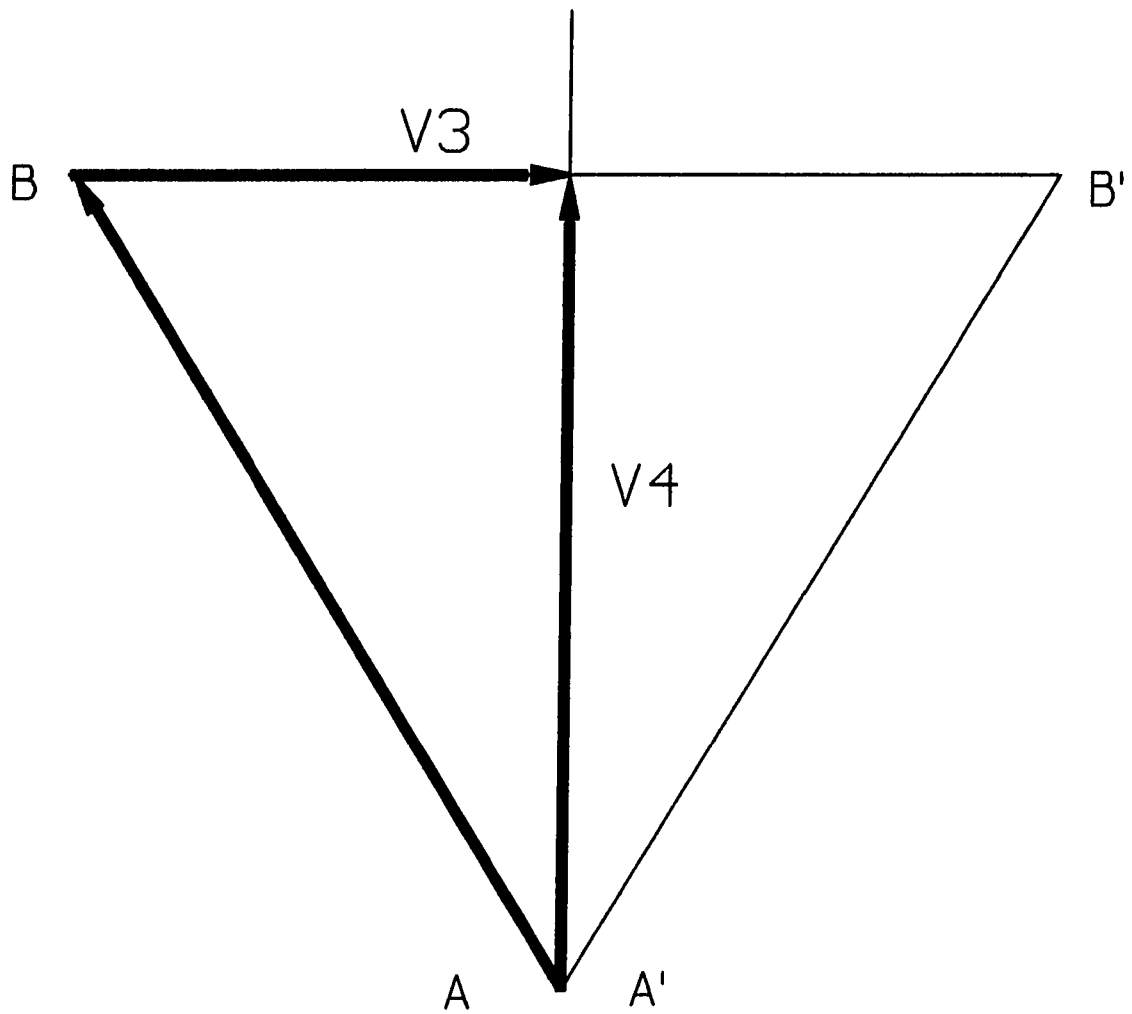

Figure 3.7. **Vector basis for V4 in terms of V3**

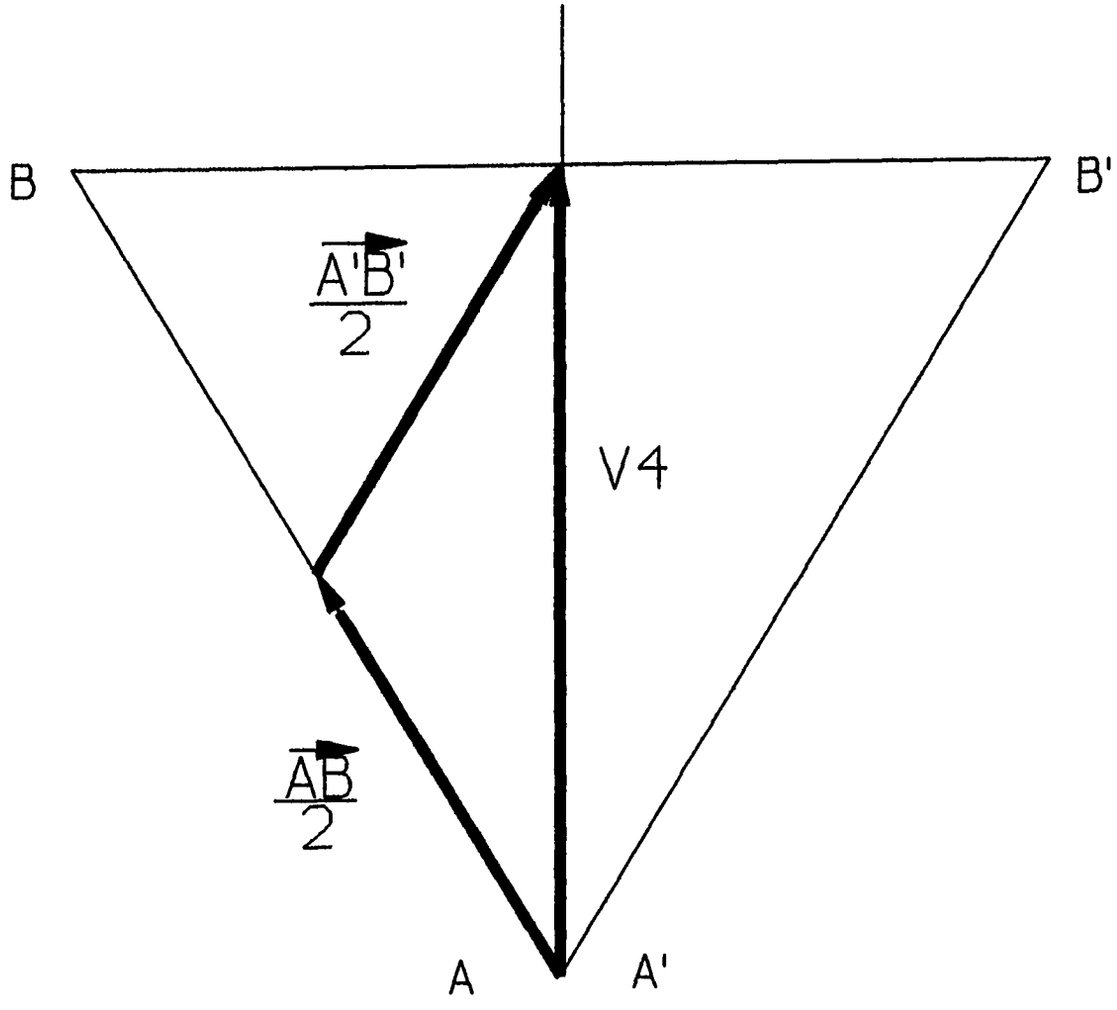

Figure 3.8. Vector basis for V4

There exist relationships between the vector pairs **AA′**, **BB′**, **AB′**, and **A′B** with the orthogonal axes **V3** and **V4** which allow for the identification of the various symmetry elements relating the vector pairs. These relationships, based on the projection of a vector pair onto one of the orthogonal axes, are outlined below.

Since the **V3**, **V4**, and **V5** axes are independent of the unit cell axes, the following cases are perfectly general. Thus, even though the following proofs use the crystallographic **b** axis as the axis of rotation and as the axis located perpendicular to the mirror plane, the proofs may be generalized to hold for these symmetry elements around other axes as well.

Since the lowest Laue symmetry which contains a mirror, glide, rotation, or screw is monoclinic (the only symmetry element available in the triclinic system is an inversion center), the most general vector product will be of the form

$$\begin{aligned} \boldsymbol{C}\cdot\boldsymbol{D} &= (x_C\boldsymbol{a}+y_C\boldsymbol{b}+z_C\boldsymbol{c}) \cdot (x_D\boldsymbol{a}+y_D\boldsymbol{b}+z_D\boldsymbol{c}) \\ &= x_Cx_Da^2+y_Cy_Db^2+z_Cz_Dc^2+(x_Cz_D+x_Dz_C)\,\boldsymbol{a}\cdot\boldsymbol{c} \qquad (3.6) \\ &= x_Cx_Da^2+y_Cy_Db^2+z_Cz_Dc^2+(x_Cz_D+x_Dz_C)\,ac\cos\beta \end{aligned}$$

Mirror plane projections

For a mirror perpendicular to the b axis, let **A** ≡ (x_A, y_A, z_A), **A′** ≡ $(x_A, -y_A, z_A)$, **B** ≡ (x_B, y_B, z_B), and **B′** ≡ $(x_B, -y_B, z_B)$, where the unit cell dimensions are omitted for simplicity and are assumed to be understood. The vector, **V3**, as defined by Equation (3.2) yields,

$$\begin{aligned} \boldsymbol{V3} &= \frac{1}{2}(\boldsymbol{BA} + \boldsymbol{A'B'}) \\ &= \frac{1}{2}[(x_A, y_A, z_A) - (x_B, y_B, z_B)] + [(x_B, -y_B, z_B) - (x_A, -y_A, z_A)] \\ &= \frac{1}{2}(0, 2y_A - 2y_B, 0) \\ &= (0, y_A - y_B, 0) \end{aligned}$$

and Equation (3.4) gives **V4** defined as

$$\begin{aligned} \boldsymbol{V4} &= \boldsymbol{AB} + \boldsymbol{V3} \\ &= (x_B - x_A, y_B - y_A, z_B - z_A) + (0, y_A - y_B, 0) \\ &= (x_B - x_A, 0, z_B - z_A) \end{aligned}$$

Using the defined vectors, **V3** and **V4**, and taking the projection of the vector **AA′** and **BB′** onto these coordinate axes yield the following relationships.

$$\boldsymbol{AA'\cdot V3} = (0,-2y_A,0)\cdot(0,y_A-y_B,0) = -2y_A(y_A-y_B)\,b^2$$

$$\boldsymbol{BB'\cdot V3} = (0,-2y_B,0)\cdot(0,y_A-y_B,0) = -2y_B(y_A-y_B)\,b^2$$

$$\therefore\ \boldsymbol{AA'\cdot V3} \neq \boldsymbol{BB'\cdot V3}$$

$$\boldsymbol{AA'\cdot V4} = (0,-2y_A,0)\cdot(x_B-x_A,0,z_B-z_A) = 0$$

$$\boldsymbol{BB'\cdot V4} = (0,-2y_B,0)\cdot(x_B-x_A,0,z_B-z_A) = 0$$

$$\therefore\ \boldsymbol{AA'\cdot V4} = \boldsymbol{BB'\cdot V4} = 0$$

Continuing with the projections of the crossed vectors **AB′** and **A′B** onto the **V3** and **V4** gives

$$\boldsymbol{AB'\cdot V3} = (x_B-x_A,-y_B-y_A,z_B-z_A)\cdot(0,y_A-y_B,0) = (y_B^2-y_A^2)\,b^2$$

$$\boldsymbol{A'B\cdot V3} = (x_B-x_A,y_B+y_A,z_B-z_A)\cdot(0,y_A-y_B,0) = (y_A^2-y_B^2)\,b^2$$

$$\therefore\ |\boldsymbol{AB'\cdot V3}| = |\boldsymbol{A'B\cdot V3}|$$

$$\boldsymbol{AB'\cdot V4} = (x_B-x_A,-y_B-y_A,z_B-z_A)\cdot(x_B-x_A,0,z_B-z_A)$$

$$= (x_B-x_A)^2a^2+(z_B-z_A)^2c^2+2(x_B-x_A)(z_B-z_A)\,accos\beta$$

$$\boldsymbol{A'B\cdot V4} = (x_B-x_A,y_B-y_A,z_B-z_A)\cdot(x_B-x_A,0,z_B-z_A)$$

$$= (x_B-x_A)^2a^2+(z_B-z_A)^2c^2+2(x_B-x_A)(z_B-z_A)\,accos\beta$$

$$\therefore\ \boldsymbol{AB'\cdot V4} = \boldsymbol{A'B\cdot V4} = |\boldsymbol{V4}|^2$$

Rotation axis projections

For the two-fold rotation about the b axis, let A ≡ (x_A, y_A, z_A), A′ ≡ $(-x_A, y_A, -z_A)$, B ≡ (x_B, y_B, z_B), and B′ ≡ $(-x_B, y_B, -z_B)$. Using the vector definition from Equations (3.2) and (3.3) gives V3 = $(x_A-x_B, 0, z_A-z_B)$ and V4 = $(0, y_B-y_A, 0)$, respectively. Projecting the vectors AA′, BB′, AB′, and A′B onto V3 and V4 generate the following relationships:

$$\begin{aligned}
\boldsymbol{AA'\cdot V3} &= (-2x_A, 0, -2z_A)\cdot(x_A-x_B, 0, z_A-z_B) \\
&= -2x_A(x_A-x_B)\,a^2 - 2z_A(z_A-z_B)\,b^2 - [2x_A(z_A-z_B) + 2z_A(x_A-x_B)]\,ac\cos\beta \\
\boldsymbol{BB'\cdot V3} &= (-2x_B, 0, -2z_B)\cdot(x_A-x_B, 0, z_A-z_B) \\
&= -2x_B(x_A-x_B)\,a^2 - 2z_B(z_A-z_B)\,b^2 - [2x_B(z_A-z_B) + 2z_B(x_A-x_B)]\,ac\cos\beta \\
&\therefore\ \boldsymbol{AA'\cdot V3 \neq BB'\cdot V3}
\end{aligned}$$

$$\begin{aligned}
\boldsymbol{AA'\cdot V4} &= (-2x_A, 0, -2z_A)\cdot(0, y_B-y_A, 0) = 0 \\
\boldsymbol{BB'\cdot V4} &= (-2x_B, 0, -2z_B)\cdot(0, y_B-y_A, 0) = 0 \\
&\therefore\ \boldsymbol{AA'\cdot V4 = BB'\cdot V4} = 0
\end{aligned}$$

$$\mathbf{AB'\cdot V3} = (-x_B-x_A, y_B-y_A, -z_B-z_A)\cdot(x_A-x_B, 0, z_A-z_B)$$

$$= (-x_B-x_A)(x_A-x_B)a^2+(-z_B-z_A)(z_A-z_B)c^2$$

$$+ [(-x_B-x_A)(z_A-z_B)+(x_A-x_B)(-z_B-z_A)]\,accos\beta$$

$$\mathbf{A'B\cdot V3} = (x_B-x_A, y_B-y_A, z_B+z_A)\cdot(x_A-x_B, 0, z_A-z_B)$$

$$= (x_B+x_A)(x_A-x_B)a^2+(z_B+z_A)(z_A-z_B)c^2$$

$$+ [(x_B+x_A)(z_A-z_B)+(x_A-x_B)(z_B+z_A)]\,accos\beta$$

$$\therefore \quad |\mathbf{AB'\cdot V3}| = |\mathbf{A'B\cdot V3}|$$

$$\mathbf{AB'\cdot V4} = (-x_B-x_A, y_B-y_A, -z_B-z_A)\cdot(0, y_B-y_A, 0) = (y_B-y_A)^2b^2$$

$$\mathbf{A'B\cdot V4} = (x_B+x_A, y_B-y_A, z_B-z_A)\cdot(0, y_B-y_A, 0) = (y_B-y_A)^2b^2$$

$$\therefore \quad \mathbf{AB'\cdot V4} = \mathbf{A'B\cdot V4} = |\mathbf{V4}|^2$$

Glide plane projections

For a c-glide perpendicular to the **b** axis, let **A** ≡ (x_A, y_A, z_A), **A'** ≡ $(x_A, -y_A, z_A+\frac{1}{2})$, **B** ≡ (x_B, y_B, z_B), and **B'** ≡ $(x_B, -y_B, z_B+\frac{1}{2})$. Using the vector definitions of **V3** and **V4** give **V3** = $(0, y_A-y_B, 0)$ and **V4** = $(x_B-x_A, 0, z_B-z_A)$. The vectors **AA'**, **BB'**, **AB'**, and **A'B** projected onto **V3** and **V4** generate the following relationships:

$$\boldsymbol{AA'\cdot V3} = (0, -2y_A, \frac{1}{2})\cdot(0, y_A-y_B, 0) = -2y_A(y_A-y_B)\,b^2$$

$$\boldsymbol{BB'\cdot V3} = (0, -2y_B, \frac{1}{2})\cdot(0, y_A-y_B, 0) = -2y_B(y_A-y_B)\,b^2$$

$$\therefore \quad \boldsymbol{AA'\cdot V3} \neq \boldsymbol{BB'\cdot V3}$$

$$\boldsymbol{AA'\cdot V4} = (0, -2y_A, \frac{1}{2})\cdot(x_B-x_A, 0, z_B-z_A) = \frac{1}{2}(z_B-z_A)\,c^2$$

$$\boldsymbol{BB'\cdot V4} = (0, -2y_B, \frac{1}{2})\cdot(x_B-x_A, 0, z_B-z_A) = \frac{1}{2}(z_B-z_A)\,c^2$$

$$\therefore \quad \boldsymbol{AA'\cdot V4} = \boldsymbol{BB'\cdot V4}$$

$$\boldsymbol{AB'\cdot V3} = (x_B-x_A, -y_B-y_A, z_B+\frac{1}{2}-z_A)\cdot(0, y_A-y_B, 0) = (y_B^2-y_A^2)\,b^2$$

$$\boldsymbol{A'B\cdot V3} = (x_B-x_A, y_B+y_A, z_B+\frac{1}{2}-z_A)\cdot(0, y_A-y_B, 0) = (y_A^2-y_B^2)\,b^2$$

$$\therefore \quad |\boldsymbol{AB'\cdot V3}| = |\boldsymbol{A'B\cdot V3}|$$

$$\mathbf{AB'\cdot V4} = (x_B-x_A, -y_B-y_A, z_B+\frac{1}{2}-z_A)\cdot(x_B-x_A, 0, z_B-z_A)$$

$$= (x_B-x_A)^2a^2+[\frac{1}{2}(z_B-z_A)+(z_B-z_A)^2]c^2$$

$$+ [(x_B-x_A)(z_B-z_A)+(x_B-x_A)(z_b+\frac{1}{2}-z_A)]accos\beta$$

$$\mathbf{A'B\cdot V4} = (x_B-x_A, y_B-y_A, z_B+\frac{1}{2}-z_A)\cdot(x_B-x_A, 0, z_B-z_A)$$

$$= (x_B-x_A)^2a^2+[-\frac{1}{2}(z_B-z_A)+(z_B-z_A)^2]c^2$$

$$+ [(x_B-x_A)(z_B-z_A)+(x_B-x_A)(z_B+\frac{1}{2}-z_A)]accos\beta$$

$$\therefore \mathbf{AB'\cdot V4} \neq \mathbf{A'B\cdot V4}$$

Screw axis projections

For the 2_1-screw rotation with rotation around and translation along the b axis, let $\mathbf{A} \equiv (x_A, y_A, z_A)$, $\mathbf{A'} \equiv (-x_A, y_A+\frac{1}{2}, -z_A)$, $\mathbf{B} \equiv (x_B, y_B, z_B)$, and $\mathbf{B'} \equiv (-x_B, y_B+\frac{1}{2}, -z_B)$. The vector definitions for V3 and V4 give $\mathbf{V3} = (x_A-x_B, 0, z_A-z_B)$ and $\mathbf{V4} = (0, y_B-y_A, 0)$. Taking the projections of the vectors $\mathbf{AA'}$, $\mathbf{BB'}$, $\mathbf{AB'}$, and $\mathbf{A'B}$ yield the following relationships:

$$\boldsymbol{AA'\cdot V3} = \left(-2x_A, \frac{1}{2}, -2z_A\right)\cdot(x_A-x_B, 0, z_A-z_B)$$

$$= -2x_A(x_A-x_B)\,a^2-2z_A(z_A-z_B)\,b^2-[2x_A(z_A-z_B)+2z_A(x_A-x_B)]\,accos\beta$$

$$\boldsymbol{BB'\cdot V3} = \left(-2x_B, \frac{1}{2}, -2z_B\right)\cdot(x_A-x_B, 0, z_A-z_B)$$

$$= -2x_B(x_A-x_B)\,a^2-2z_B(z_A-z_B)\,b^2-[2x_B(z_A-z_B)+2z_B(x_A-x_B)]\,accos\beta$$

$$\therefore\ \boldsymbol{AA'\cdot V3 \neq BB'\cdot V3}$$

$$\boldsymbol{AA'\cdot V4} = \left(-2x_A, \frac{1}{2}, -2z_A\right)\cdot(0, y_B-y_A, 0) = \frac{1}{2}(y_B-y_A)\,b^2$$

$$\boldsymbol{BB'\cdot V4} = \left(-2x_B, \frac{1}{2}, -2z_B\right)\cdot(0, y_B-y_A, 0) = \frac{1}{2}(y_B-y_A)\,b^2$$

$$\therefore\ \boldsymbol{AA'\cdot V4 = BB'\cdot V4}$$

$$\boldsymbol{AB'\cdot V3} = \left(-x_B-x_A, y_B+\frac{1}{2}-y_A, -z_B-z_A\right)\cdot(x_A-x_B, 0, z_A-z_B)$$

$$= (-x_B-x_A)\,(x_A-x_B)\,a^2+(-z_B-z_A)\,(z_A-z_B)\,c^2$$

$$+\ [(-x_B-x_A)\,(z_A-z_B)+(x_A-x_B)\,(-z_B-z_A)]\,accos\beta$$

$$\boldsymbol{A'B\cdot V3} = \left(x_B-x_A, y_B+\frac{1}{2}-y_A, z_B+z_A\right)\cdot(x_A-x_B, 0, z_A-z_B)$$

$$= (x_B+x_A)\,(x_A-x_B)\,a^2+(z_B+z_A)\,(z_A-z_B)\,c^2$$

$$+\ [(x_B+x_A)\,(z_A-z_B)+(x_A-x_B)\,(z_B+z_A)]\,accos\beta$$

$$\therefore\ \boldsymbol{|AB'\cdot V3| = |A'B\cdot V3|}$$

$$\mathbf{AB'\cdot V4} = (-x_B-x_A, y_B+\frac{1}{2}-y_A, -z_B-z_A)\cdot(0, y_B-y_A, 0)$$

$$= [\frac{1}{2}(y_B-y_A)+(y_B-y_A)^2]\,b^2$$

$$\mathbf{A'B\cdot V4} = (x_B+x_A, y_B+\frac{1}{2}-y_A, z_B-z_A)\cdot(0, y_B-y_A, 0)$$

$$= [-\frac{1}{2}(y_B-y_A)+(y_B-y_A)^2]\,b^2$$

$$\therefore \mathbf{AB'\cdot V4} \neq \mathbf{A'B\cdot V4}$$

The results of the above projection relationships are summarized in Tables 3.7 and 3.8.

Table 3.7. Comparison of projections of AA′ and BB′ onto V3 and V4 and their relationships with various symmetry elements

	|AA′ • V3|	|BB′ • V3|	|AA′ • V4|	|BB′ • V4|
mirror	α_1	β_1	0	0
2-fold	α_2	β_2	0	0
glide	α_1	β_1	ϵ_3	ϵ_3
2_1 screw	α_2	β_2	η_4	η_4

Table 3.8. Comparison of projections of **AB′** and **A′B** onto **V3** and **V4** and their relationships with various symmetry elements

	$\lvert AB' \cdot V3 \rvert$	$\lvert A'B \cdot V3 \rvert$	$\lvert AB' \cdot V4 \rvert$	$\lvert A'B \cdot V4 \rvert$
mirror	γ_1	γ_1	δ_1	δ_1
2-fold	γ_2	γ_2	δ_2	δ_2
glide	γ_1	γ_1	δ_3	δ_3'
2_1 screw	γ_2	γ_2	δ_4	δ_4'

If the atom pair does not conform to one of the above vector projection relationships, the set of atom pairs are probably unrelated. Probably here refers to the tolerance level set. If the tolerance level is too low, a symmetry relationship may be ignored. Therefore, several tolerance levels should be tried starting with a low level and gradually increasing to a higher level of tolerance.

From the projection of **AA′** and **BB′** onto **V4**, mirror and rotation symmetry can be distinguished from corresponding symmetry elements with translations (ie. glides and screws) (Figure 3.9) by noting the numerical value of the projection. For the mirror and the rotation, projection of **AA′** and **BB′** onto **V4** gives a value of zero. The glide and the screw projections yield nonzero values.

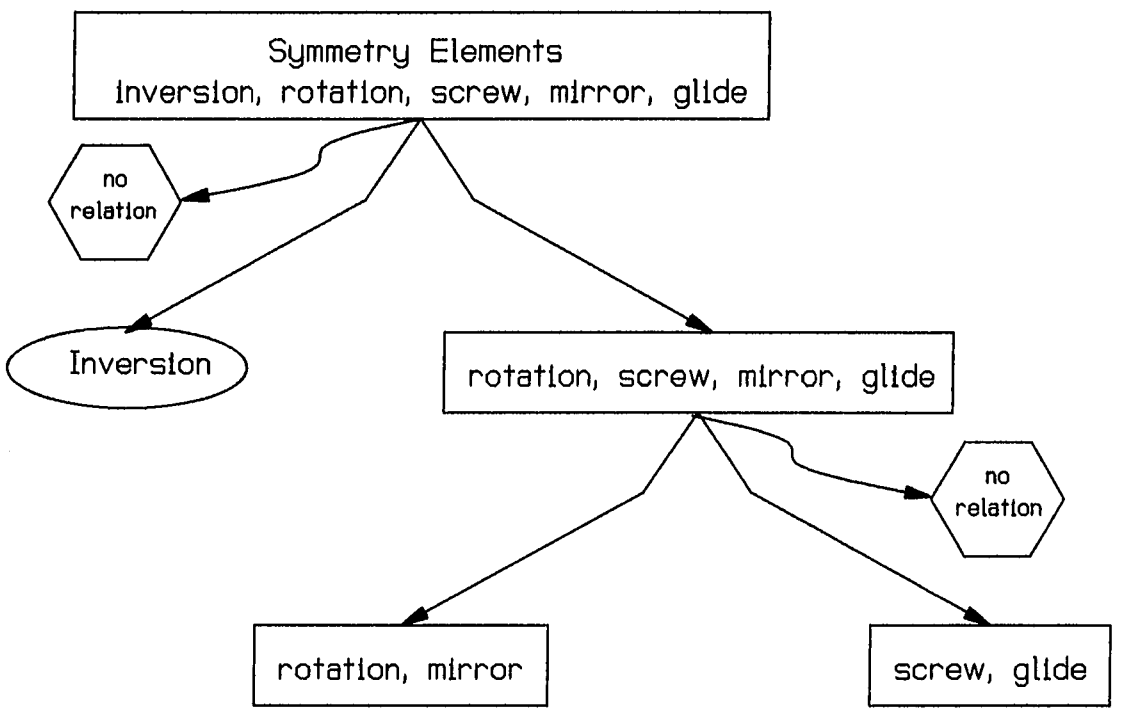

Figure 3.9. **Projection tests performed by SUPSYMM to determine translation versus non-translation symmetry elements**

Differentiation between mirror and rotation symmetry elements can be performed by noting that **AA′** can be written in terms of the orthogonal and normalized coordinates axes, **V3**, **V4**, and **V5**.

$$\mathbf{AA}' = \xi_1 \hat{V}3 + \xi_2 \hat{V}4 + \xi_3 \hat{V}4 \qquad (3.7)$$

In addition, the projection of **AA′** onto each of these orthonormal axes yields

$$\begin{aligned} \xi_1 &= \hat{V}3 \cdot \mathbf{AA}' \\ \xi_2 &= \hat{V}4 \cdot \mathbf{AA}' \\ \xi_3 &= \hat{V}5 \cdot \mathbf{AA}' \end{aligned} \qquad (3.8)$$

Inherent in the definitions of **V3**, **V4**, and **V5** is the fact that **V4** contains the axis of rotation. Therefore, if **A** is related to **A′** by a 2-fold rotation, the vector **AA′** should be perpendicular to **V4** and ξ_2 will be equal to zero. Also by definition, **V4** and **V5** describe the mirror plane. Hence, if **A** is related to **A′** by a mirror both ξ_2 and ξ_3 must equal zero. The same correlations occur for **B** and **B′**.

Because of the translations involved for screw axes and glide planes, the projections defining rotation or reflection do not hold. The ξ_2 will not equal zero for a screw and ξ_2 and

ξ_3 will not equal zero for a glide. A glide and a screw may be distinguished, however, by looking at other projections.

The effect of the translation can be negated by looking at the projection onto the V3 axis. By definition, V3 is perpendicular to any axis of rotation or plane of reflection. Therefore, the components of the dot product of the **AA'** vector and the V3 axis will reveal the requisite information. Zeroes occur when a component of **AA'** is perpendicular to a component of V3. One component equal to zero signifies a rotation axis. Two components equal to zero signifies a reflection plane.

The direction of the reflection plane and the axis of rotation for the symmetry elements can also be established based on this projection. For a 2-fold rotation or a 2_1 screw, the component of the dot product of V3 and **AA'** which is equal to zero gives the axis of rotation. The non-zero component of this same dot product yields the axis perpendicular to the reflection plane for the mirror or glide relation.

The direction of the translation for the glide plane is established using the definitions of V4 and V5. V4 and V5 are defined to contain the reflection plane. If only a mirror exists, all components of the projection of **AA'** onto either axis would yield a numerical value of zero meaning all components of **AA'** are perpendicular to V4 and V5. This can be represented by the following:

$$\mathbf{AA}' = \xi_2 \hat{V}4 + \xi_3 \hat{V}5 = 0 \qquad (3.9)$$

By vector definition in crystallographic space, Equation (3.9) can be broken down into

$$\begin{aligned} \xi_2 \hat{V}4 &= (\xi_2 \hat{V}4_x)\,\mathbf{a} + (\xi_2 \hat{V}_y)\,\mathbf{b} + \xi_2 \hat{V}4_z)\,\mathbf{c} \\ \xi_3 \hat{V}5 &= (\xi_3 \hat{V}5_x)\,\mathbf{a} + (\xi_3 \hat{V}_y)\,\mathbf{b} + (\xi_3 \hat{V}_z)\,\mathbf{c} \end{aligned} \qquad (3.10)$$

Accumulating like terms gives a numerical value for each component:

$$\begin{aligned} a\ component &\rightarrow (\xi_2 \hat{V}4_x + \xi_3 \hat{V}5_x) \\ b\ component &\rightarrow (\xi_2 \hat{V}4_y + \xi_3 \hat{V}5_y) \\ c\ component &\rightarrow (\xi_2 \hat{V}4_z + \xi_3 \hat{V}5_z) \end{aligned} \qquad (3.11)$$

If only a mirror exists, each component will add to zero. If, for example, a c-glide exists, the c components will add up to ½ while the a and b components remain zero. Both the b and the c components would add up to ½ and the a component would equal zero if an n-glide perpendicular to the a axis existed.

In general, SUPSYMM distinguishes the various symmetry elements by setting up filters based on the above distance analysis and projection tests. The overall scheme of SUPSYMM is shown is Figure 3.10.

SUPSYMM Input

SUPSYMM was designed to provide the novice crystallographer with a meaningful interpretation of a Patterson superposition map with little user intervention. To this end SUPSYMM input has been kept to a minimum. SUPSYMM requires two files to run - ALLS.CEL and SUP.PKS. Both files are created by CHES[14] and are read by SUPSYMM with no modifications required.

ALLS.CEL provides crystallographic details about the crystal. Format of ALLS.CEL is listed in Table 3.9. SUPSYMM uses only the lattice parameters and map grid spacing. SUP.PKS contains a listing of the superposition peaks. The first line of SUP.PKS contains the number of peaks in the file. The remaining lines are the x, y, z coordinates of the superposition peaks. SUPSYMM reads SUP.PKS as a free format file.

The only other input required is information about the maximum distance between peaks on which SUPSYMM performs calculations and the tolerance level to check equivalencies.

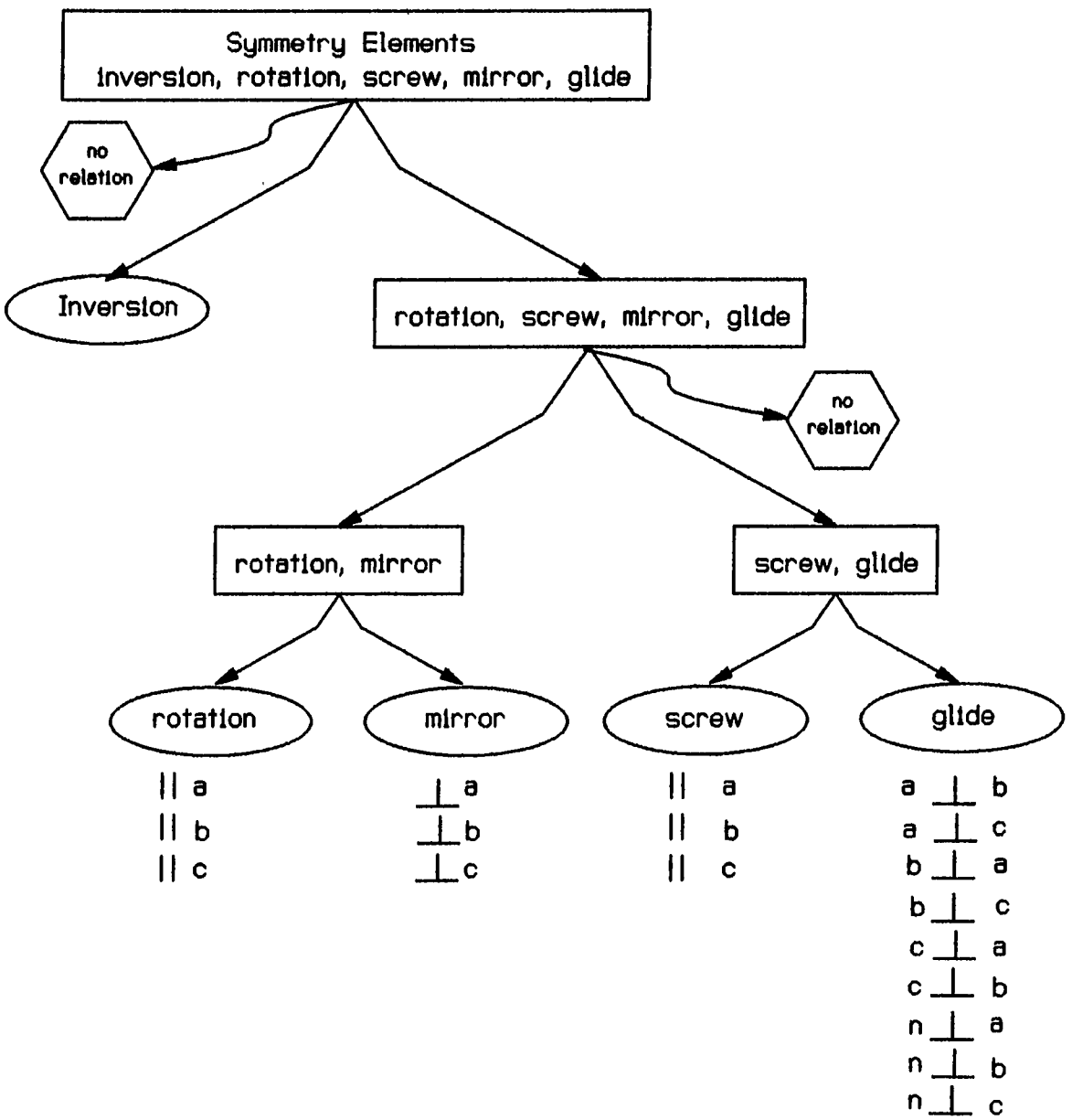

Figure 3.10. SUPSYMM scheme for the determination of symmetry elements

Table 3.9. Format for ALLS.CEL input file

Line	Variable	Format	Description
1	A,B,C,α,β,γ, Volume	6F9.6,F9.3	Lattice parameters
2	σ_A,σ_B,σ_C,σ_α,σ_β, σ_γ,Volume	6F9.6,F9.3	Parameter sigmas
3	IXGD,IYGD,IZGD	3I5	Grid spacing
	IORN	I5	Map orientation
	LAUE	I5	Laue symmetry
	NSYM	I5	# symmetry operators
	NUM,CENT,LATT,	3I5,A1	centering,lattice type
	U,D,W	3F10.5	μ,density,MW
4	SYMMETRY	A72	Symmetry operators
5	IAT	I5	Atomic numbers of all atoms in unit cell
6	IPC	I5	Number of each type of atom per unit cell

The user may use the default value or may input some maximum distance inferred from knowledge of the crystal connectivity. For example, if it is known that the maximum interatomic distance is approximately 2.3 Å, the maximum distance for calculation should be somewhat larger to allow for error in peak positions. The tolerance level is set by trial and error. The default values can be used as a first run and can be changed depending on initial results.

SUPSYMM Output

SUPSYMM calculations using distance analysis and vector projections locate peaks related by symmetry elements found in the structure. The presence of the located symmetry elements can be used to confirm the space group (if previously determined using other means such as systematic absences) or to ascertain the space group if other means failed to uniquely determine one. The fractional coordinates of peaks related to one another may be established from Harker vector analysis. More importantly, a knowledge of the symmetry elements and their positions relative to an arbitrary origin allows the conventional origin to be determined and averaged coordinates for atoms in the asymmetric unit to be found.

CHAPTER 4. PRACTICAL APPLICATIONS OF SUPSYMM

SUPSYMM uses all peaks (unless limited by the user) in the Patterson superposition map. Consequently, depending on the quality of the data, a good proportion of the atoms in the structure may be identified. The more atoms found for refinement of an initial trial model, the more likely a successful structure solution will occur especially if the structure contains a few heavy atoms which predominate the scattering. The following structures were chosen for solution by SUPSYMM due to the presence of a variety of atom types in the structure and the existence of a variety of symmetry elements. (Direct methods tend to work best when all atoms are of the same type.)

SUPSYMM Solution of $IrFe_2S_3O_5C_{24}H_{30}$

SUPSYMM was written to analyze compounds up through orthorhombic symmetry. In other words, SUPSYMM will work for compounds containing inversions, 2-fold rotations and screws, mirrors, and glide planes along or perpendicular to any axis. It could also be applied to crystals of higher symmetry using appropriate subgroup symmetry.) The compound $IrFe_2S_3O_5C_{24}H_{30}$ forms in the lowest symmetry available, triclinic. In a

triclinic system, the only symmetry operation accessible is an inversion center. This case provided a simple first test of the SUPSYMM program.

Experimental data

A black crystal provided by Robert Angelici's group (Department of Chemistry, Iowa State University) having approximate dimensions of 0.11 x 0.12 x 0.10 mm was mounted on a glass fiber. Data collection measurements were made on a Rigaku AFC6R diffractometer with graphite monochromated Mo Kα radiation. Although the crystal was a poor diffractor giving broad, ill-shaped peaks, 25 carefully centered reflections in the range $20.20 < 2\theta < 24.43^{\circ}$ revealed the crystal to have formed in the triclinic system with cell constants of a = 12.695(5), b = 13.419(6), c = 8.692(5) Å, $\alpha = 97.92$, $\beta = 103.22(5)$, and $\gamma = 83.11^{\circ}$. Complete experimental details are listed in Table 4.1.

Structure solution

Statistical analysis failed to clearly indicate a center of symmetry. Since a Patterson map automatically induces a center of symmetry, a Patterson superposition map was calculated using what looked to be an iridium-sulfur shift vector. Since the crystal was poorly diffracting and produced broad peaks only the heaviest thirty peaks were used in the SUPSYMM analysis.

Table 4.1. Experimental details for $IrFe_2S_3O_5C_{24}H_{30}$

Experimental Details	
Empirical Formula	$IrFe_2S_3O_5C_{24}H_{30}$
Formula Weight	798.59
Crystal Color, Habit	black, chunk
Crystal Dimensions (mm)	0.11 x 0.12 x 0.10
Crystal System	triclinic
Lattice Parameters	a = 12.695(5) Å
	b = 13.419(6) Å
	c = 8.692(5) Å
	α = 97.92(5)°
	β = 103.22(4)°
	γ = 83.11(4)°
Space Group	$P\bar{1}$
Z	2
Density	1.865 g/cm^3
$\mu_{(MoK\alpha)}$	59.03 cm^{-1}
Diffractometer	Rigaku AFC6R
Radiation	MoKα (λ = 0.71069)
Temperature	25°C
Scan Type	ω-2θ
$2\theta_{max}$	50.1°
Reflections Measured	5278
Reflections Observed (I>3χ(I))	1540
Variables	187
Function Minimized	Σ w ($\|F_o\| - \|F_c\|$)^2
Least-squares Weights	$4F_o^2/\sigma^2(F_o^2)$
Residuals: R; R_w	0.071; 0.079
Goodness of Fit Indicator	1.80
Maximum Peak in Final Dif. Map	1.83 e$^-$/Å^3
Minimum Peak in Final Dif. Map	-1.57 e$^-$/Å^3

Using the heaviest 30 peaks in the Patterson superposition map, SUPSYMM identified 28 inversion related atoms producing 14 atoms and their symmetry related partners (Table 4.2). The identification of an inversion center uniquely determines the space group to be $P\bar{1}$ in the triclinic system. The average position of the inversion center is located at (0.4358,0.2740,0.0982).

Table 4.2. SUPSYMM relationships and location of inversion center

peak #	peak #	x	y	z
1	2	.4360	.2732	.0970
3	4	.4356	.2735	.0978
5	6	.4358	.2735	.0971
7	8	.4361	.2742	.0975
9	10	.4359	.2732	.0966
11	12	.4358	.2735	.0972
13	15	.4366	.2732	.0990
14	17	.4356	.2744	.0984
16	18	.4336	.2771	.1018
19	27	.4368	.2730	.0995
20	22	.4348	.2734	.0997
21	24	.4353	.2764	.0978
23	28	.4362	.2740	.0971
25	26	.4364	.2732	.0988

Shifting the peak positions so that the inversion center lies at the origin allows for the selection of one symmetry unique partner to be input into a crystallographic least-squares refinement. The atoms established by SUPSYMM are listed in Table 4.3. Refinement of these 14 atoms led to an

Table 4.3. SUPSYMM positional parameters[a] for $IrFe_2S_3O_5C_{24}H_{30}$

peak #	atom	x	y	z
2	Ir	0.0640	0.2264	0.4002
3	Fe(1)	-0.2192	0.2344	0.0745
6	Fe(2)	-0.3797	0.1890	0.1675
8	S(1)	-0.2499	0.2840	0.3164
11	S(2)	-0.2334	0.0796	0.1375
9	S(3)	-0.0317	0.2015	0.1461
22	C(2A)	-0.4529	0.2998	0.1332
23	C(3)	-0.0221	0.1111	0.2811
15	C(4)	-0.1149	0.0984	0.3244
19	C(5)	-0.1608	0.1926	0.4189
18	C(6A)	-0.0615	0.3033	0.6722
25	C(7)	0.2250	0.2121	0.3410
14	C(10)	0.1684	0.3442	0.5231
13	C(11)	0.1785	0.3249	0.3734

R-factor of 14.4%. A difference electron density map revealed the remaining atoms in the structure. The final refinement, while not ideal perhaps due to high thermal motion of the outer atoms such as the carbonyl groups on the iron atoms and the methyl groups on the cyclopentyldienyl ring, led to a satisfactory R-factor of 7.1%. The final refined atom positions are listed in Table 4.4. An ORTEP drawing of the final structure is shown in Figure 4.1.

Table 4.4. Final refined positional parameters[a] for $IrFe_2S_3O_5C_{24}H_{30}$

atom	x	y	z
Ir	0.0638(2)	0.2263(2)	0.4017(2)
Fe(1)	-0.2190(5)	0.2349(5)	0.0733(8)
Fe(2)	-0.3774(5)	0.1886(6)	0.1684(8)
S(1)	-0.249(1)	0.282(1)	0.317(1)
S(2)	-0.230(1)	0.078(1)	0.136(1)
S(3)	-0.035(1)	0.198(1)	0.135(1)
O(1A)	-0.266(2)	0.164(2)	-0.265(4)
O(1B)	-0.236(3)	0.441(4)	0.008(5)
O(2A)	-0.524(3)	0.368(3)	0.109(5)
O(2B)	-0.498(3)	0.081(3)	-0.122(4)
O(2C)	-0.469(3)	0.114(3)	0.415(4)
C(1A)	-0.250(3)	0.193(3)	-0.131(5)
C(1B)	-0.229(5)	0.358(6)	0.038(7)
C(2A)	-0.463(5)	0.299(5)	0.133(6)
C(2B)	-0.456(5)	0.119(5)	-0.013(8)
C(2C)	-0.432(4)	0.145(4)	0.327(6)
C(3)	-0.011(4)	0.107(4)	0.288(5)
C(3A)	0.042(4)	0.008(4)	0.233(5)
C(4)	-0.124(3)	0.101(3)	0.323(4)
C(5)	-0.151(3)	0.190(3)	0.436(5)
C(6)	-0.046(4)	0.245(4)	0.500(6)
C(6A)	-0.062(3)	0.307(3)	0.659(5)
C(7)	0.225(3)	0.220(3)	0.340(4)
C(7A)	0.252(4)	0.171(4)	0.191(6)
C(8)	0.231(3)	0.179(4)	0.474(5)
C(8A)	0.281(4)	0.077(4)	0.514(6)
C(9)	0.207(3)	0.252(3)	0.589(5)
C(9A)	0.212(5)	0.253(5)	0.765(8)
C(10)	0.179(3)	0.346(4)	0.524(5)
C(10A)	0.151(5)	0.451(5)	0.597(7)
C(11)	0.189(3)	0.322(4)	0.375(5)
C(11A)	0.169(5)	0.401(5)	0.247(7)
C(12)	0.462(8)	0.456(6)	0.53(1)
C(13)	0.535(7)	0.396(5)	0.635(9)
C(14)	0.474(5)	0.331(5)	0.695(9)

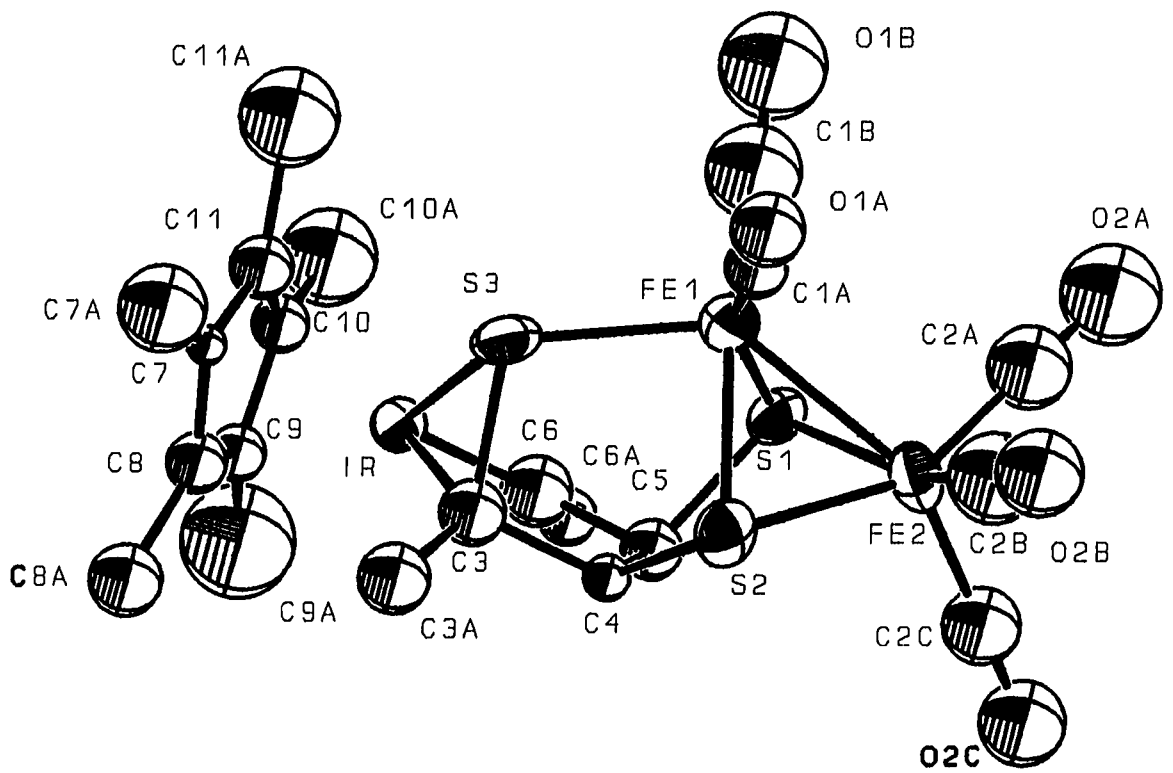

Figure 4.1. ORTEP drawing of $IrFe_2S_3O_5C_{24}H_{30}$

SUPSYMM Solution of $IrCl_2SC_{22}H_{23}$[15]

SUPSYMM was written primarily for the interpretation of Patterson superposition maps. However, since SUPSYMM looks for relationships between peaks, the origin of the peaks (whether from a Patterson map, Patterson superposition map, or electron density map) is of no importance. The $IrCl_2SC_{22}H_{23}$ crystal used SUPSYMM to search for a possible symmetry relationship between the two molecules thought to form in the asymmetric unit.

Experimental data

An orange crystal provided by Robert Angelici's group (Department of Chemistry, Iowa State University) having approximate dimensions of 0.415 x 0.320 x 0.39 mm was mounted on a glass fiber. Data collection measurements were made on a Rigaku AFC6R diffractometer with graphite monochromated Mo Kα radiation. Using setting angles of 15 carefully centered reflections in the range $12.16 < 2\theta < 15.33^\circ$, the crystal was found to have formed in the monoclinic system with cell constants of a = 16.009(5), b = 7.515(5), c = 17.125(4) Å, and $\beta = 92.70(2)^\circ$. Complete experimental details are listed in Table 4.5.

Table 4.5. Experimental details for $IrCl_2SC_{22}H_{23}$

Experimental Details	
Empirical Formula	$IrCl_2SC_{22}H_{23}$
Formula Weight	582.61
Crystal Color, Habit	orange, rectangular
Crystal Dimensions (mm)	0.415 x 0.320 x 0.39
Crystal System	monoclinic
Lattice Parameters	a = 16.009(5) Å
	b = 7.515(5) Å
	c = 17.125(4) Å
	β = 92.70(2)°
Space Group	$P2_1/c$
Z	4
Density	1.880 g/cm^3
$\mu_{(MoK\alpha)}$	68.29 cm^{-1}
Diffractometer	Rigaku AFC6R
Radiation	MoKα (λ = 0.71069)
Temperature	25°C
Scan Type	ω-2θ
$2\theta_{max}$	50.1°
Reflections Measured	4084
Reflections Observed (I>3χ(I))	3085
Variables	268
Function Minimized	Σ w ($\|F_o\| - \|F_c\|$)^2
Least-squares Weights	$4F_o^2/\sigma^2(F_o^2)$
Residuals: R; R_w	0.0298;0.0428
Goodness of Fit Indicator	2.08
Maximum Peak in Final Dif. Map	1.34 e$^-$/Å^3
Minimum Peak in Final Dif. Map	-0.96 e$^-$/Å^3

Structure solution

The systematic absences of:

h0l: l ≠ 2n

00l: l ≠ 2n

clearly indicated the presence of a c-glide perpendicular to the b axis. Unclear, however, was whether extinctions were present in the 0k0 direction. The 0k0 reflections with k = 2n were for the most part very large. Some of the 0k0 reflections with k ≠ 2n were extinct but some clearly had some intensity. With this uncertainty, the acentric space group Pc which has only the above listed extinctions was used for structure solution and refinement. The number of molecules per unit cell was four which leaves two molecules per asymmetric unit. The coordinates of the two molecules in the asymmetric unit for the solution in the Pc space group are listed in Table 4.6. The refinement proceeded to yield a satisfactory residual of 4.3%. When solving any crystal with more than one molecule per unit cell, a check for additional symmetry is standard procedure. The R-factor usually gives an obvious indication as to when a symmetry element is missing (ie. the wrong space group is used). In this case, however, neither the R-factor nor the systematic absences furnished such evidence.

Unfortunately, this is not an uncommon occurrence. Many structures have been published with the wrong space group

Table 4.6. Positional[a] parameters for $IrCl_2SC_{22}H_{23}$ for the two molecules in the asymmetric unit for solution in the Pc space group

atom	x	y	z	atom	x	y	z
IR1	0.0000	0.0870	0.0000	IR2	0.4731	0.4106	0.0201
CL1A	-0.0872	0.2065	0.0945	CL2A	0.3570	0.2897	-0.0542
CL1B	0.1203	0.2062	0.0709	CL2B	0.5647	0.2881	-0.0758
S1	-0.0045	0.3841	-0.0459	S2	0.4813	0.1128	0.0675
C1	-0.0999	0.4284	-0.1094	C1*	0.4191	0.0602	0.1453
C2	-0.1820	0.4053	-0.0926	C2*	0.3315	0.0721	0.1425
C3	-0.2407	0.4576	-0.1344	C3*	0.2845	0.0303	0.2012
C4	-0.2198	0.5152	-0.2058	C4*	0.3280	-0.0164	0.2681
C5	-0.1325	0.5392	-0.2384	C5*	0.4147	-0.0359	0.2756
C6	-0.0679	0.4920	-0.1799	C6*	0.4645	0.0082	0.2082
C7	0.0227	0.4898	-0.1928	C7*	0.5546	0.0108	0.2009
C8	0.0584	0.5465	-0.2558	C8*	0.6160	-0.0344	0.2554
C9	0.1453	0.5276	-0.2567	C9*	0.6945	-0.0192	0.2404
C10	0.1901	0.4454	-0.1903	C10*	0.7142	0.0502	0.1686
C11	0.1495	0.4006	-0.1197	C11*	0.6493	0.0880	0.1040
C12	0.0653	0.4153	-0.1233	C12*	0.5661	0.0713	0.1275
C13	-0.0872	-0.1081	-0.0464	C13*	0.5542	0.6049	0.0749
C13A	-0.1786	-0.0966	-0.0538	C13A	0.6492	0.5866	0.0911
C14	-0.0265	-0.1819	0.0150	C14*	0.5243	0.6884	0.0075
C14A	-0.0852	-0.2525	0.0812	C14A	0.5433	0.7661	-0.0694
C15	0.0438	-0.1830	0.0016	C15*	0.4196	0.6773	0.0191
C15A	0.1130	-0.2547	0.0583	C15A	0.3531	0.7424	-0.0291
C16	0.0537	-0.0938	-0.0808	C16*	0.4124	0.6033	0.0902
C16A	0.1330	-0.0791	-0.1201	C16A	0.3286	0.5744	0.1249
C17	-0.0316	-0.0590	-0.1070	C17*	0.4890	0.5604	0.1276
C17A	-0.0542	0.0117	-0.1865	C17A	0.5028	0.4841	0.2088

[a]Positional parameters are given as fractions of the unit cell.information.

The coordinates of the two molecules in the asymmetric unit were input into SUPSYMM. SUPSYMM indicated there was indeed a symmetry relationship between the two molecules. An inversion was identified at the (x,y,z) coordinates (0.236, 0.248, 0.010). Adding an inversion center to the space group Pc switches the space group to $P2_1/c$ and eliminates one of the molecules per asymmetric unit. (Looking at the 0k0 reflections and using hindsight, the k ≠ 2n reflections which showed some intensity were probably caused by overlap of the large k = 2n peaks.) After conversion of the coordinates according to the inversion center, refinement in the $P2_1/c$ space group yielded an improved residual of 2.98%. Final refinement results are listed in Table 4.7 and Figure 4.2.

SUPSYMM Solution of $[FeP_2OC_{28}H_{29}]I^{26}$

The crystal $[FeP_2OC_{28}H_{29}]I$ provided a more complicated test of SUPSYMM than the previous examples. The crystal formed in the space group $P2_1/c$ which has one of each type of symmetry element: an inversion center, a screw axis, and a glide plane.

Experimental data

A brown crystal provided by John Nelson's group (Department of Chemistry, University of Nevada - Reno) having

Table 4.7. Final refined positional parameters for $IrCl_2SC_{22}H_{23}$ in the $P2_1/c$ space group

atom	x	y	z
Ir	0.23662(2)[a]	0.16184(3)	0.01006(1)
Cl(1)	0.1183(1)	0.0415(3)	-0.0627(1)
Cl(2)	0.3263(1)	0.0411(3)	-0.0851(1)
S	0.2430(1)	-0.1356(2)	0.0568(1)
C(1)	0.1768(4)	-0.1779(8)	0.1344(4)
C(2)	0.0906(5)	-0.161(1)	0.1307(4)
C(3)	0.0476(5)	-0.207(1)	0.1960(5)
C(4)	0.0913(5)	-0.274(1)	0.2627(5)
C(5)	0.1776(5)	-0.291(1)	0.2652(4)
C(6)	0.2208(4)	-0.241(1)	0.2007(4)
C(7)	0.3110(5)	-0.240(1)	0.1908(4)
C(8)	0.3743(5)	-0.288(1)	0.2461(5)
C(9)	0.4567(5)	-0.268(1)	0.2248(5)
C(10)	0.4765(5)	-0.204(1)	0.1530(5)
C(11)	0.4146(5)	-0.160(1)	0.0973(5)
C(12)	0.3329(5)	-0.1775(8)	0.1184(4)
C(13)	0.2594(5)	0.309(1)	0.1173(4)
C(13A)	0.2800(7)	0.237(1)	0.1974(5)
C(14)	0.3201(5)	0.3562(9)	0.0613(5)
C(14A)	0.4143(6)	0.344(1)	0.0721(6)
C(15)	0.2739(5)	0.436(1)	-0.0036(4)
C(15A)	0.3140(6)	0.510(1)	-0.0752(5)
C(16)	0.1892(5)	0.4299(9)	0.0085(4)
C(16A)	0.1209(6)	0.500(1)	-0.0447(6)
C(17)	0.1782(5)	0.3487(9)	0.0840(5)
C(17A)	0.0981(6)	0.327(1)	0.1230(6)

[a] Estimated standard deviations in the least significant are given in parentheses.

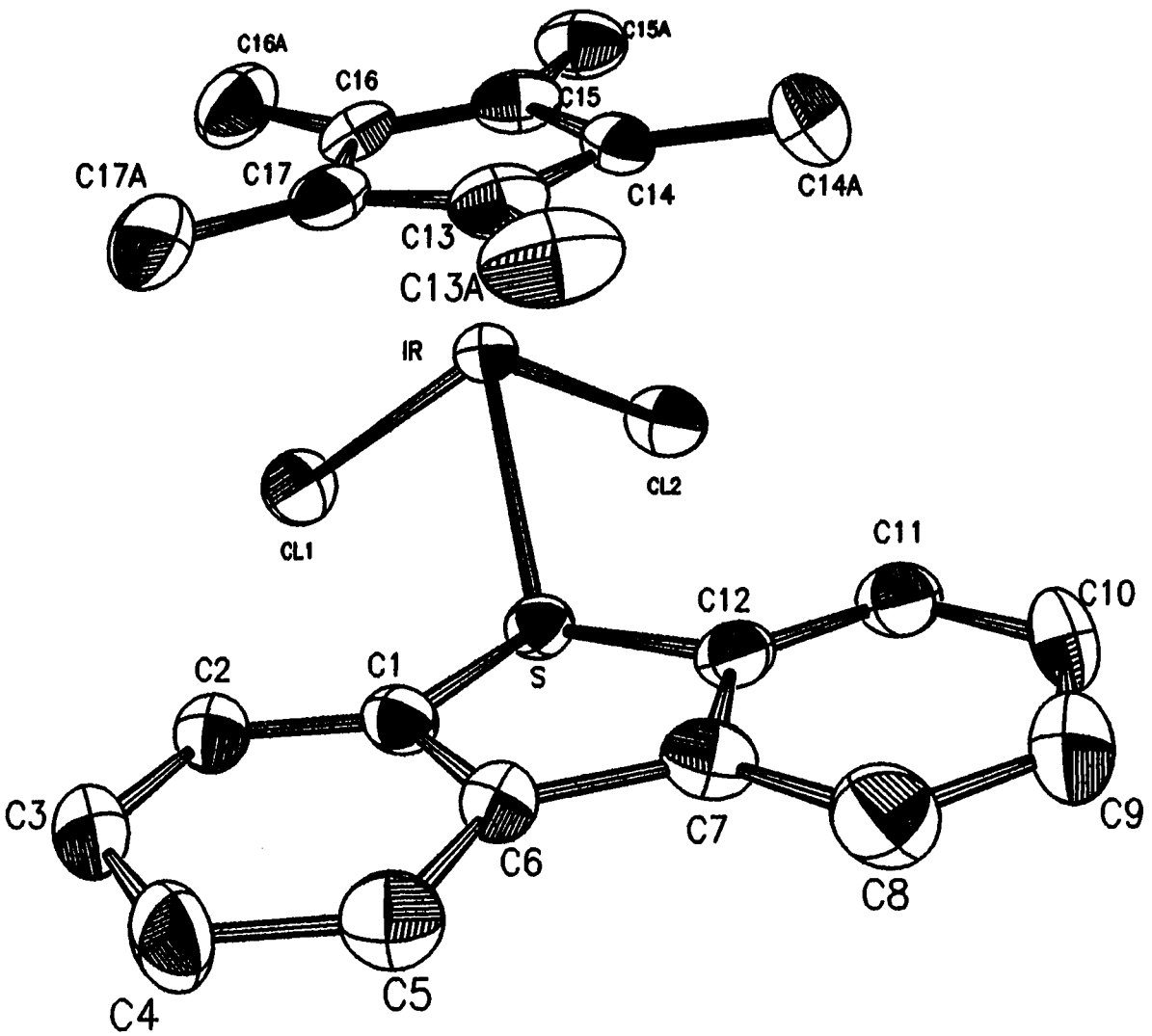

Figure 4.2. ORTEP drawing of $IrCl_2SC_{22}H_{23}$ after final refinement in space group $P2_1/c$

approximate dimensions of 0.10 x 0.11 x 0.13 mm was mounted on a glass fiber. Data collection measurements were made on a Rigaku AFC6R diffractometer with graphite monochromated Mo Kα radiation. Using setting angles of 25 carefully centered refections in the range $13.13 < 2\theta < 39.91^{\circ}$, the crystal was found to have formed in the monoclinic system with cell constants of a = 12.542(4), b = 11.488(5), c = 19.350(3) Å, and $\beta = 108.22(2)^{\circ}$. Complete experimental details are listed in Table 4.8.

Structure solution

Based on the clear systematic absences of:

$$h0l: \quad l \neq 2n$$
$$0k0: \quad k \neq 2n$$

packing considerations, a statistical analysis of intensity distribution, the space group was uniquely determined to be $P2_1/c$. The presence of the "heavy" atom, iridium, in the predominantly light molecule made this crystal a likely candidate for Patterson/Patterson superposition analysis.

A Patterson superposition map was calculated using a weighted Fe-C shift vector. The heaviest 100 peaks in the Patterson superposition map were used as input to SUPSYMM. Using tolerances varying from .01 to .1, the relationships between the peaks outlined in Table 4.9 were identified.

Table 4.8. Experimental details for $[FeP_2OC_{28}H_{29}]I$

Experimental Details	
Empirical Formula	$[FeP_2OC_{28}H_{29}]I$
Formula Weight	626.24
Crystal Color, Habit	brown, cube
Crystal Dimensions (mm)	0.10 x 0.11 x 0.13
Crystal System	monoclinic
Lattice Parameters	a = 12.542(4) Å
	b = 11.488(5) Å
	c = 19.350(3) Å
	ß = 108.22°
Space Group	$P2_1/c$
Z	4
Density	1.571 g/cm³
$\mu_{(MoK\alpha)}$	18.59 cm⁻¹
Diffractometer	Rigaku AFC6R
Radiation	MoKα (λ = 0.71069)
Temperature	25°C
Scan Type	ω
$2\theta_{max}$	50.1°
Reflections Measured	5176
Reflections Observed (I>3χ(I))	2831
Variables	415
Function Minimized	$\Sigma\ w\ (\|F_o\| - \|F_c\|)^2$
Least-squares Weights	$4F_o^2/\sigma^2(F_o^2)$
Residuals: R; R_w	0.043; 0.047
Goodness of Fit Indicator	1.57
Maximum Peak in Final Dif. Map	0.98 e⁻/Å³
Minimum Peak in Final Dif. Map	-0.63 e⁻/Å³

Table 4.9. SUPSYMM peak relationships for $[FeP_2OC_{28}H_{29}]I$

peak #	peak #	peak #	peak #	atom
1	2	5	8	I
3	6	4	7	Fe
9	15	10	14	P1
11	16	12	13	P2
17	18	24	21	C1A
19	44	26	69	C13
20	36	28	48	C11
22	51	42	31	O
23	45	67	-	C2D
25	27	43	61	C5
32	63	64	83	C8
33	40	35	-	C2A
38	47	37	39	C1B

Columns 1 and 3 are related to columns 2 and 4, respectively, by an inversion center located at (0.2926,0.1414,0.1570). SUPSYMM also identified peaks related by a 2_11 screw and a c-glide confirming the space group $P2_1/c$. The peaks listed in Table 4.9 are related as shown in Figure 4.3.

Least-squares refinement of the 14 atoms located by SUPSYMM yielded a residual of 23.8%. Difference electron density map calculations identified the remaining atoms in the structure. Refinement of the entire structure lead to a final residual of 4.3%. An ORTEP drawing after final refinement is shown in Figure 4.4.

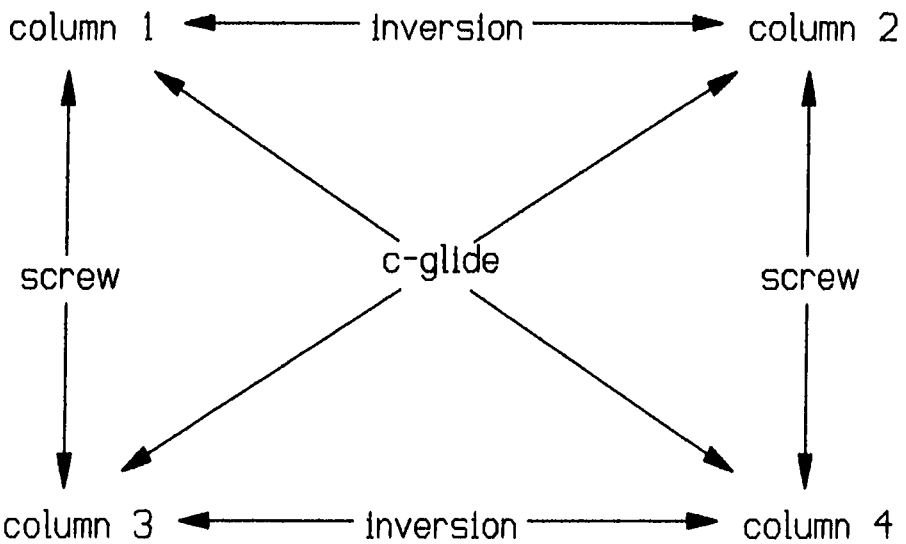

Figure 4.3. Relationships between columns in Table 4.9

SUPSYMM Solution of $Ru_2Cl_4SOC_{32}H_{32}$[17]

The crystals of $Ru_2Cl_4SOC_{32}H_{32}$ though well-formed with sharp faces were poor diffractors giving very broad peaks and asymmetric background counts. Because of the broad peaks, selection of the coordinates of the peak center was ambiguous in many cases. Therefore, this crystal presented a challenge as to whether a method based on prescribed tolerances would still give satisfactory results when the quality of the data is poor.

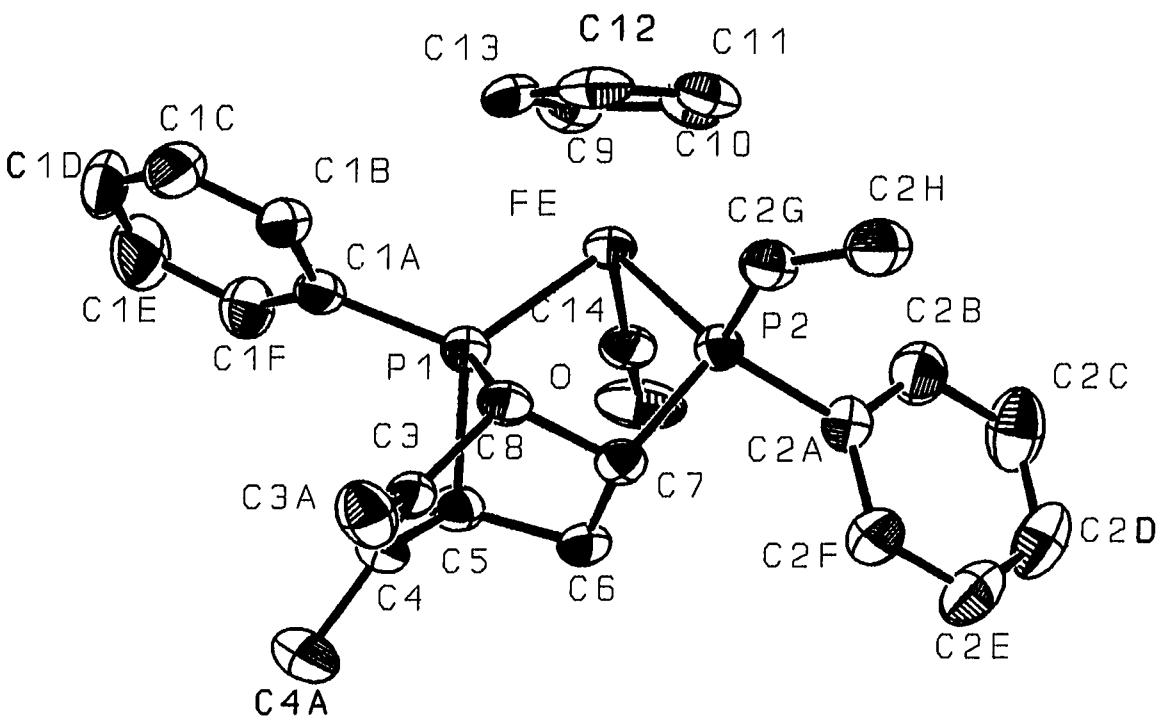

Figure 4.4. ORTEP drawing of $[FeP_2OC_{28}H_{29}]I$

Experimental data

A brown, rectangle-shaped crystal of $Ru_2Cl_4SOC_{32}H_{32}$ provided by Robert Angelici's group (Department of Chemistry, Iowa State University) having approximate dimensions of 0.200 x 0.300 x 0.300 mm was mounted on a glass fiber. Data collection measurements were made on a Rigaku AFC6R diffractometer with graphite monochromated Mo Kα radiation. Using setting angles of 15 centered reflections in the range38.17 < 2θ < 39.25°, the crystal was found to have formed in the monoclinic system with cell constants of a = 9.16(2), b = 16.8(1), c = 10.75(6) Å, and ß = 97.1(4)°. Complete experimental details are listed in Table 4.10.

Structure solution

The space group was determined to be $P2_1/n$ based on the systematic absences of:

h0l: h+l ≠ 2n

0k0: k ≠ 2n

A Patterson superposition map was calculated using a weighted Ru-C shift vector. Due to the large breadth of the peaks, only the largest 40 superposition peaks were input into SUPSYMM for analysis.

SUPSYMM identified an inversion center located at (0.0472,0.0937,0.0797). In addition, peaks related by the

Table 4.10. Experimental details for $Ru_2Cl_4SOC_{32}H_{38}$

Experimental Details	
Empirical Formula	$Ru_2Cl_4SOC_{32}H_{38}$
Formula Weight	814.66
Crystal Color, Habit	brown, rectangular
Crystal Dimensions (mm)	0.200 x 0.300 x 0.300
Crystal System	monoclinic
Lattice Parameters	a = 9.16(2) Å
	b = 16.8(1) Å
	c = 10.75(2) Å
	ß = 97.1(2)°
Space Group	$P2_1/n$
Z	2
Density	1.650 g/cm³
$\mu_{(MoK\alpha)}$	13.19 cm⁻¹
Diffractometer	Rigaku AFC6R
Radiation	MoKα (λ = 0.71069)
Temperature	25°C
Scan Type	ω-2θ
$2\theta_{max}$	50.1°
Reflections Measured	3239
Reflections Observed (I>3χ(I))	1347
Variables	183
Function Minimized	Σ w ($\|F_o\| - \|F_c\|$)²
Least-squares Weights	$4F_o^2/\sigma^2(F_o^2)$
Residuals: R; R_w	0.089; 0.094
Goodness of Fit Indicator	2.62
Maximum Peak in Final Dif. Map	2.08 e⁻/Å³
Minimum Peak in Final Dif. Map	-1.72 e⁻/Å³

screw axis and n-glide were identified and, thereby, verifying the selected space group. Tabulated results of the SUPSYMM output are shown in Table 4.11. The relationships between the columns are outlined in Figure 4.5.

Even though data quality was undeniably poor, tolerance levels in SUPSYMM were able to be set at such levels as to distinguish meaningful relationships between peaks. SUPSYMM was able, even with the poor data, to identify not only the heavy atoms but the oxygen atom located on an inversion center and two carbon atoms.

The refinement of this molecule was poor as expected. The molecule formed as a dimer with two ruthenium atoms connected by an oxygen atom which resides at the inversion center. Therefore, half of the dimer is generated by symmetry. A slightly disordered dibenzothiophene molecule is also present in the cell between the ruthenium dimers also contributing to the poor refinement. With only the atoms found by as SUPSYMM input into a least-squares refinement, the R-factor was 23.3%. The final R-factor was 8.9%. An ORTEP drawing of the final structure is shown in Figure 4.6.

Table 4.11. SUPSYMM peak relationship of $Ru_2Cl_4SOC_{32}H_{38}$

peak #	peak #	peak #	peak #	atom
1	2	4	3	Ru
5	7	8	6	Cl1
9	10	11	12	Cl2
13	14	15	16	S
19	28	--	--	O
18	20	24	33	C16
22	25	38	29	C15

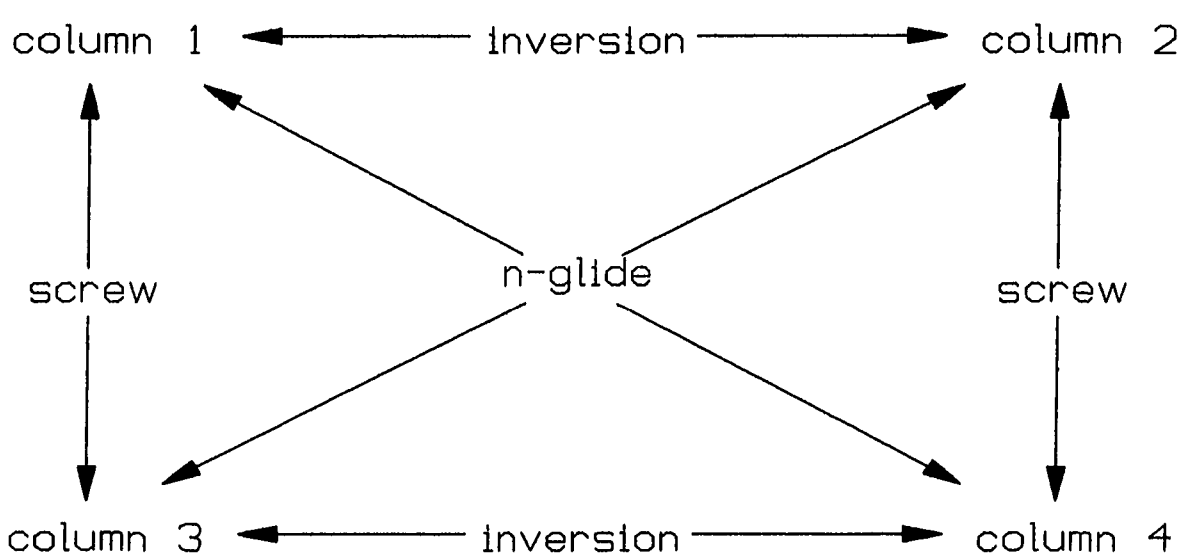

Figure 4.5. Relationships between columns in Table 4.11

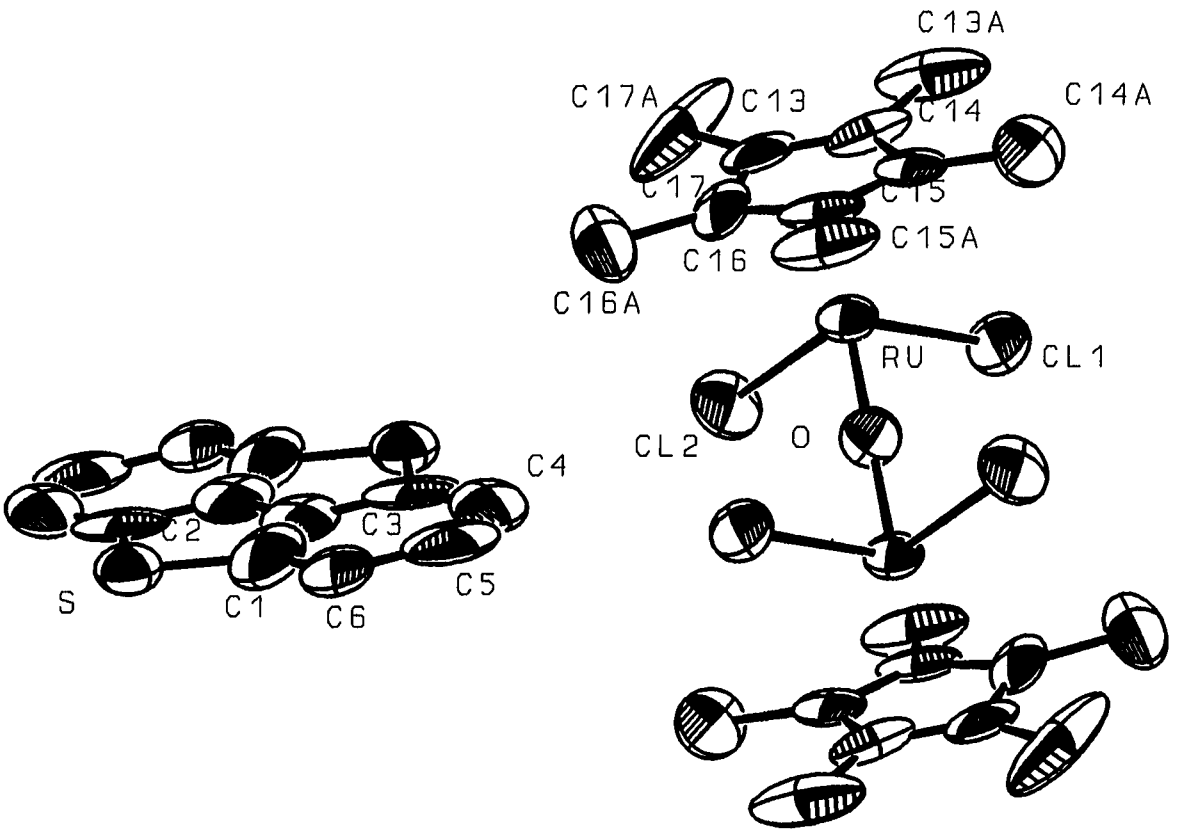

Figure 4.6. ORTEP drawing of $Ru_2Cl_4SOC_{32}H_{38}$

CHAPTER 5. COMBINING MOLECULAR MECHANICS AND CRYSTALLOGRAPHIC TECHNIQUES

As illustrated in previous chapters, Patterson and Patterson superposition methods perform best when the structure contains at least one heavy atom. On the other hand, molecular mechanics techniques rely on energy minimization approaches most widely employed with hydrocarbon structures since the most extensive and well tested empirical constants used in the energy minimizations have been accumulated for such light atoms. Utilizing the strengths of both techniques to pursue the solution of a crystal structure is the focus of this chapter.

The field of molecular mechanics has progressed to the point that applications of the techniques have expanded from such classical areas as structural and conformational study of hydrocarbons[18,19] to diverse areas such as the prediction of the rates and stereochemistries of selected chemical reactions.[20,21] While the method used in this research which combines molecular mechanics and crystallographic methods does not attempt to modify molecular mechanics approaches, it is important to know something of the pitfalls and limitations of force field methods and methods for geometry optimization.

The Basics of Molecular Mechanics

The basic ideas behind molecular mechanics or the "force field" method can be traced back to D. H. Andrews[22]. He noted that in simple cases there are forces acting on molecules that adjust their geometries such that the bonds take up some "natural" length and angle. In addition, strained systems contort in predictable ways and the strain energies can be calculated using van der Waals potential functions. It was not until 1946 that these basic concepts were put to use to rationalize certain properties involving geometries and energies of molecules.[23,24,25]

Molecular mechanics is an empirical method based on experimental data that is an alternative strategy to quantum mechanical approaches for the calculation of molecular geometry and energy. Quantum mechanics or <u>ab initio</u> methods are the obvious tool for calculating molecular properties since they can calculate exact geometry and energy of any molecule or fragment and need no experimental information concerning the system. However, the complicated nature of quantum mechanical calculations makes them computationally expensive, time-consuming and difficult to carry out for general applications.

If a system of particles is assumed to be held together by classical forces, the energy differences between molecular

systems may be estimated by classical mechanical means by assuming there exists a set of potential functions which are of the form of the classical equations of motion, thus avoiding quantum mechanical treatments. These sets of potential functions, or force fields, contain adjustable parameters that are optimized to obtain the best fit of calculated and experimental properties of the molecules. There is no limit to the equations and parameters which are necessary except that those chosen must duplicate experimental data; one also strives to find a set which is as transferable as possible from one molecular system to another.

Molecular geometries may be defined by four types of structural parameters: bond lengths, bond angles, torsional angles, and nonbonded (ie. van der Waals) interactions. These parameters give a simple molecular mechanics force field made up of these four components:

$$V = \Sigma V_{stretch} + \Sigma V_{bend} + \Sigma V_{torsion} + \Sigma V_{VDW} \qquad (5.1)$$

where the sums extend over all bonds, bond angles, torsion angles, and nonbonded interactions between all atoms not bound to each other or to a common atom. Such force fields can give reasonable approximations to geometry and energy differences. To better reproduce experimental data, a set of equations is usually assumed and the parameters involved are optimized.

The structure of the molecule will correspond to that geometry where the energy, so defined, is at a minimum. Therefore, in principle, taking the derivative of equation 5.1 with respect to each of the degrees of freedom of the molecule and finding where those derivatives are simultaneously equal to zero gives the minimum energy.

Energy minimization is carried out using an iterative geometry optimization approach where the minimum energy obtained will depend on the starting geometry of the optimization. No known general method of minimization i.e. steepest descent, Newton-Raphson, ..., finds the global energy minimum; what are found are local minima. An important point to note here is that these minimizations based on first derivatives do not strictly speaking locate minima, they locate extrema on a potential energy surface. Thus, since such procedures may lead to saddlepoints instead of minima, careful selection of starting configurations must be taken and results should be examined closely.

PCMODEL

A number of computer programs exist for molecular mechanics calculations. These programs employ different force fields utilizing different parameters and minimization techniques. The molecular mechanics software, PCMODEL, was

selected for use in the following geometry optimization of test structures. PCMODEL uses the MMX force field[26] which is a force field that extends and improves upon the widely used MM2 force field of N. L. Allinger[27]. MM2 was designed to primarily handle organic molecules; MMX handles such functional groups as radicals, cations, and anions which are not handled in MM2. The improvements employed in MMX which made PCMODEL attractive for combining with crystallographic techniques was its capacity to handle an increased number of atom types including light transition metals and its ability to accept crystallographic atomic positions as a starting basis.

MMXRAY Procedure

Patterson superposition techniques such as SUPSYMM can usually provide at least the heavy atom positions. In large organometallic complexes, however, these heavy atoms alone may not be enough to phase things properly to readily reveal the complete structure. In such cases alternative means of structure solution must be implemented.

Using the positions of the heavy atoms as a starting basis, molecular mechanics can be used to model the rest of the structure. This is accomplished by inputting the known atom positions and fixing their interatomic distances which allows them to act as anchor points. The lighter atoms are

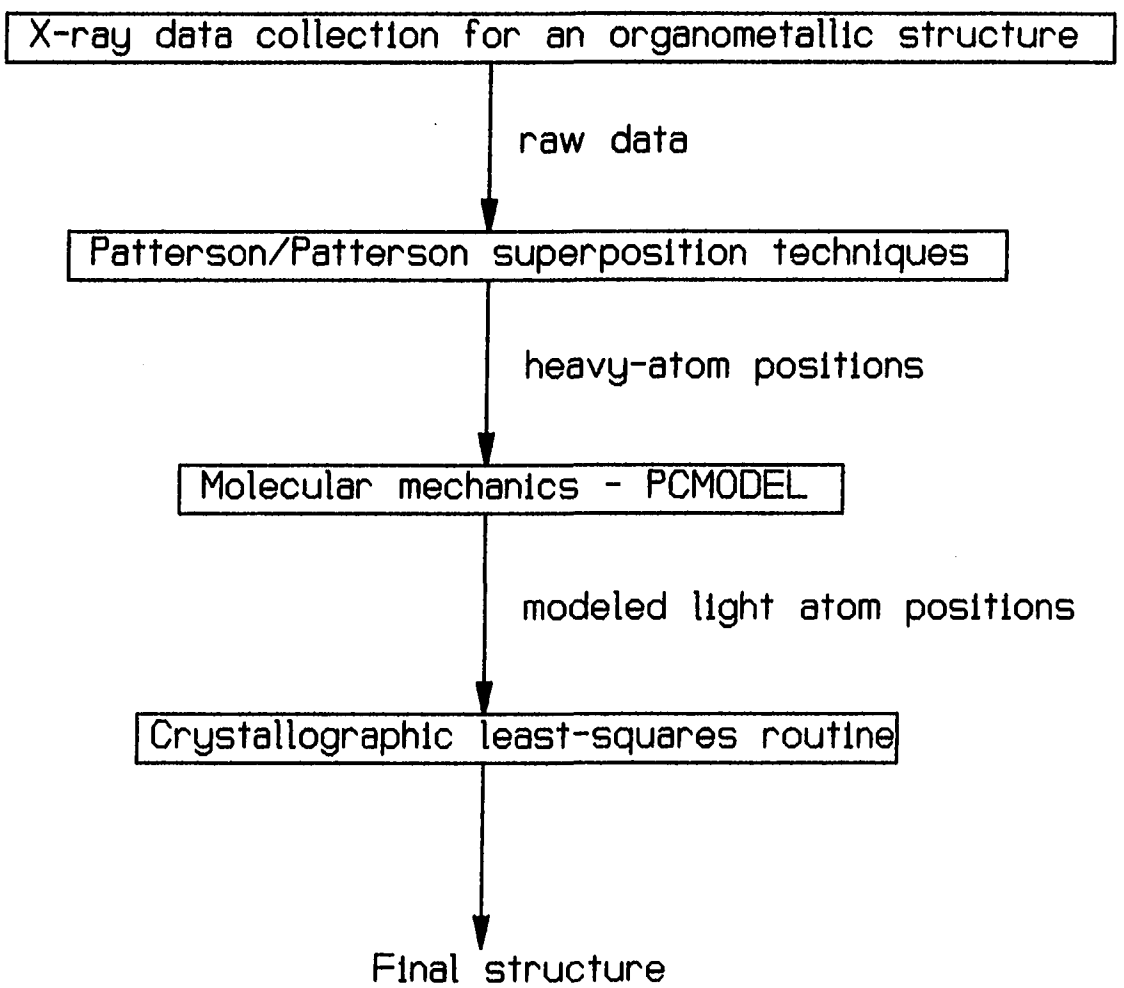

Figure 5.1. Outline of the method to combine crystallographic techniques with molecular mechanics methods

sketched onto the screen and are refined by molecular mechanics methods to find the conformation with the minimum energy. Several starting configurations are used to explore the possibility of different energy minima. After minimizing and conversion of the minimized conformations' coordinates to crystal space, the "refined" positions of the modeled atoms can be used to provide the "trial model" for an X-ray crystallographic least-squares refinement. Figure 5.1 outlines the procedure to combine molecular mechanics and crystallographic techniques.

In order to convert between crystallographic space and the molecular mechanics orthogonal space, several conversions must be performed as shown in Figure 5.2. The first conversion (a) is performed by PCMODEL. It reads in the crystallographic coordinates of the known atom positions and converts them to angstrom orthogonalized coordinates. Step (b) encompasses the process in which the additional atoms are added and the structure is adjusted to achieve a minimum energy. Although the original X-ray atoms are maintained at fixed interatomic distances, they can rotate in space during the step. In order to return to crystallographic space, step (c), the use of the program MMXRAY is required. MMXRAY uses the atomic coordinates of the original heavy atoms to define a reference system. The final positions and orientation of the heavy atoms compared with their original positions and

orientation allow MMXRAY to calculate the translation and rotation matrices necessary to convert the modeled atoms to the original crystallographic space for input into a least-squares refinement. The associated mathematical details will be given in the next chapter

.

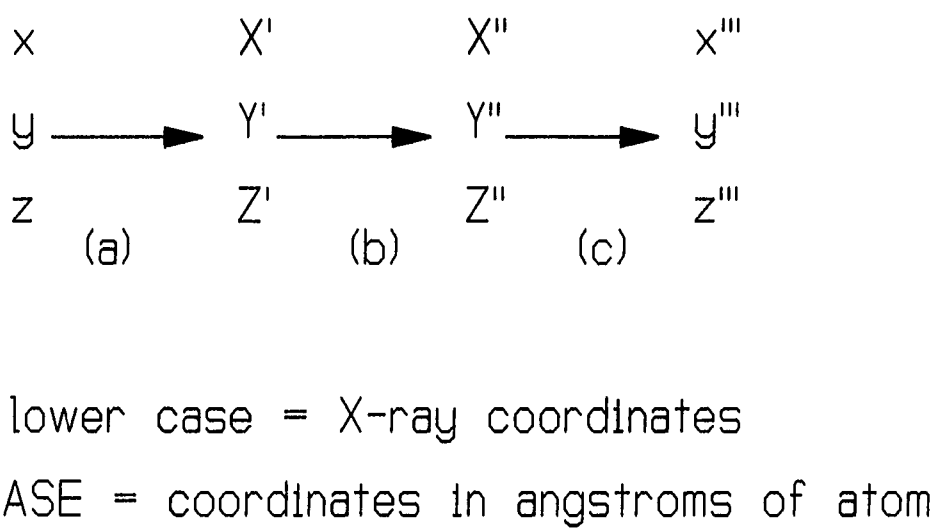

Figure 5.2. Coordinate conversions required in the combination of crystallographic and molecular mechanics techniques

CHAPTER 6. PRACTICAL APPLICATIONS OF MMXRAY

MMXRAY is a general method to utilize molecular mechanics techniques in the X-ray crystallographic solution process. Fore-knowledge of the basic molecular structure (ie. the molecular connectivity) and the ability to find at least three atoms from other determination sources such as Patterson superposition techniques are the only conditions necessary to use this technique.

The feasibility of using this process was first tested using a crystal previously solved by more standard crystallographic techniques. The results from this solution were very encouraging and led to further testing on an unknown structure and culminated in its successful determination.

MMXRAY Solution of $[FeP_2OC_{32}H_{31}]I$[16]

The crystal chosen as a likely candidate for our initial tests using MMXRAY was $[FeP_2OC_{32}H_{31}]I$ due to the highly organic nature of this organometallic compound. Crystals of the compound had previously been obtained from John Nelson's group (Department of Chemistry, University of Nevada-Reno). The original solution process included finding the iodine, iron, and two phosphorus atoms using Patterson superposition

analysis. Subsequent cycles of least-squares refinement followed by difference electron density map calculations laboriously but eventually led to the final solution with an R-factor of 4.4%.

Experimental data

A yellow crystal having approximate dimensions of 0.11 x 0.12 x 0.09 mm was mounted on a glass fiber. Data collection measurements were made on a Rigaku AFC6R diffractometer with graphite monochromated Mo Kα radiation. Using setting angles of 25 carefully centered reflections in the range $29.58 < 2\theta < 33.98^{\circ}$, the crystal was found to have formed in the orthorhombic system with cell constants of a = 9.9101(3), b = 16.5495(5) and c = 18.3383(4) Å. The extinction conditions indicated the acentric, non-standard space group $Pc2_1n$. Complete experimental details are listed in Table 6.1.

Structure solution

A vector corresponding to a Fe-P bond distance was chosen as the shift vector for a weighted superposition. Analysis of the superposition map revealed the positions of the iodine, iron, and phosphorus atoms. Since iodine is only a counter ion and plays no part in the structure, the iron and two phosphorus atoms were used as the anchor atoms for molecular modeling. The rest of the molecule was sketched onto the

Table 6.1. Experimental details for $FeP_2C_{32}OH_{31}I$

Experimental Details	
Empirical Formula	$FeP_2C_{32}OH_{31}I$
Formula Weight	676.30
Crystal Color, Habit	yellow, cube
Crystal Dimensions (mm)	0.11 x 0.12 x 0.09
Crystal System	orthorhombic
Lattice Parameters	a = 9.9101(3) Å
	b = 16.5495(5) Å
	c = 18.3383(4) Å
Space Group	$Pc2_1n$
Z	4
Density	1.502 g/cm^3
$\mu_{(MoK\alpha)}$	16.53 cm^{-1}
Diffractometer	Rigaku AFC6R
Radiation	MoKα (λ = 0.71069)
Temperature	25°C
Scan Type	ω
$2\theta_{max}$	50.1°
Reflections Measured	3008
Reflections Observed (I>3χ(I))	1451
Variables	333
Function Minimized	Σ w ($\|F_o\| - \|F_c\|$)^2
Least-squares Weights	$4F_o^2/\sigma^2(F_o^2)$
Residuals: R; R_w	0.044; 0.044
Goodness of Fit Indicator	1.42
Maximum Peak in Final Dif. Map	1.00 e$^-$/Å^3
Minimum Peak in Final Dif. Map	-0.69 e$^-$/Å^3

screen using a mouse (Figure 6.1) and allowed to shift during the energy minimization procedure.

After several minimizations from alternate starting configurations to ensure the lowest energy conformation was found, a set of orthogonal angstrom atomic coordinates for all atoms was obtained. In order to convert these atomic coordinates back to the original crystal reference system, translation and rotation matrices were obtained by MMXRAY which compared the final positions of the iron and two phosphorus atoms with their original positions. All atomic coordinates were first reconverted from angstrom coordinates to fractional coordinates and then shifted the distance of the modeled iron to the original iron. The rotation matrix was obtained by the following calculation:

$$\begin{pmatrix} x_{Fe} & x_{P1} & x_{P2} \\ y_{Fe} & y_{P1} & y_{P2} \\ z_{Fe} & z_{P1} & z_{P2} \end{pmatrix} = \boldsymbol{R} \times \begin{pmatrix} x'_{Fe} & x'_{P1} & x'_{P2} \\ y'_{Fe} & y'_{P1} & y'_{P2} \\ z'_{Fe} & z'_{P1} & z'_{P2} \end{pmatrix} \qquad (6.1)$$

or

$$\boldsymbol{X} = \boldsymbol{R} \times \boldsymbol{X}'$$

where the matrix denoted by X refers to the original X-ray coordinates, X′ refers to the molecular mechanics minimized

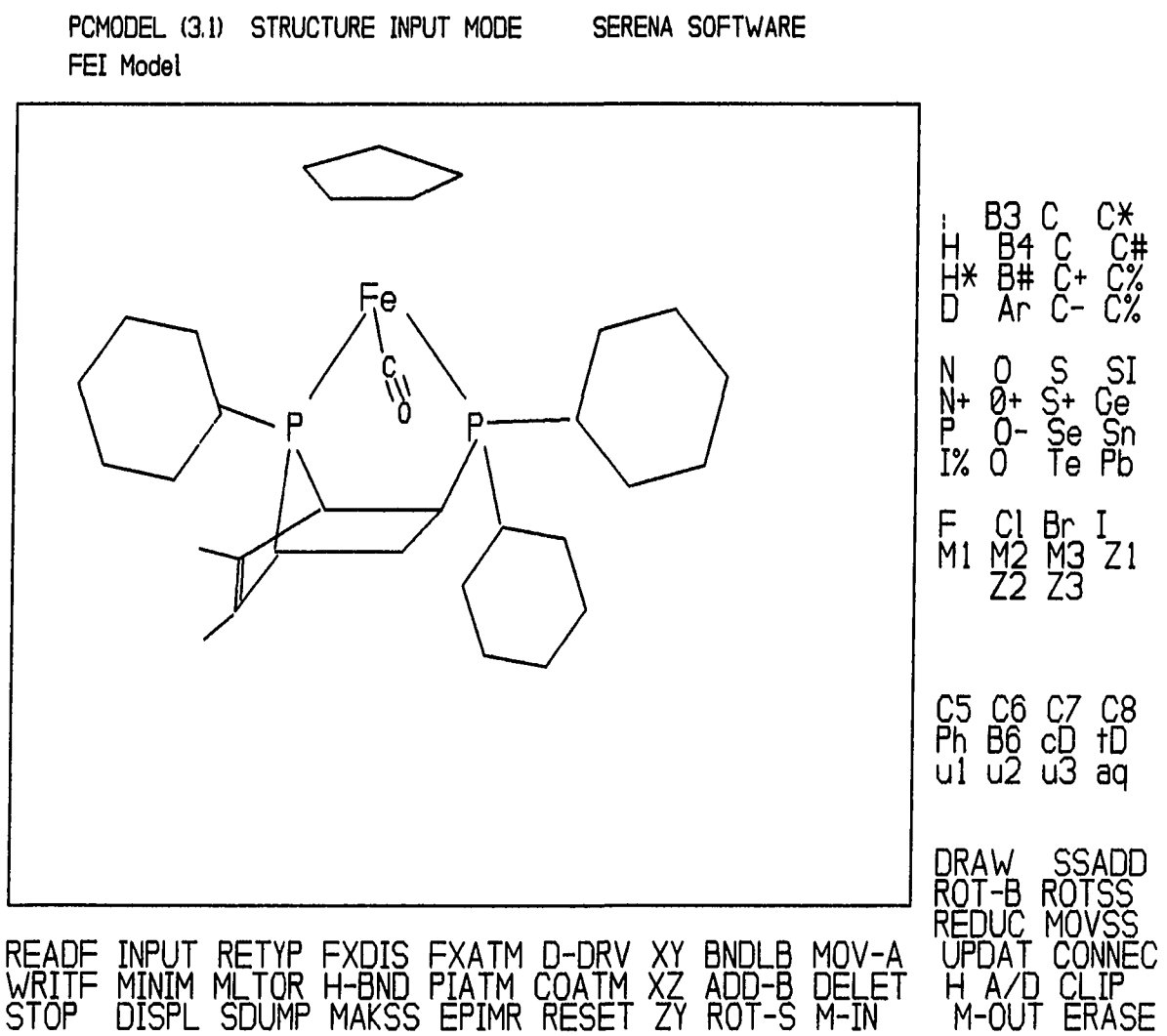

Figure 6.1. PCMODEL screen display of the modeled compound

coordinates, and R is the rotation matrix. Equation 6.1 can be rearranged to yield a relation for the rotation matrix

$$\boldsymbol{R} = \boldsymbol{X} \times (\boldsymbol{X'})^{-1} \qquad (6.2)$$

MMXRAY applies this rotation matrix to all atomic coordinates to obtain atomic coordinates in the original crystal orientation. The minimized and shifted coordinates were input into a crystallographic least-squares refinement routine.[28]

The trial model obtained by this approach gave an initial crystallographic residual of 20.3% for isotropic refinement and 8.5% for anisotropic refinement - compared to 37.7% obtained for iron, iodine, and the two phosphorus atoms only. After addition of the hydrogen atoms, refinement proceeded smoothly and quickly (within a few hours) to the final residual of 4.4% (Figure 6.2[29]).

A comparison of the molecular mechanics minimized coordinates and the final refined X-ray coordinates is shown in Table 6.2. The deviation from the final X-ray fractional coordinates from the molecular mechanics calculation averaged 0.051. The non-phenol atoms showed the best fit with an average departure of 0.009; for the phenol atoms the agreement was within an average of 0.020. The latter would be expected to show greater deviation since their spacial orientations allows greater freedom of movement. In addition, the modeling

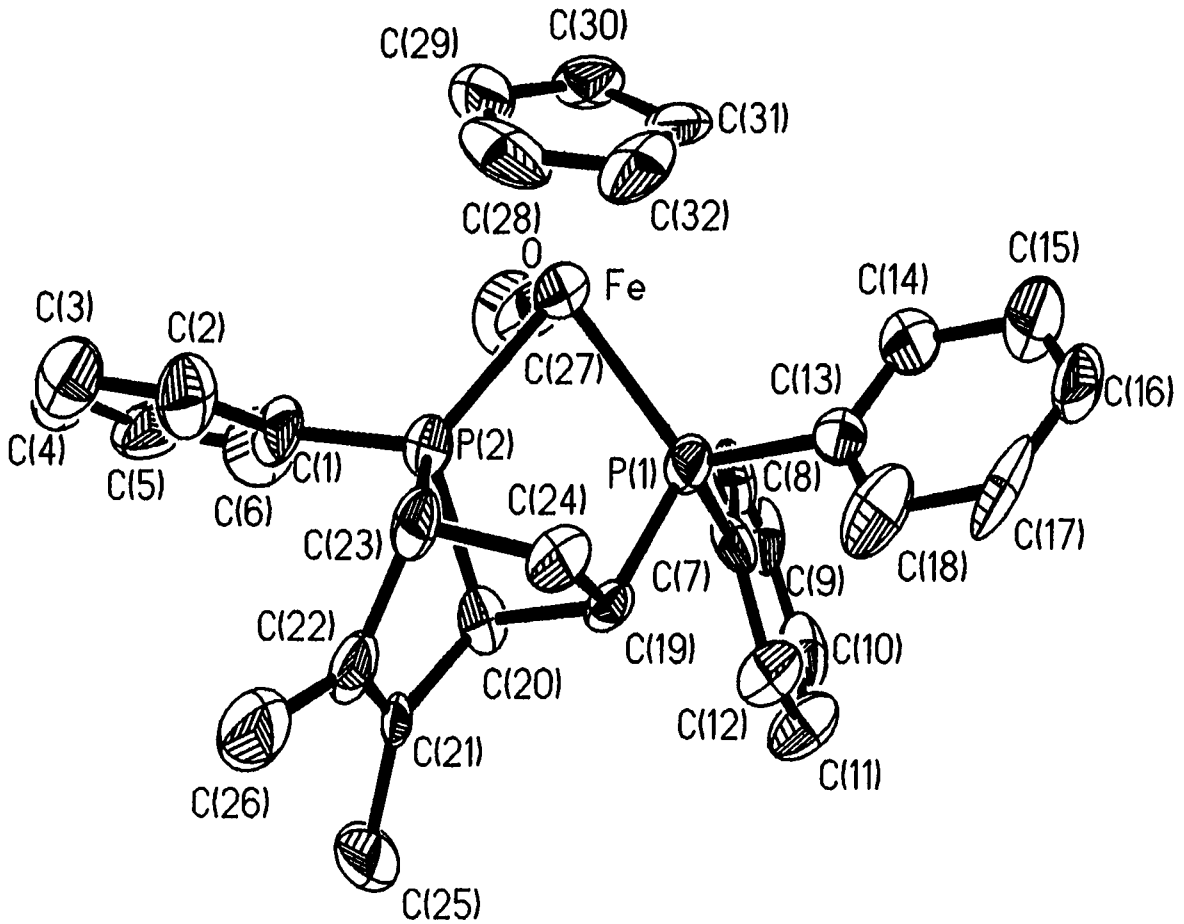

Figure 6.2. ORTEP drawing of $FeP_2C_{32}OH_{31}I$ after final refinement

Table 6.2. Comparison of molecular mechanics and refined X-ray atomic coordinates for $FeP_2C_{32}OH_{31}I$

	x-coordinate			y-coordinate			z-coordinate		
atom	MMX	X-ray	delta	MMX	X-ray	delta	MMX	X-ray	delta
I	0.206	0.206	0.000	-0.007	-0.007	0.000	0.508	0.506	0.002
Fe	0.075	0.076	-0.001	0.309	0.311	-0.002	0.057	0.057	-0.001
P1	0.207	0.212	-0.005	0.419	0.416	0.003	0.032	0.029	0.004
P2	0.255	0.253	0.002	0.269	0.268	0.000	0.117	0.114	0.002
				Carbonyl Group					
C27	0.013	-0.001	0.013	0.356	0.355	0.001	0.128	0.137	-0.009
O1	-0.023	-0.050	0.028	0.381	0.377	0.004	0.174	0.186	-0.012
				P2 Phenyl Carbons					
C1	0.235	0.237	-0.002	0.218	0.199	0.019	0.187	0.194	-0.007
C2	0.218	0.270	-0.051	0.134	0.122	0.012	0.186	0.186	0.000
C3	0.203	0.243	-0.040	0.094	0.068	0.026	0.242	0.248	-0.006
C4	0.204	0.201	0.003	0.138	0.101	0.037	0.297	0.313	-0.016
C5	0.220	0.160	0.060	0.222	0.181	0.041	0.298	0.326	-0.028
C6	0.235	0.181	0.054	0.262	0.232	0.030	0.242	0.262	-0.019
				P1 Phenyl Carbons					
C7	0.184	0.199	-0.015	0.510	0.512	-0.002	0.070	0.075	-0.005
C8	0.045	0.080	-0.035	0.533	0.537	-0.003	0.078	0.108	-0.030
C9	0.021	0.073	-0.051	0.606	0.614	-0.008	0.109	0.148	-0.039
C10	0.136	0.181	-0.045	0.656	0.664	-0.007	0.132	0.144	-0.012
C11	0.275	0.305	-0.030	0.634	0.640	-0.006	0.124	0.112	0.012
C12	0.298	0.316	-0.018	0.562	0.558	0.003	0.093	0.076	0.016
				P1 Phenyl Carbons					
C13	0.214	0.214	0.000	0.441	0.454	-0.013	-0.053	-0.069	0.016
C14	0.094	0.100	-0.006	0.474	0.483	-0.009	-0.082	-0.093	0.010
C15	0.091	0.098	-0.008	0.495	0.514	-0.020	-0.145	-0.170	0.025
C16	0.209	0.217	-0.009	0.482	0.506	-0.024	-0.178	-0.210	0.032
C17	0.330	0.324	0.005	0.449	0.475	-0.025	-0.149	-0.183	0.034
C18	0.332	0.338	-0.006	0.429	0.439	-0.010	-0.087	-0.110	0.023

Table 6.2. (Continued)

	x-coordinate			y-coordinate			z-coordinate		
atom	MMX	X-ray	delta	MMX	X-ray	delta	MMX	X-ray	delta
				Bicyclo-Ligand Carbons					
C19	0.390	0.386	0.004	0.376	0.386	-0.010	0.058	0.047	0.011
C20	0.379	0.370	0.009	0.360	0.347	0.013	0.128	0.134	-0.006
C21	0.510	0.502	0.008	0.319	0.311	0.008	0.152	0.157	-0.004
C22	0.525	0.514	0.011	0.248	0.248	0.001	0.123	0.117	0.007
C23	0.406	0.400	0.006	0.228	0.225	0.003	0.075	0.060	0.014
C24	0.419	0.408	0.011	0.294	0.302	-0.008	0.026	0.007	0.019
C25	0.611	0.605	0.006	0.358	0.343	0.015	0.202	0.207	-0.005
C26	0.643	0.625	0.018	0.192	0.186	0.007	0.136	0.117	0.019
				Cyclopentyl Carbons					
C28	0.057	0.069	-0.012	0.200	0.201	-0.001	0.007	-0.004	0.010
C29	-0.049	-0.056	0.007	0.203	0.213	-0.010	0.048	0.038	0.009
C30	-0.133	-0.126	-0.008	0.268	0.287	-0.019	0.033	0.023	0.010
C31	-0.079	-0.051	-0.028	0.306	0.313	-0.008	-0.018	-0.036	0.018
C32	0.039	0.058	-0.019	0.264	0.270	-0.006	-0.034	-0.052	0.018

routine does not account for packing that most likely effects the phenol atoms in the molecule.

Based on the successful solution of this structure, we next applied this technique of combining molecular mechanics and X-ray methods to a structure which had evaded solution through regular solution processes.

MMXRAY Solution of $TiN_4C_{50}H_{54}$[30]

The large number of non-hydrogen atoms (110, two molecules) in the asymmetric unit of the crystal (OEP)Ti(η^2-Ph-C≡C-Ph), where OEP = octaethylporphyrinato, significantly increased the difficulty and complexity of the structure determination. Attempts to solve the structure using direct methods were unsuccessful. Patterson superposition procedures established the positions of only the titanium and the coordinated nitrogen atoms. These atoms were ineffective at phasing giving a poor residual - 56%. Since no further atoms were revealed using difference electron density map calculations, the MMXRAY technique seemed a viable option for further solution attempts.

Experimental data

A purple, rectangle-shaped crystal having approximate dimensions of 0.200 x 0.100 x 0.400 mm was mounted on a glass fiber. Data collection measurements were made on a Rigaku AFC6R diffractometer with graphite monochromated Mo Kα radiation. Using setting angles of 25 carefully centered reflections in the range $36.71 < 2\theta < 40.00^\circ$, the crystal was found to have formed in the monoclinic system with cell constants of a = 49.369(7), b = 13.734(9), c = 36.622(4) Å, and $\beta = 136.622(7)^\circ$. The extinction conditions indicated the

C-centered space group C2/c with two molecules in the asymmetric unit. Complete experimental details are listed in Table 6.3.

Structure solution

A sharpened Patterson map was calculated and a Patterson superposition analysis was carried out using a vector identified as a probable Ti-Ti vector. From the resulting map, the positions of the titanium atoms plus likely positions for the coordinated nitrogens were determined. Each of the two sets of the titanium and nitrogen atoms from the asymmetric unit were input into PCMODEL. Since it was not known which direction the ethyl arms of the porphyrin ring would extend nor with which side of the porphyrin ring the diphenylacetylene ligand would coordinate, only the 20 porphyrin carbons from each ring were modeled and allowed to minimize. Since PCMODEL does not take into account packing effects, each molecule in the asymmetric unit was modeled separately and allowed to minimize. Figure 6.3 shows the screen output after minimization of one of the molecules in the asymmetric unit.

Minimizations using assorted starting configurations and using different pairs of nitrogens as the anchor points were used to ensure the lowest energy conformation was found. The two titanium and eight nitrogen atoms as well as the minimized positions of the two porphyrin rings were input into a least-

Table 6.3. Experimental details for $TiN_4C_{50}H_{54}$

Experimental Details	
Empirical Formula	$TiN_4C_{50}H_{54}$
Formula Weight	758.90
Crystal Color, Habit	purple, rectangular
Crystal Dimensions (mm)	0.200 x 0.100 x 0.400
Crystal System	monoclinic
Lattice Parameters	a = 49.369(7) Å
	b = 13.734(9) Å
	c = 36.042(7) Å
	ß = 136.622(7)°
Space Group	C2/c
Z	16
Density	1.201 g/cm³
$\mu_{(MoK\alpha)}$	2.37 cm⁻¹
Diffractometer	Rigaku AFC6R
Radiation	MoKα (λ = 0.71069)
Temperature	-40°C
Scan Type	ω
$2\theta_{max}$	50.1°
Reflections Measured	15715
Reflections Observed (I>3χ(I))	6219
Variables	992
Function Minimized	$\Sigma\ w\ (\|F_o\| - \|F_c\|)^2$
Least-squares Weights	$4F_o^2/\sigma^2(F_o^2)$
Residuals: R; R_w	0.061; 0.063
Goodness of Fit Indicator	1.69
Maximum Peak in Final Dif. Map	0.78 e⁻/Å³
Minimum Peak in Final Dif. Map	-0.42 e⁻/Å³

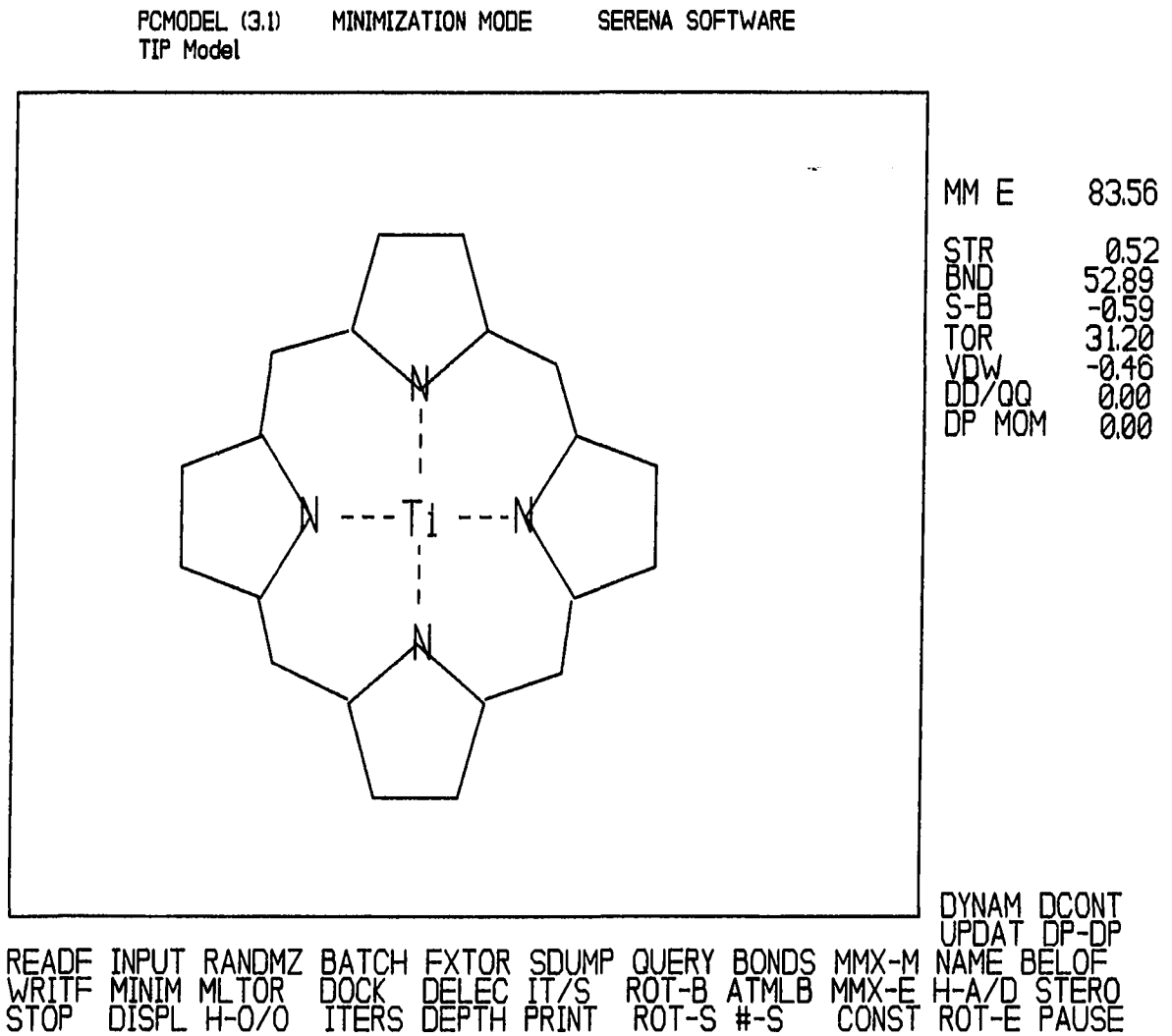

Figure 6.3. Screen output from PCMODEL after minimization

squares refinement procedure. The residual reduced to 36% which phased reflections well enough to reveal the remaining carbon atoms using difference electron density map calculations. Refinement proceeded smoothly to yield a final residual of 6.1% (Figure 6.4)[29].

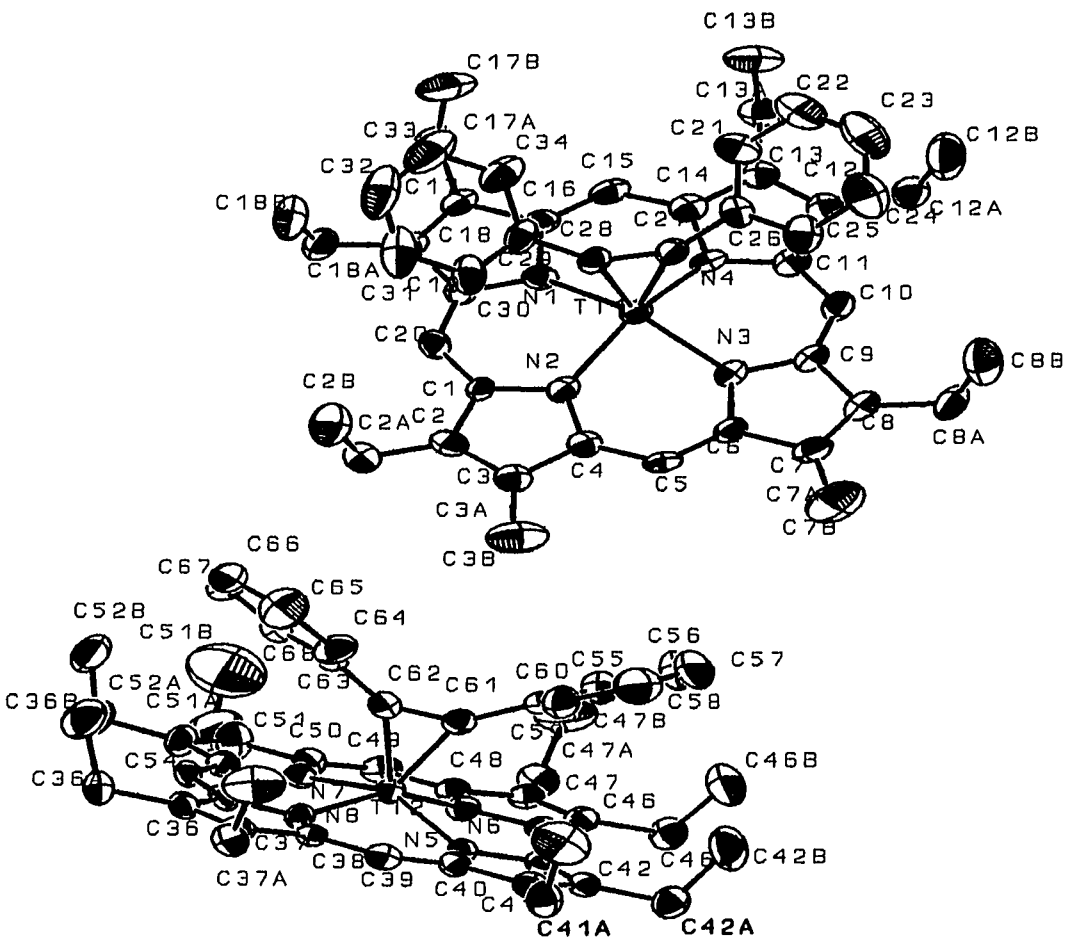

Figure 6.4. ORTEP drawing with 50% probability thermal ellipsoids and atom-labeling schemes for the molecules of the asymmetric unit of Ti(OEP)(PhC≡CPh).

A comparison of the molecular mechanics minimized coordinates and the final refined X-ray coordinates for one molecule in the asymmetric unit of the titanium porphyrin complex is shown in Table 6.4. The deviation from the final X-ray fractional coordinates from the molecular mechanics calculations averaged 0.365. These variations are significantly greater than those shown in the iron-iodide compound used for the first test. This was not an unexpected result due to the fact that molecular mechanics does not account for packing effects. As shown is Figure 6.5, the packing of the unit cell may lead to formation of intermolecular π-π interactions[31] between the pairs of porphyrins in the lattice. This interaction may affect the planarity of the molecule and thus lead to poorer molecular mechanics results.

Close agreement between the molecular-mechanics modeled coordinates and the final crystallographically refined coordinates is an important indication as to the feasibility of the MMXRAY technique. The better the agreement, the more likely crystallographic refinement will lead to a final crystal solution. However, when solving an unknown compound, the agreement will not be known until the crystal determination is complete. Therefore, the key to this technique is its ability to prod the solution to completion by either modeling the entire structure, as in the iron-iodide

Table 6.4. Comparison of molecular mechanics and refined X-ray atomic coordinates for one molecule of titanium porphyrin complex

	x-coordinate			y-coordinate			z-coordinate		
atom	MMX	X-ray	delta	MMX	X-ray	delta	MMX	X-ray	delta
Ti1	0.199	0.199	-0.000	0.200	0.201	-0.001	-0.091	-0.090	0.001
N1	0.193	0.196	-0.003	0.341	0.337	0.004	-0.067	-0.058	-0.009
N2	0.230	0.231	-0.001	0.276	0.282	-0.006	-0.097	-0.099	0.002
N3	0.232	0.233	-0.001	0.082	0.084	-0.002	-0.078	-0.078	0.000
N4	0.201	0.196	0.005	0.124	0.120	0.004	-0.033	-0.039	0.006
C1	0.263	0.227	0.036	0.374	0.389	-0.015	-0.104	-0.106	0.002
C2	0.297	0.246	0.051	0.401	0.416	-0.015	-0.122	-0.120	-0.002
C3	0.283	0.260	0.023	0.317	0.333	-0.016	-0.123	-0.124	0.001
C4	0.239	0.249	-0.010	0.238	0.259	-0.021	-0.107	-0.110	0.003
C5	0.082	0.260	-0.178	-0.025	0.164	-0.189	-0.044	-0.110	0.066
C6	0.077	0.249	-0.172	-0.090	0.074	-0.164	-0.049	-0.097	0.048
C7	0.128	0.258	-0.130	-0.036	-0.025	-0.011	-0.073	-0.097	0.024
C8	0.164	0.244	-0.080	0.063	-0.076	0.139	-0.083	-0.084	0.001
C9	0.446	0.229	0.217	0.355	-0.010	0.365	0.005	-0.070	0.075
C10	0.492	0.212	0.280	0.564	-0.046	0.610	0.024	-0.053	0.077
C11	0.476	0.198	0.278	0.478	0.023	0.455	0.023	-0.038	0.061
C12	0.474	0.181	0.293	0.498	-0.006	0.504	-0.006	-0.022	0.016
C13	0.231	0.168	0.063	0.426	0.066	0.360	-0.079	-0.017	-0.062
C14	0.223	0.180	0.043	0.486	0.146	0.340	-0.066	-0.028	-0.038
C15	0.172	0.166	0.006	0.427	0.250	0.177	-0.042	-0.034	-0.006
C16	0.147	0.179	-0.032	0.330	0.335	-0.005	-0.039	-0.043	0.004
C17	0.265	0.169	0.096	0.442	0.423	0.019	-0.097	-0.042	-0.055
C18	0.211	0.182	0.029	0.142	0.480	-0.338	-0.102	-0.061	-0.041
C19	0.467	0.197	0.270	0.554	0.418	0.136	0.016	-0.072	0.088
C20	0.151	0.213	-0.062	0.194	0.445	-0.250	-0.059	-0.092	0.043

case, or modeling part of the structure, as in the titanium porphyrin case. If least-squares refinement of the modeled structure is successful, regardless of the final agreement, MMXRAY has performed effectively.

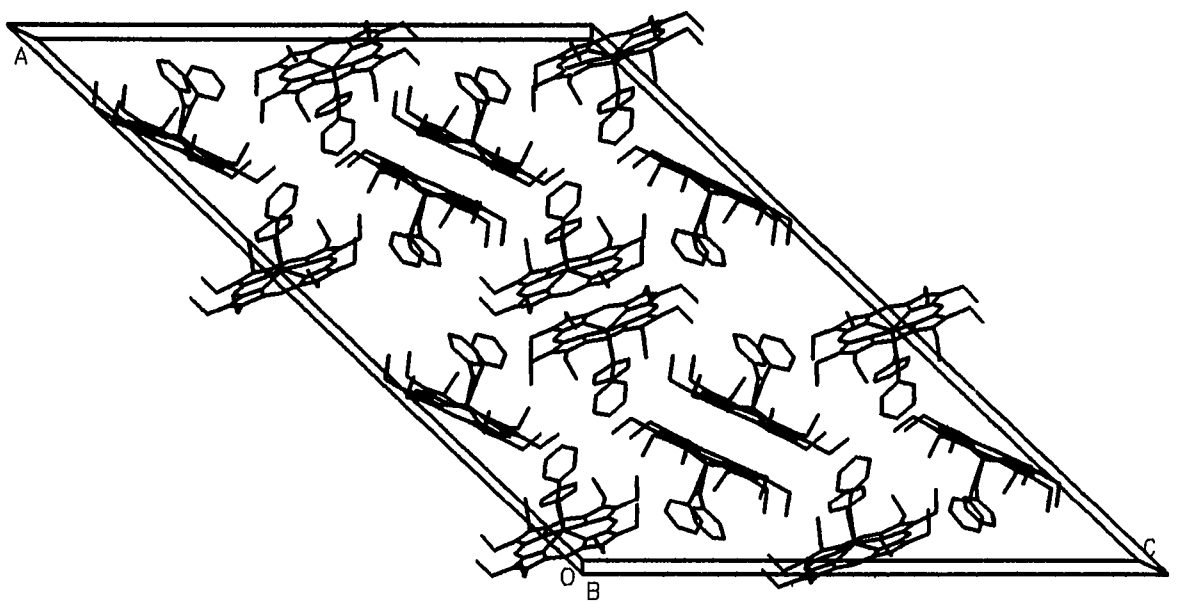

Figure 6.5. Crystal-packing diagram for Ti(OEP)(η^2-PhC≡CPh)

CHAPTER 7. DISCUSSION AND FUTURE WORK

The development of X-ray crystallography has paralleled that of computers. With today's fast computers has also come advanced "user-friendly" software making use of the latest improvements in crystallographic techniques. Where less than 50 years ago, a crystal structure determination involved months of tedious hand calculations; today synthetic chemists, with only rudimentary knowledge of crystallographic theory, can solve routine crystal structures in a matter of hours or days. In fact, crystallography has become a black box tool for structural characterization of new compounds. Where does the synthetic chemist turn when these black box methods fail to yield a structure solution?

Both MMXRAY and SUPSYMM were designed for the novice crystallographer as structure solution tools for use when normal crystallographic routines fail. When normal model development routines such as the widely used direct methods fail to yield even a starting point for the crystal determination, SUPSYMM can be used to interpret Patterson superposition maps to find at least the heavy atoms in the structure. SUPSYMM was designed to aid the less experienced crystallographer in the meaningful interpretation of a Patterson superposition map. Using distance analysis and

vector projections, SUPSYMM determines if symmetry relationships exist between superposition peaks. These relationships lead to identification of symmetry elements and peak positions.

SUPSYMM is designed to produce results for crystal systems of orthorhombic or lower symmetry with little intervention by the user. It should be noted that this takes care of about 90% of the crystal structure solutions performed on organometallic substances. Nevertheless, SUPSYMM theory was set up to be completely general and, therefore, for completeness SUPSYMM needs to be extended to include the higher symmetry crystal systems.

SUPSYMM is limited by the quality of the data. Because peaks in a Patterson superposition map have a certain breadth associated with them, extraneous peaks caused by incidental overlapping may be produced. As shown in chapter 4, even with poor data quality, all of the heavy atoms and a few light atoms in the structure can be identified. Further study is needed to improve superposition map calculations to eliminate some of the uncertainties in the peak positions and thereby allowing for more of the structure to be elucidated.

Patterson superposition techniques such as SUPSYMM can usually provide at least a few atom positions. In large organometallic complexes, however, these atom alone may not be enough to phase reflections properly to readily reveal the

rest of the structure. The technique, MMXRAY, uses the known atom positions as a starting point and then uses molecular mechanics to model the rest of the structure. Refinement of the modeled positions using a crystallographic least-squares routine has been shown to lead the difficult structure solution to completion.

MMXRAY has been shown to lead to the solution of the structure when tested on both a known and an unknown organometallic molecule. To fully understand the limitations and pitfalls one may encounter when using molecular mechanics, MMXRAY should be further tested using a wider range of molecular structures. The range of structures MMXRAY may be able to handle may be extended by exploring the use of different force fields.

Combining SUPSYMM and MMXRAY gives the novice crystallographer a nonroutine but still easy-to-implement path to find a structure solution for a structure that has resisted solution by routine crystallographic methods.

LITERATURE CITED

1. Patterson, A. L., Phys. Rev., 46, 372 (1934).

2. Stout, G. and Jensen, L., X-ray Structure Determination-A Practical Guide, New York, Macmillan, pp. 271 (1968).

3. Harker, D., J. Chem. Phys., 4, 381 (1936).

4. Nordman, C. E., Trans. Am. Cryst. Assoc., 2, 29 (1966).

5. Mighell, A. D. and Jacobson, R. A., Acta. Cryst., 16, 443-445 (1963).

6. Egert, E., Acta. Cryst., 39, 936-940 (1983).

7. TEXSAN - TEXRAY Structure Analysis Package, Molecular Structure Corporation, The Woodlands, TX (1985).

8. Sheldrick, G. M., Crystallographic Computing 3, New York, Oxford University Press (1985).

9. Buerger, M. J., Vector Space, New York, Wiley (1959).

10. Jacobson, R. A., Wunderlich J. A. and Lipscomb, W. N., Acta. Cryst., 14, 598 (1961).

11. Clastre, J. and Gray, R., Compt. Rend., 230, 1876 (1950).

12. Jacobson, R. A., Trans. Am. Cryst. Assoc., 2, (1966).

13. Jacobson, R. A., Crystallographic Computing, F. R. Ahmed, Ed., Munksgaard, Copenhagen, Denmark, pp. 81-86 (1970).

14. CHES - Structure Analysis Package, Ames Laboratory, Ames, IA (1978).

15. Rao, K. M., Day, C. L., Jacobson, R. A., Angelici, R. J., Inorg. Chem., 30, 5046 (1991).

16. Bhaduri, D., Nelson, J. H., Day, C. L., Jacobson, R. A., Solujic, L. and Milosavlyevic, E., Organometallics, submitted for publication.

17. Rao, K. M., Day, C. L., Jacobson, R. A., Angelici, R. J., Organometallics., 11, 2303 (1992).

18. Allinger, N. L. and Chang, S. H. M., Tetrahedron, 33, 1561 (1977).

19. Bartell, L. S. and Brugi, H. B., J. Am. Chem. Soc., 94, 5239 (1972).

20. Williams, D. E., Act. Cryst. Sect. A, 36, 715 (1980).

21. Simonetta, M., Acc. Chem. Res., 7, 345 (1974).

22. Andrews, D. H., Phys. Rev., 36, 544, (1930).

23. Hill, T. L., J. Chem. Phys., 14, 465 (1946).

24. Dostrovsky, I., Hughes, E. D., Ingold, C. K., J. Chem. Soc., 3200 (1955).

25. Westheimer, F. H., Mayer, J. E., J. Chem. Phys., 14, 733 (1946).

26. Gajewski, J. J. and Gilbert, K. E., "PCMODEL: Molecular Modeling Software", Serena Software, Bloomington, Indiana (1987).

27. Allinger, N. L., J. Amer. Chem. Soc., 99, 8 (1977).

28. Lapp, R. L. and Jacobson, R. A., "ALLS: A generalized Crystallographic Least-Squares Program", USDOE Report IS-4708, Iowa State University, Ames, Iowa (1978).

29. Johnson, C. K., "ORTEP II", Report ORNL-5138, Oak Ridge National Laboratory, Oak Ridge, Tennessee (1976).

30. Woo, L. K., Hays, J. A., Jacobson, R. A., and Day, C. L., Organometallics, 10, 2102 (1991).

31. Scheidt, W. R. and Lee, T. J., Struct. Bonding, 64, 1 (1987).

32. Dunitz, J. D., Acta. Cryst., 307 (1957).

ACKNOWLEDGEMENTS

This dissertation is the culmination of five years of graduate study. While it is impossible to acknowledge the many individuals who have had some impact on my life over the course of my graduate work, key to the completion of this project was the guidance and encouragement of Dr. Robert Jacobson. Also, the friendship and support of Brenda "B" Smith cannot go without mention.

Finally, I would like to thank my parents and Phyllis and Cecil Stewart for always being there in both the good times and the not so good times.

This work was performed at Ames Laboratory under contract No. W-7405-eng-82 with the U. S. Department of Energy. The United States government has assigned the DOE Report number IS-T 1620 to this thesis.

APPENDIX A. COMPUTER ASSISTED INSTRUCTION TO ELEMENTARY CRYSTALLOGRAPHIC METHODS

Introduction

Addressing a significant part of the may facets of crystallographic methodology is not feasible in the undergraduate chemistry curriculum. Though X-ray diffraction has led the way to significant structural discoveries, crystallographic techniques, at best, receive only a cursory review during the undergraduate course of study. POWDER and XTALLAB and their accompanying supplements were designed to provide the undergraduate junior or senior physical chemistry student hands-on computational experience with crystallographic methods to supplement knowledge obtained through course lectures.

These experiments are each broken into two parts - a description of the crystallographic theory and calculations involved and an interactive computer program. Knowledge gained from the descriptive material is applied to the solution of a practical x-ray diffraction problem. POWDER helps the student index a powder photograph, decide the cubic lattice to which the crystal belongs, and find the crystal's lattice constant. XTALLAB was designed to acquaint the student with the method of crystal structure determinations

based upon x-ray diffraction data obtained with single crystals. To simplify calculations and viewing of the trial molecule, the structure determination is carried out on a relatively planar structure with a short cell axis which allows for 2-dimensional analysis. Used in conjunction, POWDER and XTALLAB mesh to provide the student with a basic understanding of crystal structure determination based upon X-ray diffraction data obtained from powder photographs and single crystals.

POWDER

Descriptive handout

The descriptive material for POWDER describes the basic concepts needed for the interpretation of x-ray powder photographs. No previous knowledge of crystallography is assumed. The descriptive material begins with general information about crystal regularity to define the crystal systems, symmetry classes and space groups. The scattering of x-rays by the regularly arranged atoms in the lattice is explained by introducing the Bragg relationship. Starting with Bragg's law, the student is guided through the derivations for the indexing of a crystal in the cubic system, the calculation of the lattice constant and Z (the number of molecules in the unit cell).

Experimental procedure

Depending on the availability of experimental apparatus, powder photographs may be provided to the student or the student may prepare their own. Before proceeding to POWDER, the student is instructed to accurately measure the position of 6-10 lines on the photograph and the density of the material. After entering the measured lines, POWDER guides the student stepwise through the indexing procedure previously outlined in the descriptive handout. Once the indexing has been accomplished, the choice of cubic lattice is made by on-screen direct comparison with the three types of cubic systems - simple, face-centered, or body-centered. (Figure A.1) The next stage of POWDER guides the student through calculation of the 'best' lattice constant. The lattice constant, the molecular weight, and the measured density are then used to calculate the number of molecules per unit cell (Z).

At various stages throughout the program, explanations or further detail of the calculations can be brought onto the screen by typing ? for help. After the completion of POWDER, a file is created containing the students indexing results. The information in this file is used in the student's lab report. Also included in the student's lab report should be a discussion of unaccounted lines, if any, in their indexing, how they determined the value of a_o and Z, and whether their

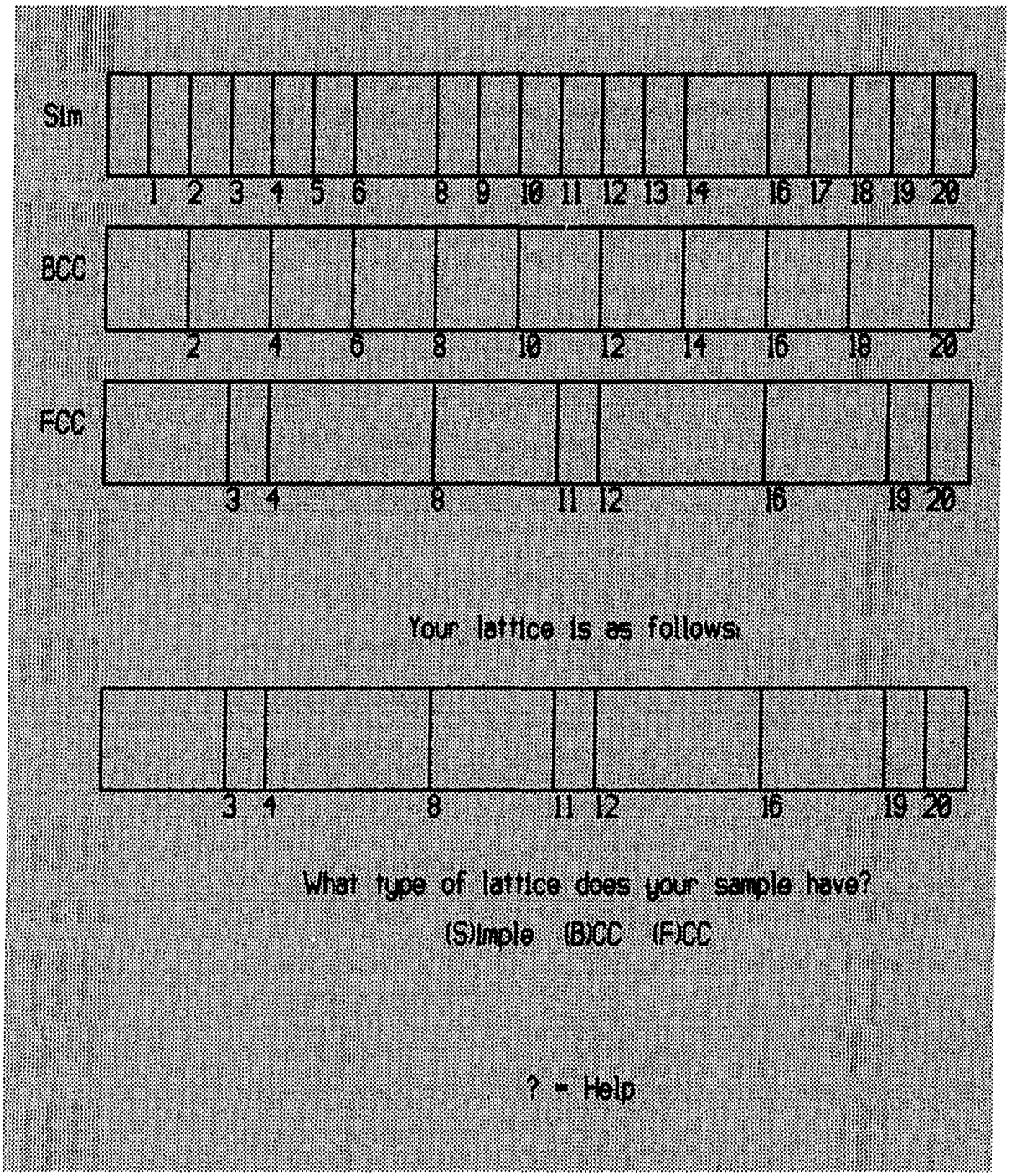

Figure A.1. POWDER screen for comparison of cubic systems and sample.

calculated Z value is consistent with the determined lattice type.

XTALLAB

Descriptive handout

This experiment was designed to acquaint the undergraduate chemistry student with the method of crystal structure determinations based upon x-ray diffraction data obtained from single crystals. The supplementary handout for XTALLAB provides further detail as to the theoretical and mathematical concepts of x-ray diffraction introduced in POWDER. It describes x-ray scattering, constructive versus destructive interference, crystal symmetry, and electron density and Patterson map calculations that lead to trial structures. It also explains how a trial structure is tested for viability by the residual factor, R.

Experimental procedure

Using the knowledge gleaned from the descriptive material, the student must calculate the volume, the number of molecules per unit cell, Z, and must answer some rudimentary questions about the symmetry of the experimental crystal. These calculations and questions must be completed before the student is allowed to proceed with the XTALLAB program.

XTALLAB is broken into three main sections - XTAL, ATOM, and MAP. (Figure A.2)

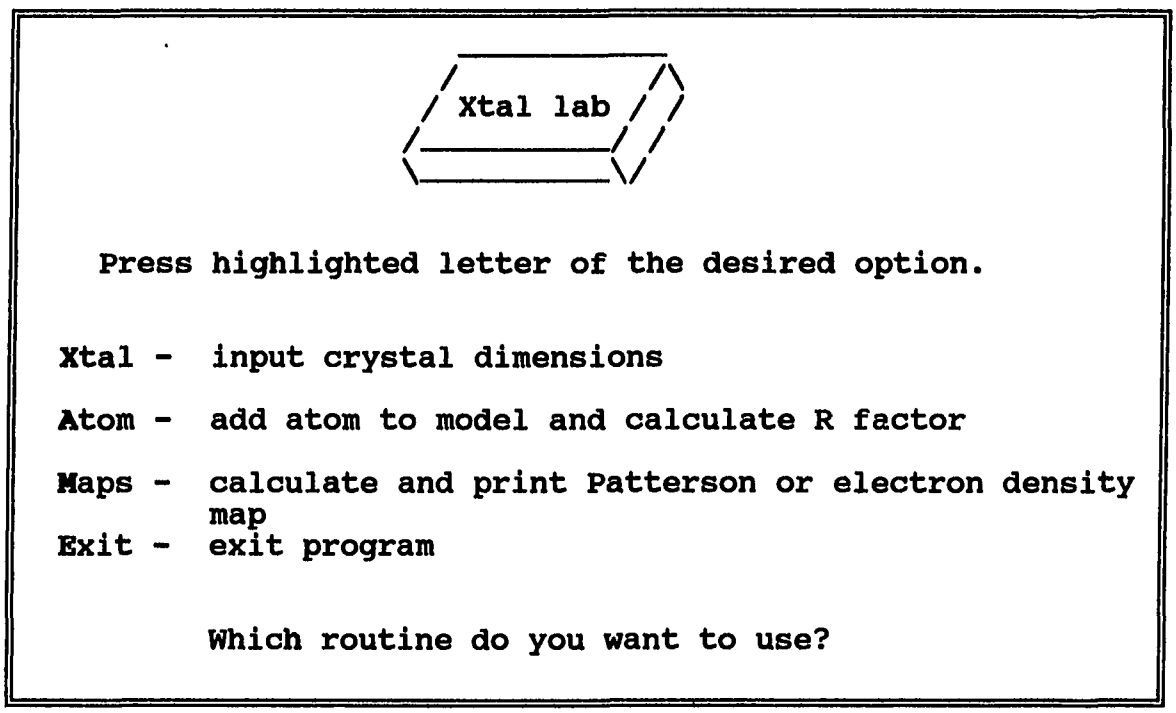

Figure A.2. XTALLAB main menu screen

XTAL - XTAL prompts the user for crystal information - lattice parameters and space group symmetry for the test crystal (copper dipyridine dichloride). The information entered into XTAL is used by both ATOM and MAP.

ATOM - ATOM is an interactive program for developing and manipulating a model structure.

Atom names, positions, and occupancy are the required input. (See Figure A.3) As more atom positions are revealed by electron density map calculations, they may be added to the trial structure and manipulated using the various commands in ATOM. ATOM allows the user to add, delete, or edit the atoms in the model structure. To help the user decide the feasibility of the input atoms, ATOM will calculate interatomic distances, angles, and the residual.

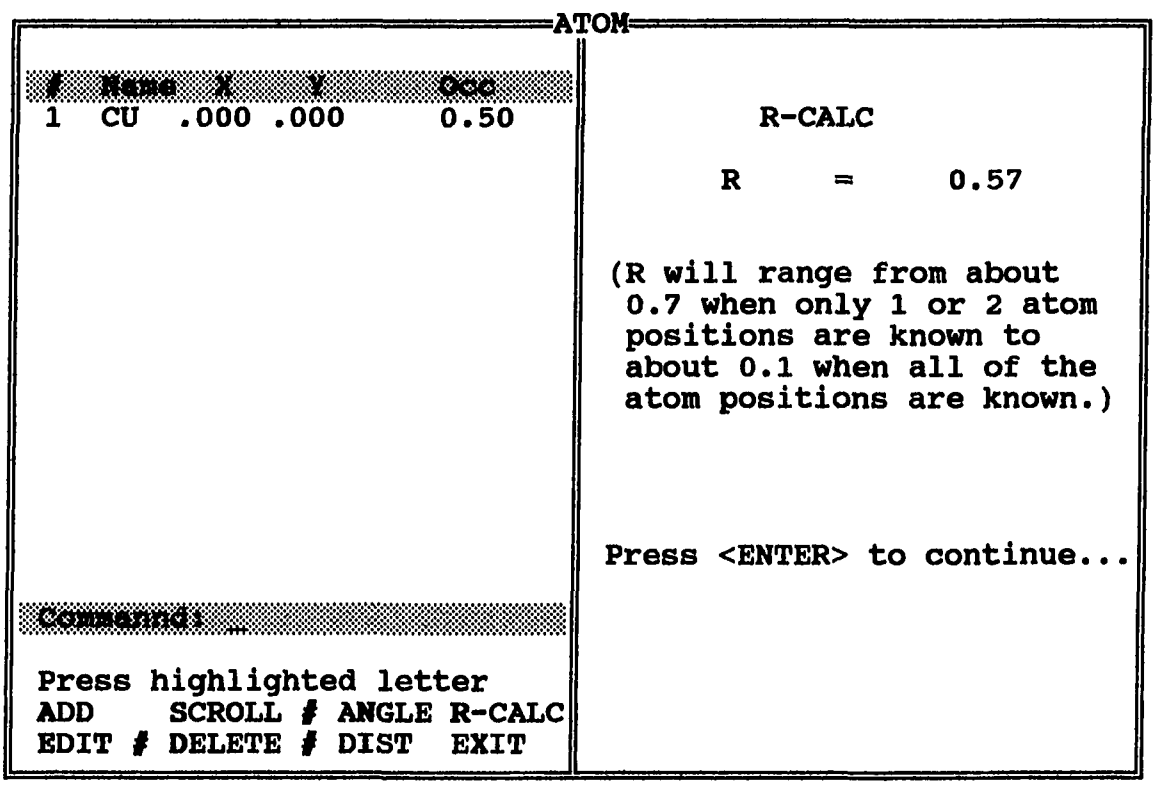

Figure A.3. ATOM input screen

MAPS - MAPS will calculate, display, and print either a Patterson or an electron density map projection. (See Figure A.4) On the printed map, the x-axis is 32 grid points across and the y-axis is 32 grid points down. The display at the bottom of the map lists the fractional coordinates of the cursor position. The maps use a one character color code (1-9(blue), a-z(orange), and A-Z(yellow)) to represent an electron density or Patterson value scaled between 1-62. A value less than or equal to 0.0 is displayed on the map as a period.

As more of the structure is input into ATOM and the residual decreases, more of the structure will be elucidated by subsequent electron density map calculations until the final structure is obtained.

The sample crystal copper dipyridine dichloride (Dunitz, J. D., 1957)[32] was chosen because it lies relatively flat in the xy-plane and has a short c-axis allowing a 2-dimensional structure determination to be completed. Data for the sample crystal is included with the program; however, the sample crystal can be changed with only a few modifications

Section 0

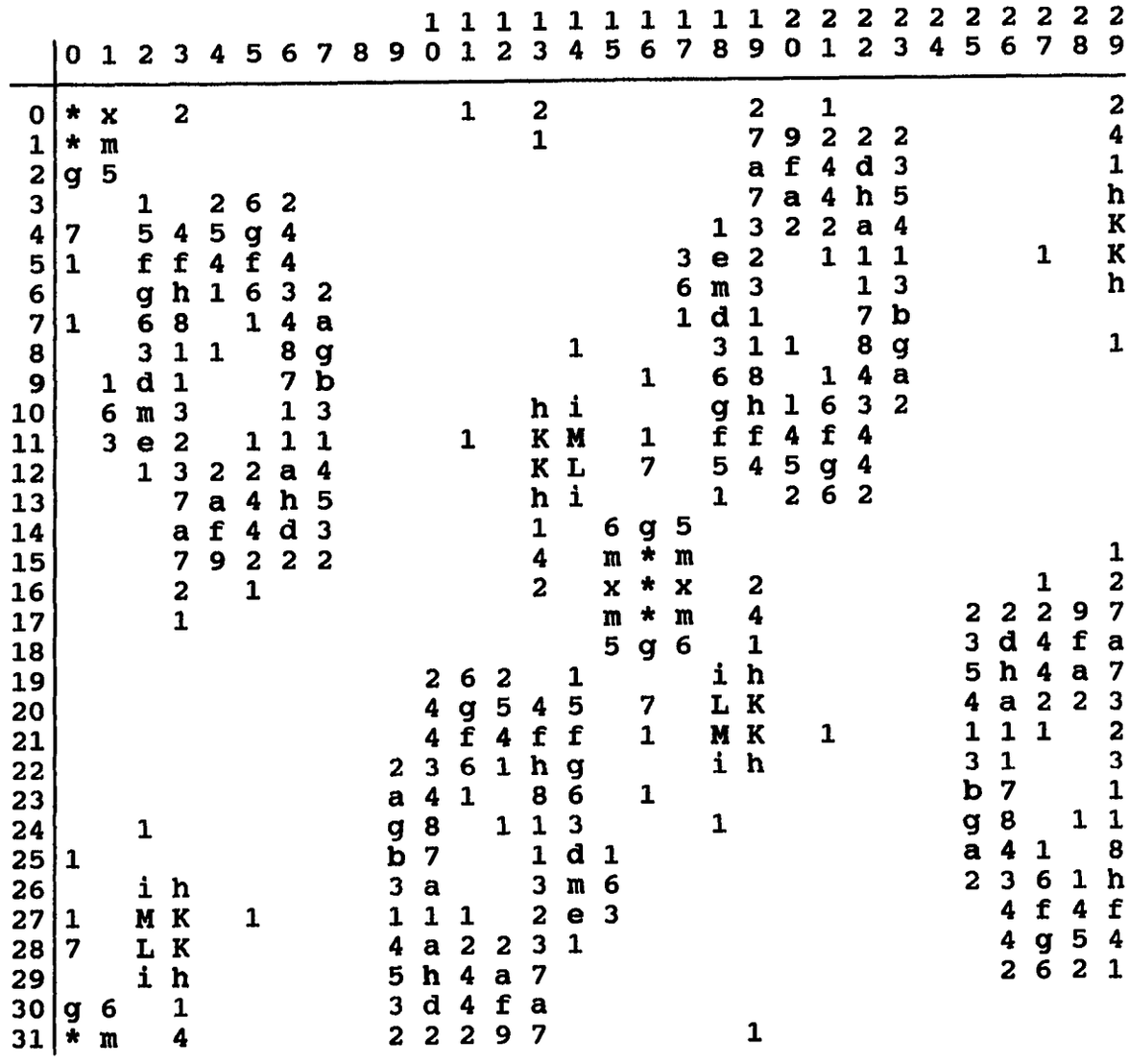

Figure A.4. MAPS screen showing an electron density map

APPENDIX B. ROUTINE CRYSTAL STRUCTURE DETERMINATIONS

The major emphasis of this research has been the development of two new techniques for solution of crystal structures that have resisted solution through normal crystallographic means. In addition to the crystal structures presented in the main body as illustrations of these techniques, several other compounds have been solved. The details of these additional crystal solutions are presented in this appendix.

Structure Determination of $[BrC_{15}NO_4H_{24}]Cl \cdot CCl_2H_2$

Data collection

A transparent, cube-shaped crystal of $[BrC_{15}NO_4H_{24}]Cl \cdot CCl_2H_2$ provided by George Kraus' group (Iowa State University) having approximate dimensions of 0.485 x 0.500 x 0.505 mm was mounted on a glass fiber. The crystal had a tendency to be moisture sensitive and, therefore, was coated with epoxy glue. All measurements were made on a Rigaku AFC6R diffractometer with graphite monochromated Mo Kα radiation and a 12KW rotating anode generator.

Cell constants and an orientation matrix for data collection, obtained from a least-squares refinement using the

setting angles of 25 carefully centered reflections in the range $14.00 < 2\theta < 35.00^{\circ}$ corresponded to an orthorhombic cell with dimensions :

$a = 13.250\ (4)\text{Å}$
$b = 16.144\ (6)\text{Å}$ $\quad V = 2047\ (1)\text{Å}^3$
$c = 9.570\ (4)\text{Å}$

For Z = 4 and F.W. = 481.64, the calculated density is 1.563 g/cm. Based on the systematic absences of:

h00: h ≠ 2n
0k0: k ≠ 2n
00l: l ≠ 2n

and the successful solution and refinement of the structure, the space group was determined to be:

$P2_12_12_1$ (#19)

The data were collected at a temperature of 23 ± 1°C using the ω-2θ scan technique to a maximum 2θ value of 50.1°. Omega scans of several intense reflections, made prior to data collection, had an average width at half-height of 0.43° with a take-off angle of 6.0°/min (in omega). The weak reflections ($I < 10.0\sigma(I)$) were rescanned (maximum of 2 rescans) and the

counts were accumulated to assure good counting statistics. Stationary background counts were recorded on each side of the reflection. The ratio of peak counting time to background counting time was 2:1. The diameter of the incident beam collimator was 0.5 mm and the crystal to detector distance was 400.0 mm.

Data reduction

Of the 2103 reflections which were collected, 2101 were unique (R_{int} = 0.037). The intensities of three representative reflections which were measured after every 150 reflections remained constant throughout data collection indicating crystal and electronic stability (no decay correction was applied).

The linear absorption coefficient for Mo Kα is 24.0 cm^{-1}. An empirical absorption correction, based on azimuthal scans of several reflections, was applied which resulted in transmission factors ranging from 0.86 to 1.00. The data were corrected for Lorentz and polarization effects.

Structure solution and refinement

The structure was solved by Patterson methods. The non-hydrogen atoms were refined anisotropically. The final cycle of full-matrix least-squares refinement was based on 1203 observed reflections($I > 3.00\sigma(I)$) and 226 variable parameters and converged (largest parameter shift was 0.03 times its esd) with unweighted and weighted agreement factors of:

$$R = \Sigma \, ||Fo| - Fc|| \, / \, \Sigma \, |Fo| = 0.052$$

$$R_w = [(\Sigma \, w \, (|Fo| - |Fc|)^2 \, / \, \Sigma \, w \, Fo^2)]^{1/2} = 0.058$$

The standard deviation of an observation of unit weight was 2.35. The weighting scheme was based on counting statistics and included a factor (p = 0.03) to downweight the intense reflections. Plots of Σ w $(|Fo| - |Fc|)^2$ versus $|Fo|$, reflection order in data collection, sin θ/λ, and various classes of indices showed no unusual trends. The maximum and minimum peaks on the final difference Fourier map corresponded to 0.49 and -0.37 $e^-/Å^3$, respectively.

Full crystallographic details are presented in Table B.1. Final positional parameters are given in Table B.2. An ORTEP drawing is shown in Figure B.1.

Structure Determination of $[Re(CO)_2(C_5H_5)_2]_2(SC_8H_4)$

Data collection

A brown, cube-shaped crystal of $[Re(CO)_2(C_5H_5)_2]_2(SC_8H_6)$ provided by Dr. Angelici's group (Iowa State University) having approximate dimensions of 0.200 x 0.200 x 0.200 mm was mounted on a glass fiber. The crystals had a tendency to grow in complex twin formations. The crystal used for data collection was cut from one of these complex formations. All

Table B.1. Experimental details for $[BrC_{15}NO_4H_{24}]Cl \cdot CCl_2H_2$

Experimental Details	
Empirical Formula	$[BrC_{15}NO_4H_{24}]Cl \cdot CCl_2H_2$
Formula Weight	481.64
Crystal Color, Habit	transparent,cube
Crystal Dimensions (mm)	0.485 x 0.500 x 0.505
Crystal System	orthorhombic
Lattice Parameters	a = 13.250(4) Å
	b = 16.144(6) Å
	c = 9.570(4) Å
Space Group	$P2_12_12_1$
Z	4
Density	1.563 g/cm^3
$\mu_{(MoK\alpha)}$	24.01 cm^{-1}
Diffractometer	Rigaku AFC6R
Radiation	MoKα (λ = 0.71069)
Temperature	25°C
Scan Type	ω-2θ
$2\theta_{max}$	50.1°
Reflections Measured	2103
Reflections Observed (I>3χ(I))	1203
Variables	226
Function Minimized	Σ w ($\|F_o\| - \|F_c\|$)^2
Least-squares Weights	$4F_o^2/\sigma^2(F_o^2)$
Residuals: R; R_w	0.052; 0.058
Goodness of Fit Indicator	2.35
Maximum Peak in Final Dif. Map	0.49 e$^-$/Å^3
Minimum Peak in Final Dif. Map	-0.37 e$^-$/Å^3

Table B.2. Positional parameters[a] for $[BrC_{15}NO_4H_{24}]Cl \cdot CCl_2H_2$

atom	x	y	z
Br	0.0377(1)	0.9679(1)	0.3355(2)
Cl	0.2567(2)	0.7570(3)	0.8693(4)
Cl(2)	0.4466(4)	0.0379(4)	0.2757(6)
Cl(3)	0.3206(5)	-0.0114(4)	0.5008(6)
O(1)	0.1946(7)	0.5874(6)	0.294(1)
O(2)	0.2918(7)	0.6972(6)	0.300(1)
O(3)	0.2022(7)	0.8437(5)	0.254(1)
O(4)	0.1716(7)	0.6681(7)	0.603(1)
N(1)	-0.0145(7)	0.7546(7)	0.103(1)
C(1)	-0.059(1)	0.817(1)	0.395(1)
C(2)	-0.0614(9)	0.724(1)	0.415(1)
C(3)	0.046(1)	0.6884(8)	0.425(1)
C(4)	0.1100(9)	0.7135(8)	0.302(1)
C(5)	0.126(1)	0.8058(8)	0.334(1)
C(6)	0.149(1)	0.803(1)	0.493(2)
C(7)	0.102(1)	0.725(1)	0.551(2)
C(8)	-0.021(1)	0.750(1)	-0.054(1)
C(9)	-0.051(1)	0.668(1)	-0.106(1)
C(10)	0.280(2)	0.479(2)	0.401(4)
C(11)	0.027(1)	0.8464(7)	0.303(1)
C(12)	0.285(1)	0.533(1)	0.298(3)
C(16)	0.325(1)	0.027(1)	0.334(2)
C(17)	0.0033(9)	0.8413(8)	0.147(2)
C(18)	0.211(1)	0.6659(9)	0.297(1)
C(19)	0.0706(9)	0.6976(8)	0.152(1)

[a]Estimated standard deviations in the least significant are given in parentheses.

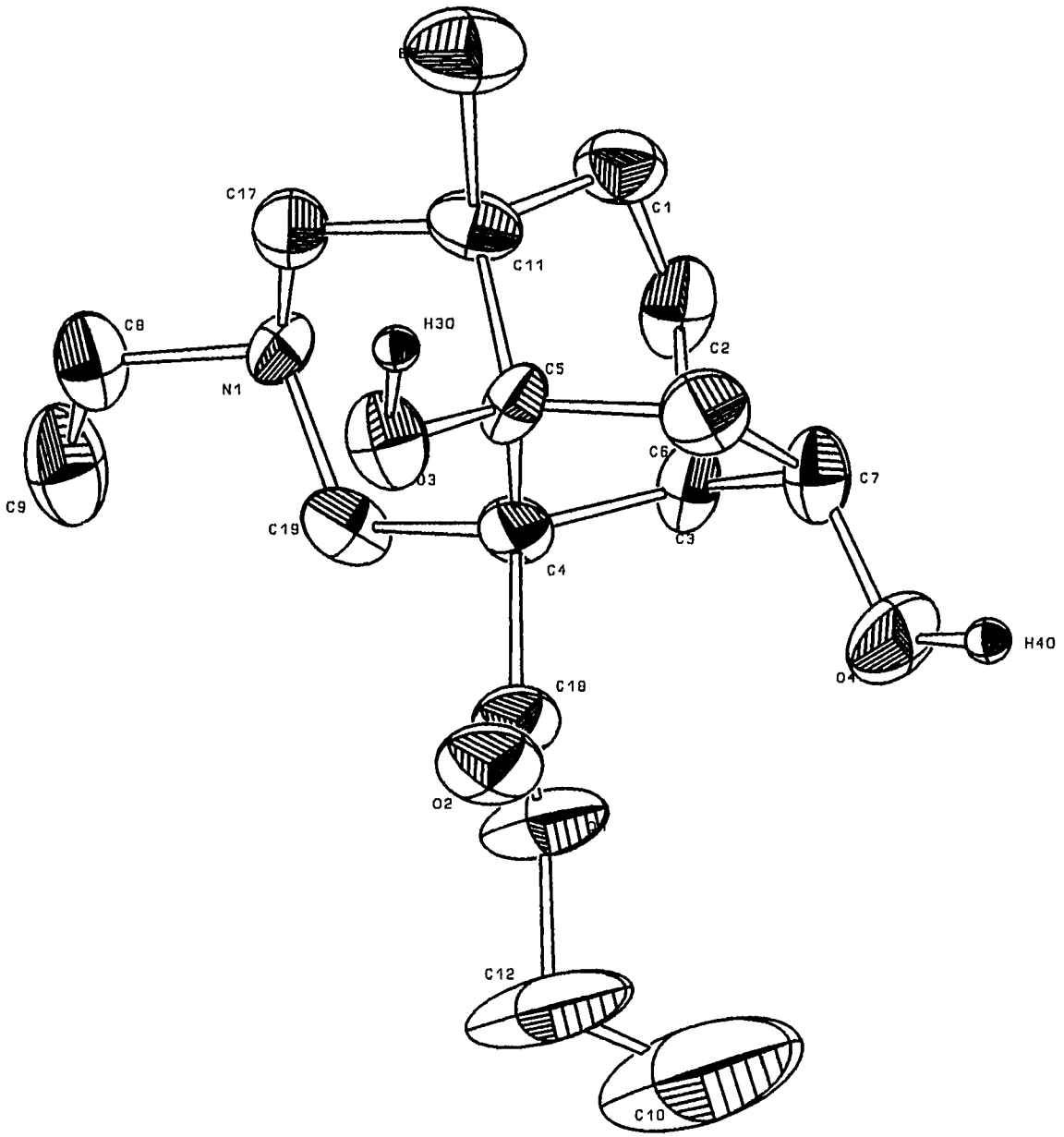

Figure B.1. ORTEP drawing of $[BrC_{15}N_1O_4H_{24}]Cl \cdot CCl_2H_2$

measurements were made on a Rigaku AFC6R diffractometer with graphite monochromated Mo Kα radiation and a 12KW rotating anode generator.

Cell constants and an orientation matrix for data collection, obtained from a least-squares refinement using the setting angles of 24 carefully centered reflections in the range $12.82 < 2\theta < 17.17^{\circ}$ corresponded to an monoclinic cell with dimensions :

$a = 12.265\ (7)\text{Å}$
$b = 11.162\ (6)\text{Å}$ $\quad V = 2044\ (2)\text{Å}^3$
$c = 15.816\ (5)\text{Å}$
$\beta = 109.28\ (3)^{\circ}$

For Z = 4 and F.W. = 746.82, the calculated density is 2.427 g/cm. Based on the systematic absences of:

h0l: $l \neq 2n$
0k0: $k \neq 2n$

and the successful solution and refinement of the structure, the space group was determined to be:

$P2_1/c$ (#14)

The data were collected at a temperature of 23 ± 1°C using the ω-2θ scan technique to a maximum 2θ value of 50.2°. Omega scans of several intense reflections, made prior to data collection, had an average width at half-height of 0.53° with

a take-off angle of 6.0°/min (in omega). Scans of (1.42 + 0.30 tan θ)° were made at a speed of 16.0°/min (in omega). The weak reflections ($I < 10.0\sigma(I)$) were rescanned (maximum of 2 rescans) and the counts were accumulated to assure good counting statistics. Stationary background counts were recorded on each side of the reflection. The ratio of peak counting time to background counting time was 2:1. The diameter of the incident beam collimator was 0.5 mm and the crystal to detector distance was 400.0 mm.

Data reduction

Of the 4024 reflections which were collected, 3837 were unique (R_{int} = 0.103). The intensities of three representative reflections which were measured after every 150 reflections remained constant throughout data collection indicating crystal and electronic stability (no decay correction was applied).

The linear absorption coefficient for Mo Kα is 121.2 cm^{-1}. An empirical absorption correction, based on azimuthal scans of several reflections, was applied which resulted in transmission factors ranging from 0.60 to 1.00. The data were corrected for Lorentz and polarization effects.

Structure solution and refinement

The structure was solved using a combination of Direct methods and a local fourier program. The non-hydrogen non-carbon atoms were refined anisotropically. The carbon atoms

constrained by the aromatic thiophene ring were also refined anisotropically. The carbon atoms of the cyclopentadienyl rings and the carbonyl ligands were refined isotropically. These carbons could not adequately be refined anisotropically perhaps due to slight disorder and/or thermal motion. The final cycle of full-matrix least-squares refinement was based on 1521 observed reflections($I > 3.00\sigma(I)$) and 263 variable parameters and converged (largest parameter shift was 0.40 times its esd) with unweighted and weighted agreement factors of:

$$R = \Sigma \; ||Fo| - Fc|| \; / \; \Sigma \; |Fo| = 0.044$$

$$R_w = [(\Sigma \; w \; (|Fo| - |Fc|)^2 \; / \; \Sigma \; w \; Fo^2)]^{1/2} = 0.046$$

The standard deviation of an observation of unit weight was 1.36. The weighting scheme was based on counting statistics and included a factor (p = 0.03) to downweight the intense reflections. Plots of Σ w $(|Fo| - |Fc|)^2$ versus $|Fo|$, reflection order in data collection, sin θ/λ, and various classes of indices showed no unusual trends. The maximum and minimum peaks on the final difference Fourier map corresponded to 1.35 and -1.38 $e^-/Å^3$, respectively.

Full crystallographic details are presented in Table B.3. Final positional parameters are given in Table B.4. An ORTEP drawing showing anisotropic thermal ellipsoids is shown in Figure B.3.

Table B.3. Experimental details for $[Re(CO)_2(C_5H_5)_2]_2(SC_8H_4)$

Experimental Details	
Empirical Formula	$[Re(CO)_2(C_5H_5)_2]_2(SC_8H_4)$
Formula Weight	746.82
Crystal Color, Habit	brown,cube
Crystal Dimensions (mm)	0.200 x 0.200 x 0.200
Crystal System	monoclinic
Lattice Parameters	a = 12.265(7) Å
	b = 11.162(6) Å
	c = 15.816(5) Å
	β = 109.28°
Space Group	$P2_1/c$
Z	4
Density	2.427 g/cm^3
$\mu_{(MoK\alpha)}$	121.20 cm^{-1}
Diffractometer	Rigaku AFC6R
Radiation	MoKα (λ = 0.71069)
Temperature	25°C
Scan Type	ω
$2\theta_{max}$	50.1°
Reflections Measured	4024
Reflections Observed (I>3χ(I))	1521
Variables	263
Function Minimized	Σ w ($\|F_o\| - \|F_c\|$)^2
Least-squares Weights	$4F_o^2/\sigma^2(F_o^2)$
Residuals: R; R_w	0.044; 0.046
Goodness of Fit Indicator	1.36
Maximum Peak in Final Dif. Map	1.35 e$^-$/Å^3
Minimum Peak in Final Dif. Map	-1.38 e$^-$/Å^3

Table B.4. Positional parameters for $[Re(CO)_2(C_5H_5)_2]_2(SC_6H_6)$

atom	x	y	z
Re(1)	0.0931(1)	0.0730(2)	0.3054(1)
Re(2)	0.3281(1)	-0.2713(1)	0.5566(1)
S	0.1445(9)	-0.0445(9)	0.4365(8)
O(1AA)	0.299(3)	-0.003(4)	0.255(2)
O(1BB)	0.239(3)	0.288(2)	0.397(2)
O(2AA)	0.379(3)	-0.163(3)	0.736(2)
O(2BB)	0.077(2)	-0.303(3)	0.550(2)
C(1AA)	0.219(4)	0.024(4)	0.277(3)
C(1BB)	0.181(3)	0.200(3)	0.367(3)
C(2AA)	0.363(3)	-0.207(2)	0.670(3)
C(2BB)	0.171(4)	-0.283(3)	0.553(3)
C(1A)	0.355(5)	-0.410(4)	0.455(3)
C(1B)	0.450(4)	-0.348(4)	0.485(4)
C(1C)	0.495(4)	-0.370(4)	0.584(4)
C(1D)	0.419(5)	-0.445(4)	0.594(3)
C(1E)	0.334(3)	-0.467(4)	0.509(5)
C(2A)	-0.080(3)	-0.021(4)	0.246(3)
C(2B)	-0.097(3)	0.078(4)	0.289(3)
C(2C)	-0.081(3)	0.175(4)	0.247(3)
C(2D)	-0.038(3)	0.156(3)	0.187(3)
C(2E)	-0.039(3)	0.025(4)	0.175(3)
C(2)	0.273(3)	-0.131(3)	0.455(2)
C(3)	0.366(3)	-0.087(3)	0.520(2)
C(4)	0.400(3)	0.099(4)	0.629(3)
C(5)	0.357(4)	0.186(4)	0.662(3)
C(6)	0.244(5)	0.210(4)	0.631(3)
C(7)	0.170(3)	0.142(4)	0.563(2)
C(8)	0.337(3)	0.014(3)	0.563(3)
C(9)	0.218(3)	0.052(3)	0.527(2)

[a]Estimated standard deviations in the least significant are given in parentheses.

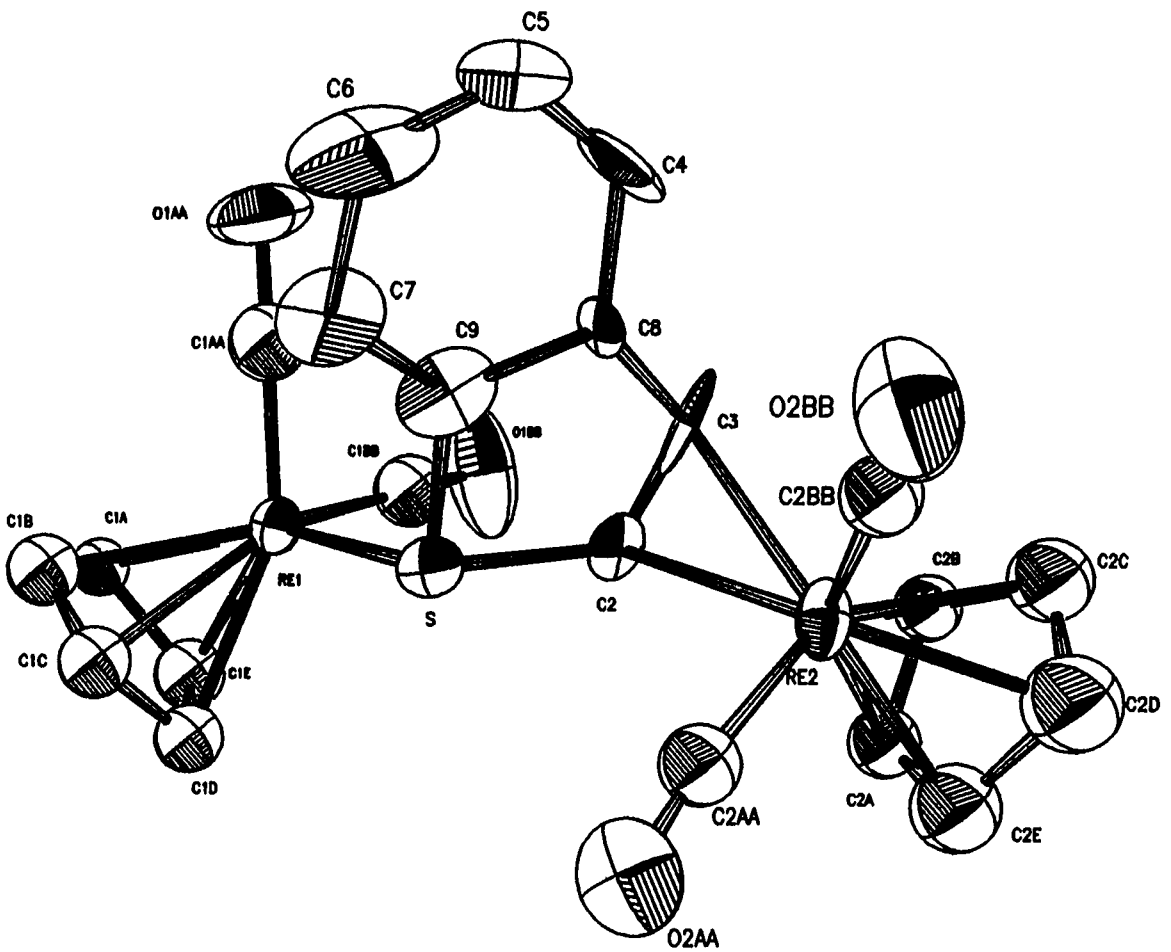

Figure B.2. ORTEP drawing of $[Re(CO)_2(C_5H_5)_2]_2(SC_8H_4)$

Structure Determination of $[FeP_2OC_{30}H_{31}]I$[16]

Data collection

A orange, cube-shaped crystal of $[FeP_2OC_{30}H_{31}]I$ provided by John Nelson's group (Department of Chemistry, University of Nevada - Reno) having approximate dimensions of 0.18 x 0.22 x 0.22 mm was mounted on a glass fiber. All measurements were made on a Rigaku AFC6R diffractometer with graphite monochromated Mo Kα radiation and a 12KW rotating anode generator.

Cell constants and an orientation matrix for data collection, obtained from a least-squares refinement using the setting angles of 22 carefully centered reflections in the range $12.55 < 2\theta < 21.09^\circ$ corresponded to a monoclinic cell with dimensions :

a = 10.710 (4)Å
b = 17.983 (4)Å V = 2905 (2)Å^3
c = 15.490 (5)Å
ß = 103.20 (4)°

For Z = 4 and F.W. = 652.27, the calculated density is 1.491 g/cm^3. Based on the systematic absences of:

h0l: l ≠ 2n
0k0: k ≠ 2n

packing considerations, a statistical analysis of intensity distribution, and the successful solution and refinement of the structure, the space group was determined to be:

$P2_1/c$ (#14)

The data were collected at a temperature of 23 ± 1°C using the ω-2θ scan technique to a maximum 2θ value of 50.1°. Omega scans of several intense reflections, made prior to data collection, had an average width at half-height of 0.41° with a take-off angle of 6.0°/min (in omega). Scans of (1.57 + 0.30 tan θ)° were made at a speed of 16.0°/min (in omega). The weak reflections ($I < 10.0\sigma(I)$) were rescanned (maximum of 2 rescans) and the counts were accumulated to assure good counting statistics. Stationary background counts were recorded on each side of the reflection. The ratio of peak counting time to background counting time was 2:1. The diameter of the incident beam collimator was 0.5 mm and the crystal to detector distance was 400.0 mm.

Data reduction

Of the 10875 reflections which were collected, 5330 were unique(R_{int} = 0.087); equivalent reflections were merged. The intensities of three representative reflections which were measured after every 150 reflections remained constant throughout data collection indicating crystal and electronic stability (no decay correction was applied).

The linear absorption coefficient for Mo Kα is 17.0 cm^{-1}. An empirical absorption correction, based on azimuthal scans of several reflections, was applied which resulted in

transmission factors ranging from 0.79 to 1.00. The data were corrected for Lorentz and polarization effects.

Structure solution and refinement

The structure was solved by direct methods. The non-hydrogen atoms were refined anisotropically. The hydrogens are in calculated positions. The final cycle of full-matrix least-squares refinement was based on 2831 observed reflections ($I > 3.00\sigma(I)$) and 317 variable parameters and converged (largest parameter shift was 2.86 times its esd) with unweighted and weighted agreement factors of:

$$R = \Sigma \; ||Fo| - Fc|| \; / \; \Sigma \; |Fo| = 0.042$$
$$R_w = [(\Sigma \; w \; (|Fo| - |Fc|)^2 \; / \; \Sigma \; w \; Fo^2)]^{1/2} = 0.049$$

The standard deviation of an observation of unit weight was 1.74. The weighting scheme was based on counting statistics and included a factor ($p = 0.03$) to downweight the intense reflections. Plots of $\Sigma \; w \; (|Fo| - |Fc|)^2$ versus $|Fo|$, reflection order in data collection, $\sin \theta/\lambda$, and various classes of indices showed no unusual trends. The maximum and minimum peaks on the final difference Fourier map corresponded to 0.77 and -0.65 $e^-/Å^3$, respectively.

Full crystallographic details are presented in Table B.5. Final positional parameters are given in Table B.6. An ORTEP drawing is shown in Figure B.3.

Table B.5. Experimental details for $[FeP_2OC_{30}H_{31}]I$

Experimental Details	
Empirical Formula	$[FeP_2OC_{30}H_{31}]I$
Formula Weight	652.27
Crystal Color, Habit	orange, cube
Crystal Dimensions (mm)	0.18 x 0.22 x 0.22
Crystal System	monoclinic
Lattice Parameters	a = 10.710(4) Å
	b = 17.983(4) Å
	c = 15.490(5) Å
	ß = 103.20(4)°
Space Group	$P2_1/c$
Z	4
Density	1.491 g/cm³
$\mu_{(MoK\alpha)}$	16.99 cm⁻¹
Diffractometer	Rigaku AFC6R
Radiation	MoKα (λ = 0.71069)
Temperature	25°C
Scan Type	ω-2θ
$2\theta_{max}$	50.1°
Reflections Measured	10875
Reflections Observed (I>3χ(I))	2930
Variables	317
Function Minimized	Σ w ($\lvert F_o \rvert - \lvert F_c \rvert$)²
Least-squares Weights	$4F_o^2/\sigma^2(F_o^2)$
Residuals: R; R_w	0.042; 0.049
Goodness of Fit Indicator	1.74
Maximum Peak in Final Dif. Map	0.77 e⁻/Å³
Minimum Peak in Final Dif. Map	-0.65 e⁻/Å³

Table B.6. Positional parameters[a] for $[FeP_2OC_{30}H_{31}]I$

atom	x	y	z
I	0.21598(5)	0.03938(4)	0.76217(4)
Fe	0.25923(8)	0.06839(5)	0.13096(6)
P(1)	0.3486(1)	0.10112(9)	0.2678(1)
P(2)	0.3076(1)	0.1744(1)	0.0724(1)
O	0.0125(4)	0.1307(3)	0.1368(4)
C	0.1104(6)	0.1073(4)	0.1359(4)
C(1)	0.3914(7)	-0.0162(4)	0.1213(5)
C(2)	0.2979(8)	-0.0421(4)	0.1628(5)
C(3)	0.1758(8)	-0.0373(4)	0.1029(6)
C(4)	0.1969(7)	-0.0058(4)	0.0258(6)
C(5)	0.3296(8)	0.0073(4)	0.0360(5)
C(10)	0.2886(6)	0.0557(3)	0.3553(4)
C(11)	0.3592(6)	0.0584(4)	0.4422(4)
C(12)	0.3124(7)	0.0284(4)	0.5101(5)
C(13)	0.1975(8)	-0.0076(4)	0.4921(6)
C(14)	0.1257(7)	-0.0115(4)	0.4062(6)
C(15)	0.1706(6)	0.0204(4)	0.3385(5)
C(16)	0.5187(5)	0.0936(4)	0.2982(4)
C(17)	0.5709(5)	0.1613(4)	0.3195(4)
C(17A)	0.7117(6)	0.1760(5)	0.3413(5)
C(18)	0.4781(6)	0.2206(3)	0.3194(4)
C(18A)	0.5178(7)	0.2991(4)	0.3417(5)
C(19)	0.3559(6)	0.1975(3)	0.2966(4)
C(21)	0.4735(6)	0.2037(4)	0.0852(4)
C(22)	0.5009(7)	0.2777(4)	0.0797(5)
C(23)	0.6260(8)	0.3025(5)	0.0869(6)
C(24)	0.7249(7)	0.2509(6)	0.1012(6)
C(25)	0.6976(7)	0.1774(6)	0.1067(5)
C(26)	0.5726(6)	0.1528(4)	0.0994(5)
C(27)	0.2298(6)	0.1765(4)	-0.0433(4)
C(28)	0.1384(6)	0.2276(4)	-0.0595(4)
C(28A)	0.0461(7)	0.2393(5)	-0.1468(5)
C(29)	0.1344(5)	0.2739(3)	0.0185(4)
C(29A)	0.0390(7)	0.3345(4)	0.0148(5)
C(30)	0.2212(6)	0.2557(3)	0.0920(4)

[a]Estimated standard deviations in the least significant figure are given in parentheses.

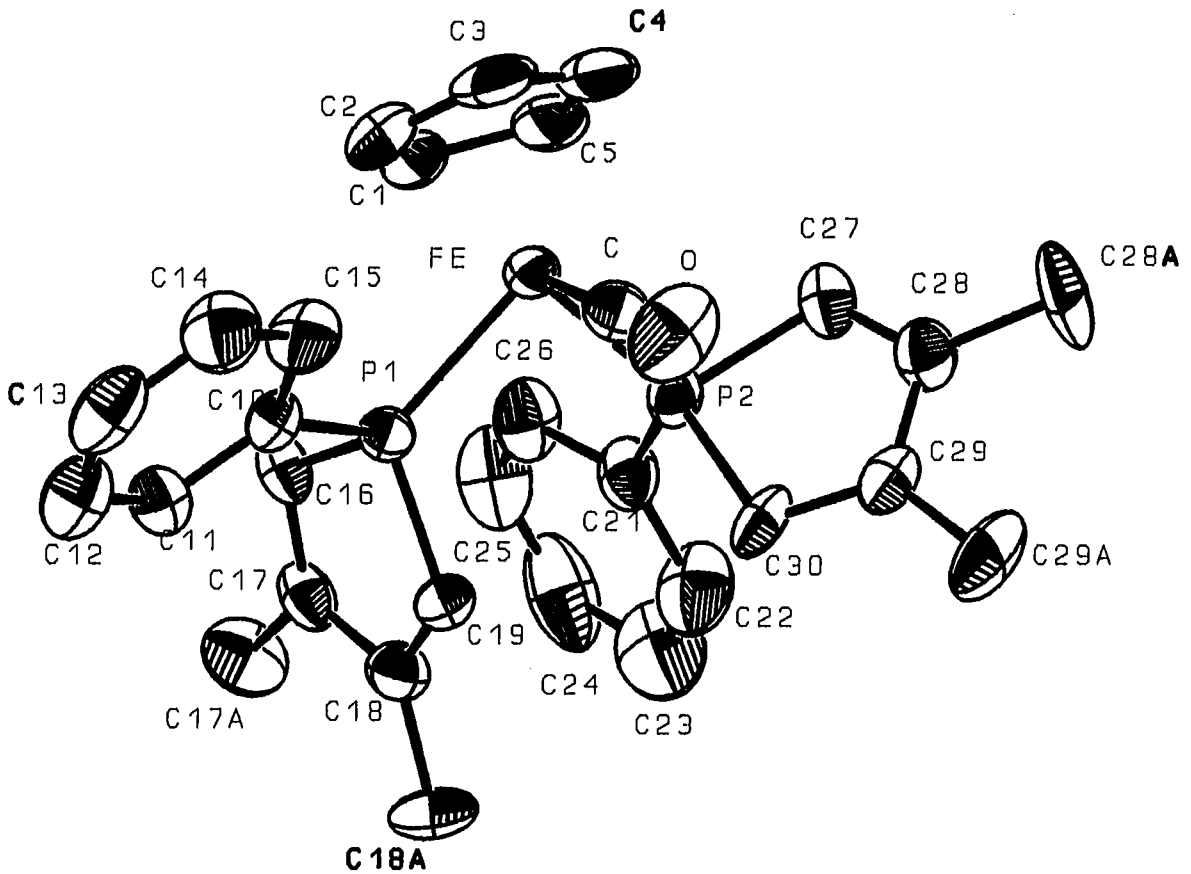

Figure B.3. ORTEP drawing of $[FeP_2OC_{30}H_{31}]I$